

Gold Nanostars: Sensitive, Highly Capturable Reporters Improving Visual Lateral Flow Assay Limit of Detection

By
Parisa Ansari

A thesis submitted to the Department of Chemistry,
College of Natural Science and Mathematics
in partial fulfillment of the requirements for the degree of

Master of Science

in Chemistry

Chair of Committee: Dr. T. Randall Lee

Co-Chair of Committee: Dr. Richard C. Willson

Committee Member: Dr. Allan J. Jacobson

Committee Member: Dr. Scott Gilbertson

Committee Member: Dr. P. Shiv Halasiyamani

University of Houston
May 2020

ACKNOWLEDGMENT

I learned a lot from all the challenges coming on the way that boost my problem-solving ability. I have received enormous support, passion, and encouragement from different individuals. I would like to acknowledge their help and supports. First, I want to express my most profound appreciation to my advisors, Professors T. Randall Lee and Richard C. Willson, whom I took advantage of for knowledge and guidance. I would like to express the deepest appreciation for their dedicated help, with constant encouragement and expert advice, and most importantly, their full support during my research. They were always available, involved with my project, let me make mistakes, and learn from them. I am also very grateful to my dissertation committee members Prof. Allan J. Jacobson, Prof. Scott Gilbertson, and Prof P. Shiv. Halasyamani for their willingness to take time to review my work and offer their valuable comments.

I would like to thank Dr. Francissco Robles Hernandez for his help in obtaining HRTEM images with high quality for this thesis.

I would also like to thank Dr. Katerina Kourentzi, Dr. Binh Vu, and Dr. Hung-Vu Tran for helping me with the review of this thesis.

I would also like to thank Dr. Boris Makarenko for his excellent assistance with the XPS and Dr. Wang for the great training sessions for TEM.

I would also appreciate all the lab members in the two groups I had the advantage to be a member of for all their help.

I dedicate this work to my beloved family, the dearest spouse in the world, Amirhesam Khalafi, and my lovely son, Adrian. Without their love, sincerity, support, and understanding, I could never have gone through this challenging chapter of my life.

Last but not least, I am grateful for my adorable family, whose great leaders are my parents. The champions who have always helped me and prayed the best for my life. Just like my awesome siblings and friends do.

ABSTRACT

Lateral flow assay (LFA) is a point-of-care (POC) diagnostic testing method. LFA is advantageous over many other POC tests for its diverse applications, simplicity, convenience of use, quick time-to-result, low cost, and independence of elaborate equipment or trained labor. However, the lack of desired sensitivity of the so-far-reported reporters limits LFA applications. This thesis reports the use in LFA of gold nanostars (AuNSs) synthesized by applying a seed growth method, systematically functionalized with antibodies without any aggregation, and fully characterized. The influence of the morphology of the particles on the sensitivity and limit of detection (LOD) of the LFA for human chorionic gonadotropin (hCG) hormone was studied. The results were compared to those with standard commercial 40 nm gold nanospheres (AuNPs). The gold nanostars used in this study produce low LODs owing to their high capturability and high optical detectability related to their localized surface Plasmon resonance (LSPR). Preliminary experiments on engineering and evaluation of hCG-targeted LFA using AuNSs colloid gave a visual LOD of 2 pg/mL, about 50-fold magnitude more sensitive than colloidal gold LFA (~100 pg/mL) at the same conditions.

TABLE OF CONTENTS

ACKNOWLEDGMENT.....	III
TABLE OF CONTENTS.....	VI
LIST OF TABLES	VIII
LIST OF FIGURES	IX
CHAPTER 1. INTRODUCTION	1
1.1 LATERAL FLOW ASSAY (LFA).....	1
1.2 LOCALIZED SURFACE PLASMON RESONANCE (LSPR).....	8
1.3 GOLD NANOPARTICLES.....	11
1.4 SYNTHESIS OF GOLD NANOSTARS	14
1.5 SURFACE MODIFICATION OF GOLD NANOPARTICLES	17
1.6 APPLICATION OF GOLD NANOPARTICLES IN LFA	19
1.7 APPLICATION OF GOLD NANOSTARS IN LFA	21
CHAPTER 2. GOLD NANOSTARS: SENSITIVE, HIGHLY CAPTURABLE, FAST REPORTERS IMPROVING VISUAL LIMIT OF DETECTION OF LATERAL FLOW ASSAYS	22
2.1 INTRODUCTION	22
2.2 MATERIALS.....	31
2.3 APPARATUS AND METHODS	32
2.4 SPECTROSCOPIC TECHNIQUES	32
2.5 SYNTHESIS OF GOLD NANOSTARS	33
2.5.1 PREPARATION OF GOLD NANOSEEDS	33
2.5.2 PREPARATION OF GOLD NANOSTARS GROWTH SOLUTION.	33

2.5.3 PREPARATION OF GOLD NANOSTARS.....	34
2.6 ORGANIC SYNTHESIS OF THE LINKER BMPHA AND SAM FUNCTIONALIZATION OF GOLD NANOSTAR.....	34
2.7 THIOLATE- FUNCTIONALIZATION OF THE GOLD NANOSTARS.....	35
2.8 BIO-FUNCTIONALIZATION OF GOLD NANOSTARS WITH ANTIBODIES	36
2.9 ASSEMBLING HALF STRIPS (DIPSTICKS)	37
RUNNING THE LFA TESTS	38
2.10 CHARACTERIZATION OF GOLD NANOSTAR REPORTERS	39
2.11 DISCUSSION ON GOLD NANOSTARS FORMATION TO BIOCONJUGATION.....	47
2.12 GOLD NANOSTARS BIOCONJUGATION	49
2.13 LFA DATA OBTAINING.....	51
2.14 AMOUNT OF ANTIBODIES USED	52
2.15 PARTICLE NUMBER OPTIMIZATION.....	53
2.16 COMPARISON OF LFA BASED ON GOLD NANOSPHERES AND GOLD NANOSTARS	54
2.17 KINETIC ANALYSIS OF THE GOLD NANOSTAR-LATERAL FLOW ASSAY	58
2.18 CONCLUSION.....	60
2.19 FUTURE WORKS.....	61
BIBLIOGRAPHY.....	62

LIST OF TABLES

TABLE 1.1. HCG CONCENTRATION DURING PREGNANCY PERIOD.....	5
TABLE 2.1. SUMMARY OF AUNS-BASED LFAS USED FOR SENSITIVITY ENHANCEMENT	28
TABLE 2.2. THE ELEMENTAL PERCENTAGE OBTAINED BY EDX AND XPS FOR GOLD NANOSTARS.	47
TABLE A.1. FREQUENTLY USED ABBREVIATION TABLE	85

LIST OF FIGURES

FIGURE 1.1. SCHEMATIC REPRESENTATION OF LATERAL FLOW ASSAY	3
FIGURE 1.2. HUMAN CHORIONIC GONADOTROPIN (hCG) AND ITS A-hCG AND B-hCG SUBUNITS ..	4
FIGURE 1.3. SCHEMATIC ILLUSTRATION OF THE LSPR WHICH RISES FROM THE INTERACTION OF THE ELECTROMAGNETIC WAVE WITH THE OSCILLATING ELECTRONS ON THE SURFACE OF THE NANOPARTICLES.	9
FIGURE 1.4. CALCULATED EXTINCTION, ABSORPTION, AND SCATTERING OF (A) 20, (B) 40, AND (C) 80 NM SILVER NANOPARTICLES, AND (D) 20, (E) 40, AND (F) 80 NM GOLD NANOPARTICLE USING THE COMPUTATIONAL BOUNDARY ELEMENT (BME) METHOD.....	10
FIGURE 1.5. EXTINCTION SPECTRA OF (A) SPHERICAL AuNPs, (B) AuNSs, AND (C) AuNRs; AND THEIR CORRESPONDING TEM IMAGES FOR (D) SPHERICAL AuNPs, (E) AuNSs, AND (F) AuNRs	13
FIGURE 1.6. SCHEMATIC ILLUSTRATION OF GOLD NANOSTARS' APPLICATIONS (A) IN PHOTO TUMOR ABLATION-THERAPY, AND (B) DRUG DELIVERY USING NIR IRRADIATION.	17
FIGURE 1.7. AuNP SHAPES, SIZES, SURFACE COATING, AND FUNCTIONALIZATION.	18
FIGURE 2.1. SCHEMATIC REPRESENTATION OF GOLD NANOSTARS LATERAL FLOW ASSAY AND GOLD NANOSPHERES LATERAL FLOW ASSAY.....	30
FIGURE 2.2. THE SYNTHESIS PROCEDURE OF BMPHA	35
FIGURE 2.3. EXTINCTION SPECTRA OF THE SYNTHESIZED SAM-FUNCTIONALIZED AuNSs.....	39
FIGURE 2.4. SEM IMAGES OF THE AuNSs.	40
FIGURE 2.5. (A), (C), (E) TEM IMAGES OF THE AuNSs AND (B), (D),(F) THEIR CORRESPONDING X- RAY DIFFRACTION PATTERN	41

FIGURE 2.6. (A), (B) TEM IMAGES OF THE AUNSS REPRESENTING GOLD FACE-CENTERED CUBIC (FCC) STRUCTURE	42
FIGURE 2.7. (A) TEM IMAGE OF ONE ARM OF AUNSS, (B) THE SULFUR, AND (C) THE GOLD ABUNDANCE ALONG THE DRAWN LINE PERPENDICULAR TO IT MEASURED BY EDX-TEM.	42
FIGURE 2.8. PARTICLE SIZE DISTRIBUTION RESULTS OF THE AUNSS MEASURED BY (A) NANOSIGHT AND (B) ARCHIMEDES MICROCHANNEL RESONATOR; MEDIAN=62 NM, MEAN=84 NM, AND STANDARD DEVIATION=28 NM. THE NANO-CHIP USED IN ARCHIMEDES COULD NOT SENSE THE PARTICLES WITH THE SIZE OF <50 NM.	43
FIGURE 2.9. FTIR SPECTRA OF BMPHA (BLUE), 4-MBA (PURPLE), THE MIXTURE OF BMPHA/ 4-MBA (1:3) (RED), AND THE SAM-FUNCTIONALIZED AUNSS (BLACK).	44
FIGURE 2.10. XPS SPECTRA OF THE SAM-FUNCTIONALIZED AUNSS IN THE (A) AU 4F, (B) S 2P, AND (C) C 1s, AND AG 3D (D) REGIONS.	45
FIGURE 2.11 DECONVOLUTION OF S 2P PEAK OF XPS OF THE AUNSS AND ITS CORRELATED BOUND AND UNBOUND THIOL PERCENTAGE	46
FIGURE 2.12. EDX-TEM ELEMENTAL MAPPING OF THE BMPHA FUNCTIONALIZED STARS.....	46
FIGURE 2.13. SCHEMATIC ILLUSTRATION DEPICTING THE GROWTH OF THE AUNSS WHERE: (I) THE SURFACTANT STABILIZES THE [111] FACET OF THE GOLD PARTICLE; (II) TIPS GROW FROM THE STABILIZED [111] FACET; AND FINALLY, (III) MULTI-TWIN DEFECTS LEAD TO THE FORMATION OF THE STARS	48
FIGURE 2.14. SAM FUNCTIONALIZATION OF THE AUNSS	49
FIGURE 2.15. OVERALL STEPS OF BIO-FUNCTIONALIZATION OF THE AUNSS.....	50

FIGURE 2.16. PEAK AREA VS EXPOSURE TIME FOR THE DATA OBTAINED BY LUMOS USING DIFFERENT LIGHT SOURCES AND EXPOSURE TIMES FOR A) AuNSs AND B) SPHERICAL AuNPs.	52
FIGURE 2.17. PEAK AREA VS. NUMBER OF THE AuNSs FOR THE DATA OBTAINED BY LUMOS USING DIFFERENT AMOUNTS OF ANTIBODIES FOR BIOCONJUGATION FOR CL	53
FIGURE 2.18. THE INTENSITY OF PEAKS FOR TL AND CL OBTAINED BY LUMOS USING DIFFERENT CONCENTRATIONS OF HCG AND AuNS-LFA REPORTERS.	54
FIGURE 2.19. TL/CL RATIO FOR DIFFERENT CONCENTRATIONS OF HCG USING AuNSs AND SPHERICAL AuNPs WITH (A) LONGER Y-AXIS AND (B) SHORTER Y-AXIS	55
FIGURE 2.20. (A) SPHERICAL- AND STAR- SHAPED GOLD NANOPARTICLES' CAPTURABILITY COMPARISON EXPERIMENT. (B) LIGHT SENSITIVITY EXPERIMENT DONE FOR GOLD NANOSTARS (BLUE), GOLD NANOSPHERES (RED).....	57
FIGURE 2.21. KINETIC COMPARISON OF NANOSTARS (BLUE), GOLD NANOSPHERES (RED).	59
FIGURE A.1. H NMR OF THE 16-(3,5 BIS (MERCAPTOMETHYL) PHENOXY) HEXADECANOIC ACID (BMPHA).....	73
FIGURE A.2. THE INTENSITY OF CL AND TL VS. DETECTION LINES POSITIONS ON LFA USING AuNSs REPORTERS WITH THE WHITE LS OF LUMOS TRYING DIFFERENT EXPOSURE TIMES, FROM 1 MSEC. TO 10 MSEC.	74
FIGURE A.3. THE INTENSITY OF CL AND TL VS. DETECTION LINES POSITIONS ON LFA USING AuNSs REPORTERS WITH THE GREEN LS OF LUMOS TRYING DIFFERENT EXPOSURE TIMES, FROM 1 MSEC. TO 10 MSEC.	74

FIGURE A.4. THE INTENSITY OF CL AND TL VS. DETECTION LINES POSITIONS ON LFA USING AuNSs REPORTERS WITH THE BLUE LS OF LUMOS TRYING DIFFERENT EXPOSURE TIMES, FROM 1 MSEC. TO 10 MSEC.	75
FIGURE A.5. THE INTENSITY OF CL AND TL VS. DETECTION LINES POSITIONS ON LFA USING AuNSs REPORTERS WITH THE RED LS OF LUMOS TRYING DIFFERENT EXPOSURE TIMES, FROM 1 MSEC. TO 10 MSEC.	76
FIGURE A.6. THE INTENSITY OF CL AND TL VS. DETECTION LINES POSITIONS ON LFA USING AuNSs REPORTERS WITH THE “COLLOIDAL OLD” LS OF LUMOS TRYING DIFFERENT EXPOSURE TIMES, FROM 1 MSEC. TO 10 MSEC.	77
FIGURE A.7. THE INTENSITY OF CL AND TL VS. DETECTION LINES POSITIONS ON LFA USING AuNSs REPORTERS WITH THE RED-BLUE LS OF LUMOS TRYING DIFFERENT EXPOSURE TIMES, FROM 1 MSEC. TO 10 MSEC.	77
FIGURE A.8. AuNSs PEAK AREA OF TL AND CL VS. DIFFERENT EXPOSURE TIMES USING THE VARIOUS LIGHT SOURCES OF LUMOS READER.	78
FIGURE A.9. THE INTENSITY OF CL AND TL VS. DETECTION LINES POSITIONS ON LFA USING SPHERICAL AuNPs REPORTERS WITH THE RED LS OF LUMOS TRYING DIFFERENT EXPOSURE TIMES, FROM 1 MSEC. TO 10 MSEC.	79
FIGURE A.10. THE INTENSITY OF CL AND TL VS. DETECTION LINES POSITIONS ON LFA USING SPHERICAL AuNPs REPORTERS WITH THE “COLLOIDAL GOLD” LS OF LUMOS TRYING DIFFERENT EXPOSURE TIMES, FROM 1MSEC. TO10 MSEC.	80

FIGURE A.11. THE INTENSITY OF CL AND TL VS. DETECTION LINES POSITIONS ON LFA USING SPHERICAL AUNPS REPORTERS WITH THE RED-GREEN LS OF LUMOS TRYING DIFFERENT EXPOSURE TIMES, FROM 1 MSEC. TO 10 MSEC.....	80
FIGURE A.12. THE INTENSITY OF CL AND TL VS. DETECTION LINES POSITIONS ON LFA USING SPHERICAL AUNPS REPORTERS WITH THE RED-BLUE LS OF LUMOS TRYING DIFFERENT EXPOSURE TIMES, FROM 1 MSEC. TO 10 MSEC.	81
FIGURE A.13. THE INTENSITY OF CL AND TL VS. DETECTION LINES POSITIONS ON LFA USING SPHERICAL AUNPS REPORTERS WITH THE GREEN LS OF LUMOS TRYING DIFFERENT EXPOSURE TIMES, FROM 1 MSEC. TO 10 MSEC.....	81
FIGURE A.14. THE INTENSITY OF CL AND TL VS. DETECTION LINES POSITIONS ON LFA USING SPHERICAL AUNPS REPORTERS WITH THE BLUE LS OF LUMOS TRYING DIFFERENT EXPOSURE TIMES, FROM 1 MSEC. TO 10 MSEC.....	82
FIGURE A.15. THE INTENSITY OF CL AND TL VS. DETECTION LINES POSITIONS ON LFA USING SPHERICAL AUNPS REPORTERS WITH THE WHITE LS OF LUMOS TRYING DIFFERENT EXPOSURE TIMES, FROM 1 MSEC. TO 10 MSEC.....	83
FIGURE A.16. THE INTENSITY OF CL AND TL VS. DETECTION LINES POSITIONS ON LFA USING SPHERICAL AUNPS REPORTERS WITH THE GREEN-BLUE LS OF LUMOS TRYING DIFFERENT EXPOSURE TIMES, FROM 1 MSEC. TO 10 MSEC.....	84
FIGURE A.17. LFA RESULTS USING GOLD NANOSTARS WITH DIFFERENT CONCENTRATIONS OF HCG (ON TOP) AND SPHERICAL GOLD NANOPARTICLES IN DIFFERENT CONCENTRATIONS OF HCG (ON BOTTOM).....	84

CHAPTER 1. Introduction

1.1 Lateral Flow Assay (LFA)

Lateral flow assays (LFAs) are point-of-care (POC) diagnostic tests that have been the center of scientific research due to their commercial and free-of-specialist usage, as well as their applications in detection of manifold analytes like toxins in agriculture, food, environmental monitoring, safety control, and drug industry to medical diagnosis and animal health.^{1,2} However, LFAs often lack desirable sensitivity or limit of detection (LOD), and their results are semi-quantitative in many cases.^{3,4}

The LFA strip contains four important porous parts with the capacity of spontaneous transport of fluid by capillary wicking. (Figure 1.1)

- 1) The sample pad: the first part made mainly from glass fiber that acts like a sponge on which the sample containing the analyte (the antigen, e.g., hCG) is applied.
- 2) The conjugate release pad: commonly made from cellulose, contains dried antibody-functionalized reporter nanoparticles.^{5,6}
- 3) The nitrocellulose (NC) membrane: the last part on which two or more (in multiplex LFA) colorful lines can potentially be observed during testing of the analyte; the control line (CL) and the test line(s) (TL).
- 4) Absorbent pad: this part is located on the very top end of the strip and is made of cellulose, and controls the flow rate and assists the forward movement of the sample. All four parts mentioned above are assembled on a polyvinyl chloride adhesive backing card.⁵

In commercial versions, all mentioned parts of LFA are put inside a housing case. The sample, which is dripped on the sample pad, might be blood, milk, urine, serum, plant material, or

food. Once the sample is loaded onto the sample pad region, capillary forces cause its migration toward the absorbent pad, which is located at the other end of the strip. During this migration, the sample dissolves the LFA reporters on the conjugate pad. If the target analyte is present in the sample, it will react with the detecting reporters. The analyte conjugated with the detection reagents keeps moving on the porous nitrocellulose membrane until it reaches the TL and CL zones⁷. Figure 1.1 illustrates the different parts of the LFA strips as well as the sandwich immunoassay mechanism that causes the TL and CL formations. In reality, there is an overlap between different parts of the LFA.

On the CL and TL zone located on the NC membrane, there might be two mechanisms applied to detect the presence of the analyte in the sample.

a) Competitive mechanisms for small molecules

In this format, the same molecule as the analyte competes with the analyte in attaching to the TL antibodies. The competitive format itself splits up into two categories. In the first one, the analyte and the same molecule placed on reporters in the conjugation pad compete with one another in their conjugation to the capturing antibodies plotted in the TL. In the second one, the mechanism includes the attachment of the analyte molecules to the capturing agents placed on the reporters on the conjugation pad. This mechanism causes the blocking of these capturing agents. This blockage prevents their attachment to the “immobilized antigens” in the TL zone. In both formats, the signal gained from the LFA strips is inversely related to the concentration of the analyte.

b) Sandwich immunoassay format for large molecules

In a sandwich immunoassay format, the presence of analyte will cause the capture of reporting particles on the TL resulting in a detectable signal whose intensity increases with analyte concentration.⁸

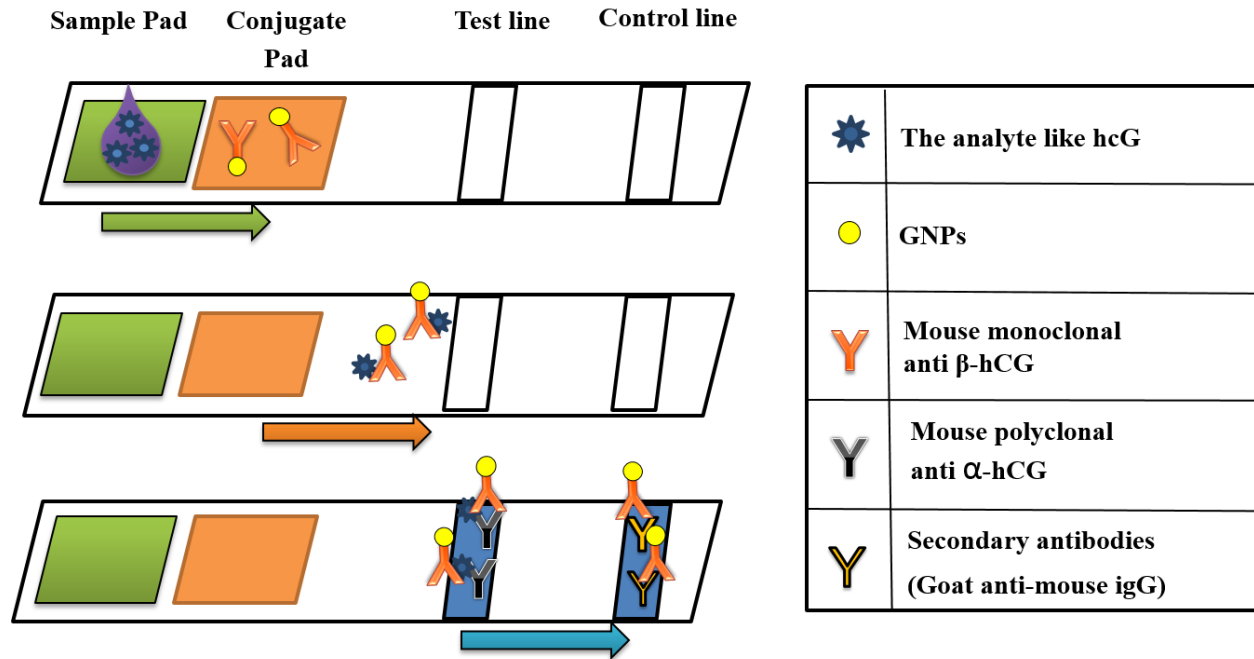


Figure 1.1. Schematic representation of lateral flow assay

A detectable signal appears on the TL zone decreasing with increasing of the analyte concentration, in the competitive mechanism, and rising directly by the enhancement of the analyte concentration in the sandwich immunoassay format, cause the target detection.⁸ If the analyte being studied is human chorionic gonadotropin (hCG) in a sandwich immunoassay format, the control line is plotted with secondary antibodies like anti-mouse IgG. The formation of the line there indicates the proper liquid flow through the porous membrane and is independent of the presence or not of the analyte (hCG) in the sample. The CL formation also shows if the test works

well or not, by capturing the antibody functionalized nanoparticles. The test line is plotted with the primary antibodies like goat polyclonal anti- β hCG. If the sample contains hCG, the hCG would be sandwiched between antibody functionalized gold nanoparticles and the polyclonal antibodies on the strip at the test line. Therefore, the appearance of color on the test line confirms the formation of the sandwich immunoassay and the existence of the analyte in the sample, which is hCG hormone on the pregnancy LFA test.^{5, 6}

hCG (Figure 1.2) is a hormone possessing a glycoprotein structure composing of 237 amino acids with a molecular weight of 36.7 KDa. These 237 amino acids are composed of two main subunits called: α -hCG with 92 amino acids (Mw = 14.5 KDa) and β -hCG with 145 amino acids (Mw = 22.2 KDa). The two units of α -hCG and β -hCG create a hydrophobic core with a high surface to volume ratio surrounded by the hydrophilic amino acids.^{9, 10} hCG is produced usually after implantation and during pregnancy. Table 1.1 represents the hCG levels during pregnancy.

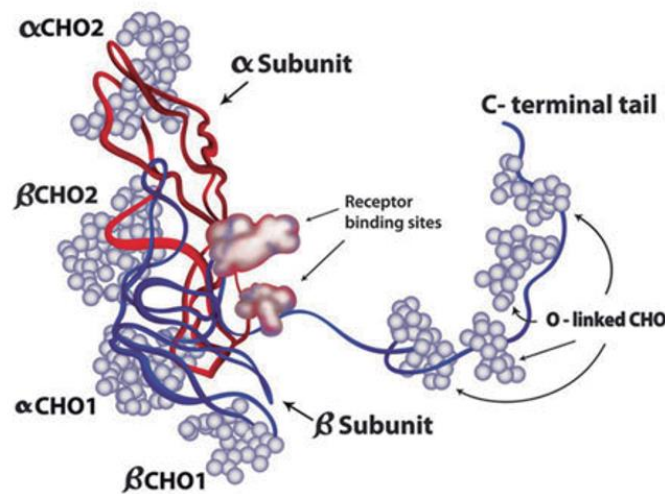


Figure 1.2. Human chorionic gonadotropin (hCG) and its α -hCG and β -hCG subunits¹¹

Table 1.1. hCG concentration during pregnancy period¹²

weeks since last menstrual period (LMP)	mIU/mL	weeks since LMP	mIU/mL
3	5 – 50	13 – 16	13,300 – 254,000
4	5 – 428	17 – 24	4,060 – 165,400
5	18 – 7,340	25 – 40	3,640 – 117,000
6	1,080 – 56,500	Non-pregnant females	<5.0
7 – 8	7,650 – 229,000	Postmenopausal females	<9.5
9 – 12	25,700 – 288,000		

The β -hCG subunit also is produced by some cancerous cells. Therefore, detection of hCG can also be used in cancer diagnosis or paraneoplastic syndromes if the patient is not pregnant.¹³ Each international unit of concentrations of hCG which is (mIU/mL) is equivalent to 2.35×10^{-12} moles/mL, or about 6×10^{-8} grams/mL. The normal range for men is between 0-5 mIU/mL.^{14, 15} Besides, hCG is as an established clinical biomarker of pregnancy or some illnesses like metro-carcinoma. Hence, in time detection of low concentrations of hCG within blood or urine tests helps early diagnosis of cancers or pregnancy at the very early stages.²

The most common method of detection of hCG is using LFA. One of the drawbacks of LFA is its incapability of simultaneous detection of two biomarkers, like the prediction of the

reoccurrence of some cancers. Another case is the monitoring of the germ cell tumors, in which the level of hCG is needed to be reported along with α -fetoprotein.¹⁶ The appearance of multiplex LFA solved this problem. In case of having a multiplex strip, the existence of the additional test lines on the NC membrane, with different targets with the same or different reporters on a single strip allow simultaneous detection of multiple analytes. Multiplex LFA is popular for being more economical in application when the detection of more than one analyte at the same time is desired, like in some cancer infection diagnoses.¹⁷

In order to have an efficient LFA, the shape and properties of the reporters are vital factors.¹⁸ There are many forms of the reporters, like quantum dots, latex beads, gold nanoparticles, magnetic nanoparticles, electrochemical active tags, SERS active tags, and enzymatic tags, to be used in LFA for the detection of various target analytes. The choice of the reporters in LFA depends on the detection technique used in capturing analyte. The on-site detection of the analyte is done through applying different methods including (a) visual-, (b) magnetic-, (c) fluorescent-, (d) surface enhanced Raman spectroscopy (SERS-), (e) electrochemical- based methods.⁸

(a) Visual-based detection in LFA

As it is obvious from its name, the visible, colorful appearance of the TL zone of LFA strips reveals if the target is present in the sample. The need for the formation of the visible line requires the use of colorful particles. The necessity of colorful particles drives use of light-driven nanotechnology in their structure, like different sized and shaped gold nanoparticles or silver nanoparticles, explained in the following, or latex particles.¹⁹

(b) Magnetic-based detection in LFA

Magnetic beads and nanoparticles like Fe_3O_4 ²⁰ or magnetized carbon nanotubes²⁰ are the examples of the reporters used in this technique. The use of these reporters has gained attention

due to their stability over time. However, a magnetic reader is needed to assess the signal in this technique.

(c) Luminescent-based detection in LFA

Sometimes, to increase the signal intensity, the chemiluminescence tags are used. However, it also requires an expert user most of the time.¹⁸ Organic fluorophores, quantum dots, and fluorescent dyes are the common fluorescent reporters used in this method.^{18, 21} Moreover, the low photostability of the fluorophores,^{22, 23} the high cost and intermittent on/off behavior of quantum dots,²⁴ and low colloidal stability of the dyes¹⁸ limit their application. These drawbacks can be addressed by using persistent luminescent nanophosphors (PLNPs).²⁵ In this case, the LFAs coupled with minimal hardware on a smartphone can detect the signal with high sensitivity toward different biomarkers.²⁵⁻²⁷

(d) SERS-based detection in LFA

Surface-enhanced Raman scattering (SERS)-based lateral flow immunoassay (LFA) is a technique in which Raman reporter-labeled nanoparticles are used as SERS detection probes. SERS allows the highly sensitive quantitative evaluation of the analyte by measuring the signals from the test zone. Although this method can trace very low concentrations of the analyte, it is not a costly-effective or simple technique.^{28, 29} This is due to the need for highly expensive and specialized equipment with tunable laser sources, beside an expert technician.

(e) Electrochemical- based detection in LFA

Another option is the conjugation of an electrochemical technique with a calorimetric detection of the analyte in LFA that leads to the quantification of the results usually by using red/ox properties of some the reporters in LFA.¹⁸

Sometimes, the combination of two of the detection techniques mentioned above is used. In the dual detection mode LFA, the visual-based detection LFA along with other detection techniques are used to decrease the systematic error of the detection and lead the simultaneous qualitative and quantitative results. However, these coupled techniques enhance their cost and brings up the requirement of a special reader and specialized expert.³⁰

The low sensitivity of LFA and its aforementioned valuable advantages, at the same time, caused the evolution of the LFA research by applying nanotechnology-driven enhancement of its technology, to increase their sensitivity.³¹ AuNPs are the most popular so-far reported reporters of LFA. The prevalence of the AuNPs as LFA reporters is from their easy synthesis protocols, facile surface modification with sulfur-based coatings⁸, affordability, and naked-eye detection.^{6, 32}

The colorimetric detection is related to the nanoplasmonics properties of the gold nanoparticles. Nanoplasmonic is considered as one of the most interesting light-driven technologies, particularly for bio-sensing applications.

1.2 Localized Surface Plasmon Resonance (LSPR)

The optical phenomena experienced by plasmonic materials, in general, originates from the interaction of light with the free electrons of the material, which will lead to the coherent oscillation of those electrons, also known as surface plasmon resonance.³³ When the size of the plasmonic material is smaller than the wavelength of the incoming light (i.e., on the nanometer scale), coherent localized plasmon oscillations will result. This is also known as localized surface plasmon resonance (LSPR) and is illustrated in Figure 1.3.³⁴

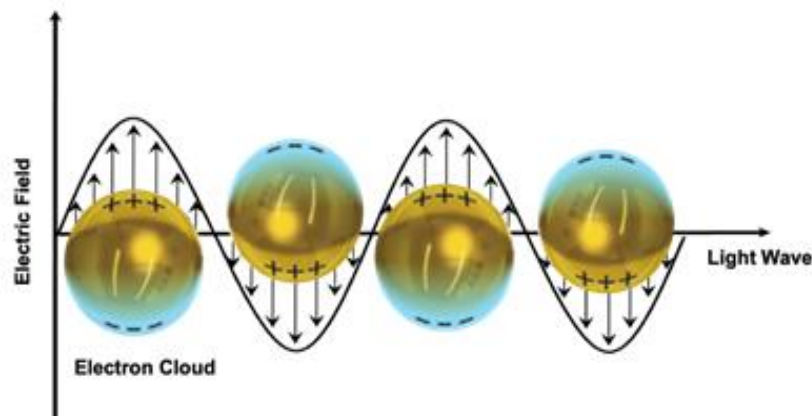


Figure 1.3. Schematic illustration of the LSPR which rises from the interaction of the electromagnetic wave with the oscillating electrons on the surface of the nanoparticles.

The LSPR spectrum of a metallic nanoparticle depends on its size, shape, material, and the dielectric constant of its environment, which itself depends on the refractive index of the surrounding media of the nanoparticle.³⁵

The LSPR inherent to plasmonic nanoplatforms enables the use of these nanostructures in cost-effective point-of-care (POC) diagnostic devices. The LSPR peak position depends on the dielectric nanoplatform/nanoparticle environment. For example, a small change in refractive index of the AuNPs environment results in changes in their LSPR frequency. Since it is easy to track the LSPR frequency, nanoscale sensing application is possible using nanoparticles..⁴ Therefore, plasmonic-based bio-sensing has been predominantly used for its fast and real-time capture of biological analytes, such as antibodies, enzymes, and nucleic acids.³⁶

There are many kinds of materials exhibiting plasmonic properties like gold, silver, aluminum, copper, and doped semiconductors and metal oxides. Among them, gold and silver are the most common ones due to the more enhanced LSPR, which is even higher in silver comparing to gold. However, the simplicity of the synthesis procedure, inertness, and facile surface modification of gold made it the most popular candidate for LSPR-based applications.³⁷ Figure

1.4 shows calculated absorption, scattering, and extinction (sum of absorption and scattering) of different sized silver or gold nanoparticle using the computational boundary element method.³⁸ Increasing of the size of the spherical AuNPs and Ag nanoparticles cause the redshift of their LSPR peak. Also, the 20 nm Au and Ag NPs extinction is mainly for their high absorption of the incident light. However, the increase of the NPs size from 20 nm to 80 nm results in higher intensity of the scattering peak as the main component of extinction.

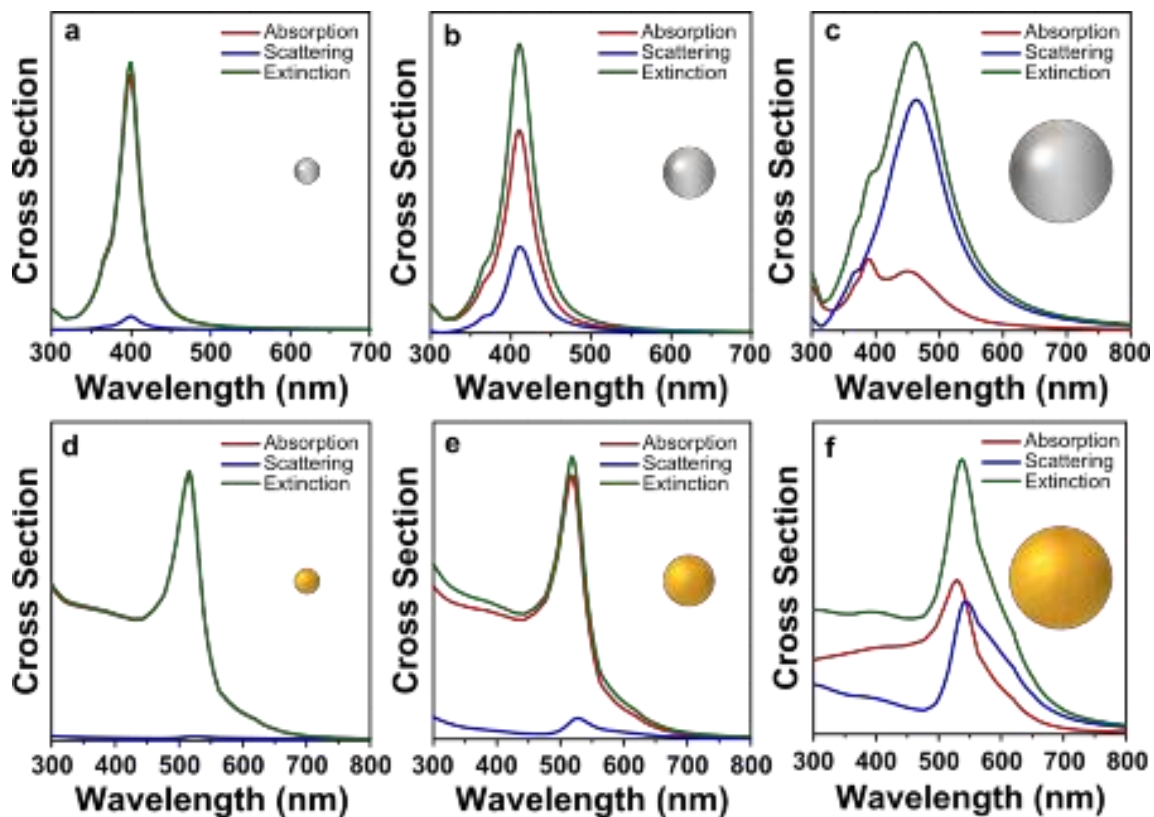


Figure 1.4. Calculated extinction, absorption, and scattering of (a) 20, (b) 40, and (c) 80 nm silver nanoparticles, and (d) 20, (e) 40, and (f) 80 nm gold nanoparticle using the computational boundary element (BME) method³⁸

1.3 Gold Nanoparticles

The LSPR peak of the gold nanoparticles (AuNPs) is related to electron oscillations on their surface. Generally, the wavelength of the light absorbed red shifts with increasing the size of the AuNPs,³⁹ and enhancement of the refractive index of their environments.⁴⁰ Accordingly, gold nanoparticles have been widely adopted for different types of applications since tuning of their LSPR can be achieved through modification of the shape, size, and composition.⁴¹ Some recent reviews summarize various applications of gold nanoparticles mentioned below.^{32, 42, 43} These applications include using of AuNPs in:

- *Drug delivery*- AUNPS can do nano-drug delivery to difficult sites like brain, tumors, retina, and intracellular organelles.⁴⁴
- *Tumor detection and imaging of tumors*- AuNPs in different shapes can provide SERS signal using Raman tags on their surface. Coating of their surface with thiol modifying PEG, they can target tumors and their SERS signal can be detected..⁴⁵ The AuNPs accumulation in cancerous textures enhances the contrast in the imaging of the cancerous cells versus healthy cells.^{46, 47}
- *Using them as photothermal agents*- Because AuNPs absorb at the near infrared (NIR) region, they can be used to destroy tumor cells. This is due to the ability of NIR wavelength to penetrate human skin and tissue.⁴⁸
- *Gene therapy*- Owing to the facile surface modification of the AuNPs with DNA, AuNPs are used in gene therapy applications.⁴⁹
- *Radiotherapy dose enhancer*- The local deposition of the dose of the radiotherapy near the AuNPs and the greater cellular uptake of the tumor cells compared to the normal ones provides this feature of their application.⁵⁰

- *Bio-sensing in any form of optical, electrochemical, and immunological-* AuNPs LSPR sensitivity to the refractive index of its environment is the main reason for being able to apply them in any sensing applications. Furthermore, the controllable surface modification of AuNPs with peptides and glycans develop the detection biological assays for capturing antibodies in human serum.⁵¹ A recent review by Priyadarshini, *et al.* (2017) summarizes various bio-sensing applications of gold nanoparticles as sensors in calorimetric detection of toxic metal ions.⁵²
- *Toxic gas detection-* AuNPs are also used to detect the poisonous gases like the aggregation response of the AuNPs in absence of a toxic gas like H₂S and NO₂ and the disaggregation of them in presence of H₂S in an alkaline medium as the form of HS⁻ cause the AuNPs stabilization and prevent them from aggregation which cause LSPR redshift.⁵³

There have been many gold NP shape and size to improve the aforementioned applications' performance. AuNPs in different shapes from spherical to anisotropic shapes, including gold nanorods (AuNR)⁵⁴, gold nanocubes (AuNC)⁵⁵, gold nanoprisms⁵⁶, gold nanoflowers⁵⁷, and gold nanostars⁵⁸ have been reported. Sau *et al.* (2004) provided different structural architectures for AuNPs like rod, rectangle, hexagon, cube- triangle, and stars at high yields at room temperature.⁵⁹ Control the size and shape of the gold nanoparticles' crystal structure requires the knowledge of thermodynamic and kinetic parameters of their synthesis procedure. These parameters might be the additives concentration, thermal energies provided for different steps, light exposure and their combinations.^{60, 61 62, 63} The diversity of the shapes of the gold nanoparticles is the result of an interplay between the faceting inclination of the stabilizing agent, decreasing the surface energy of particular facet more than the others, and the speed of their growth which is kinetically controlled.⁶⁴⁻⁶⁶ The evolution of the synthesis of the gold nanoparticles from nanospheres toward

fancy anisotropic shapes like gold nanostars happened due to the higher wavelength of LSPR that anisotropic shapes could provide leading to a broader range of implementation of the AuNPs.⁶⁷

The anisotropic shapes of the gold nanoparticles provide the electron oscillation alongside different directions. For example, in gold nanorods (AuNR), longitudinal and transverse LSPR modes correspond with oscillation of the surficial electrons along the AuNRs larger and smaller axes, respectively. The aspect ratio of these axes defines the extinction peaks position on their UV-Vis spectrum.⁶⁸ The pointy shape of the AuNSs makes the electron oscillation along with their tips (central broad LSPR peak) as well as core surface (less intense peak at a lower wavelength). Figure 1.5 shows different LSPR that obtained from a spherical, rod-shaped, and star-shaped gold nanoparticles.^{68, 69}

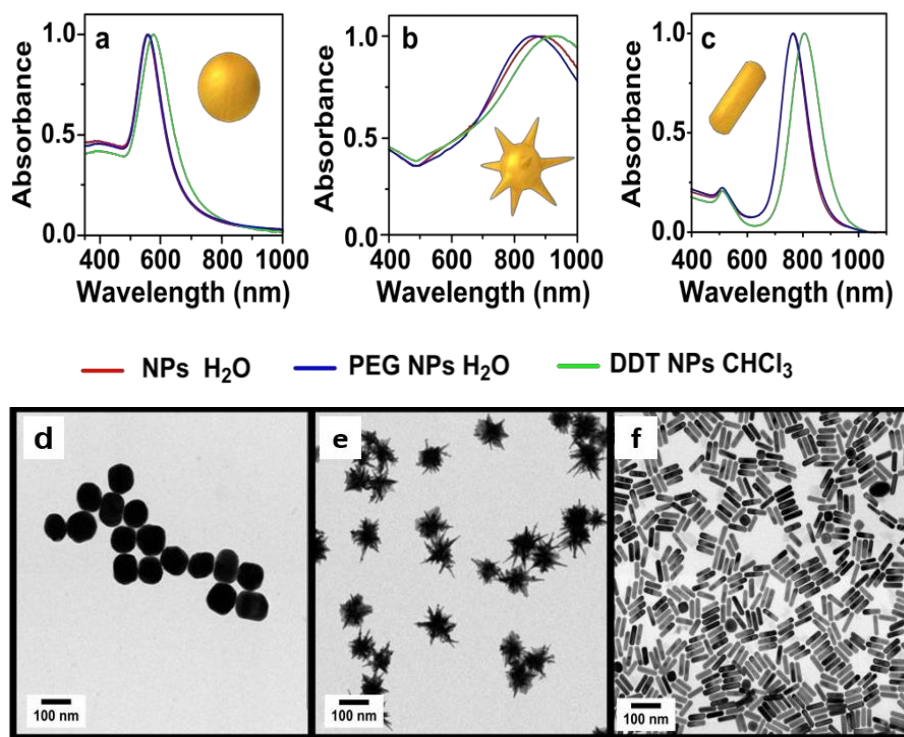


Figure 1.5. Extinction spectra of (a) spherical AuNPs, (b) AuNSs, and (c) AuNRs; and their corresponding TEM images for (d) spherical AuNPs, (e) AuNSs, and (f) AuNRs.^{68, 69}

Moreover, the gold nanoparticles not only exhibit unique features like the LSPR but also are easily functionalized with organic coatings, making them applicable in a variety of biomedical and sensing applications.⁵⁸

1.4 Synthesis of Gold Nanostars

In general, there have been several approaches to synthesis of AuNSs with narrow size and shape distribution with a special branching degree. These approaches include: ^{3, 70}

- Seed growth method- A method developed in the recent 15 years, which is also widely used for the synthesis of AuNRs and is the most common method of synthesis of the AuNSs. This method is based on the reduction of chloroauric acid with ascorbic acid in the presence of a surfactant. The surfactant used for growth solution usually has the same concentration as the surfactant used for the gold nano seeds stabilization.⁷¹
- Non “seed-mediated” methods- This method is usually a water-based synthesis technique, that unlike the seed-mediated approaches, is a direct method in which the nucleation and growth of the AuNSs’ arms are done at the same step. They trigger by addition of small quantity of silver nitrate to a solution containing the surfactant, reducing agent and gold precursor. Multi-spiked AuNSs formation doesn’t require preparation of the seeds.⁷²
- One-pot synthesis methods- The precursor solution is directly produced while the proper reducing agent and surfactant are both present, varying the reaction time and the reactant concentration in this method can produce the star-like shapes of gold nanoparticles.^{73, 74}

- Electron beam lithographic approaches- These expensive methodologies can be used for the fabrication of the AuNSs as a bottom-up procedure. The advantage of this technique is the production of the stars with controllable, sharp tips compared to other methods.^{75, 76}

Although beam lithographic techniques provide organized sharp tips surface features with the tunable LSPR, they are neither timely nor economically competitive with the chemical methods.⁷⁰ Among all the wet procedures available for the synthesis of the gold nanostars, the seed growth method is a robust way to get desirable size and shape of the AuNSs since it is based on a step-by-step enlargement method. The method is generally composed of two steps: seed preparation step, and growth step.⁵⁸ The use of surfactant as a capping agent in seed growth methods not only causes preferential adsorption on certain crystalline facets allowing anisotropic growth but also controls the formation speed of the spikes along with preferred directions on the surface of the particles. That produces the nanostars with the desired size and shape.²⁵ Using a mild reducing agent also plays a significant role in the formation of the arms of the AuNSs. Slow and mild reduction of the available gold ions on the surface of the seeds is controlled by using a mild reductant and certain concentration of the surfactant. Because of the choice of the surfactant, reagents, and reducing agent, their concentration, and the order they are added to the reaction yields yet different wavelengths of LSPR exhibited by the star-shaped gold nanoparticles.⁷⁷

The first synthesis of gold nanostars possessing a spherical core surrounded with pointy arms was inspired by the synthesis procedure of gold nanorods by a seed growth method. This synthesis was based on first making the seeds out of HAuCl_4 by adding NaBH_4 and subsequent reduction of gold on the gold seeds' surface using ascorbic acid (AA) in the presence of cetyltrimethylammonium bromide (CTAB) and silver nitrate (AgNO_3).⁷⁸

In this method, the formation of AuNSs due to modifying growth rate along specific crystallographic directions using CTAB as a capping agent besides adding silver nitrate at a different step. Comparing to the AuNRs, the AuNSs possess the advantage of a higher surface to volume ratio and a broad absorbance peak in the higher wavelengths.⁷⁹ During the synthesis, certain facets of the gold nanoseeds were blocked by the CTAB, the surfactant, and the silver ions. However, the CTAB toxicity, and the aggregation of the AuNSs during the washing steps, needed for surfactant removal limit this synthesis method's applications. Hence, several different protocols were developed to solve these problems and make the AuNSs candidates for the desired applications.

The NIR optical activity of AuNSs allows the excitation of them with NIR laser. NIR laser provides wavelengths at which light has its maximum depth of penetration in tissue. Therefore, AuNSs are better candidates among other shapes of AuNPs for bio-imaging, tissue-based assays, and therapies (like photothermal tumor ablation), drug-delivery applications.⁵⁸ A recent review by Mousavi *et al.* (2020) summarizes various applications of gold nanostars for diagnosis, bio-sensing, and biomedical applications.⁸⁰ Figure 1.6 (a) illustrates the application of AuNSs in SERS imaging of the lung cancerous cells of mice. Mice cancerous lung is imaged using SERS detection of the AuNSs. This imaging technique can be applied in chemotherapy of cardiovascular diseases.⁸¹ Also AuNSs embedded within tumors produce heat as a result of absorbing NIR laser irradiation, allowing selective cancer treatment. The small size of the AuNSs cause their facile penetration through the cancerous cells.⁸²

The targeted drug delivery using AuNSs is showed as a pictorial sketch of drug functionalized AuNSs releasing the drug from the surface of the nanoparticles to the target cell in exposing to the NIR laser irradiation.⁵⁸

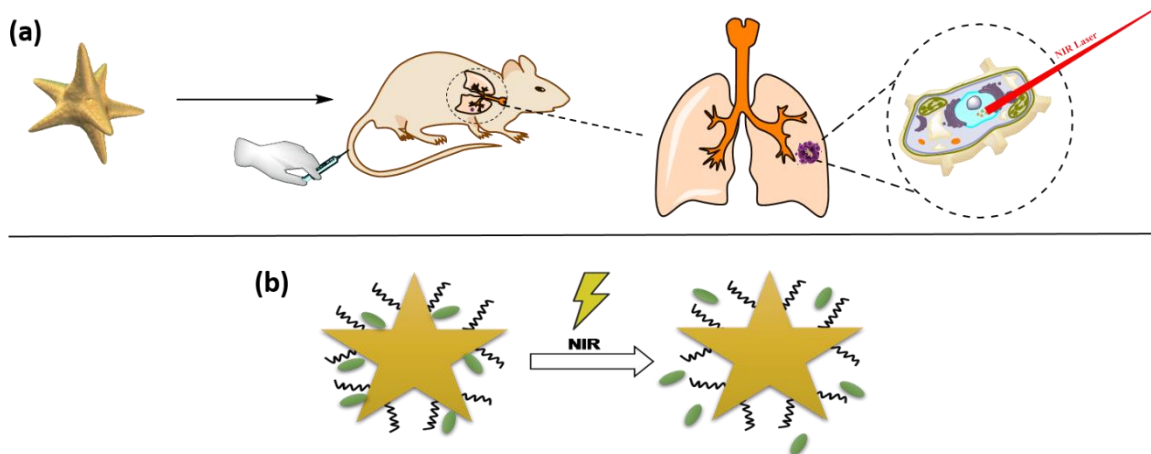


Figure 1.6. Schematic illustration of gold nanostars' applications (a) in photo tumor ablation-therapy, and (b) drug delivery using NIR irradiation.

1.5 Surface Modification of Gold Nanoparticles

The wide range of application of gold nanoparticles, especially AuNSs, the tunable LSPR optical properties of them, and the inertness of gold, all caused the importance of their surface modification. Proper surface modification of AuNPs ensures particle stability and aggregation-free modification of their surface.⁸³ Since the surface functionalization is mainly related to the property of the metal material, which is being functionalized, the surface functionalization and modification of AuNSs are similar to the other gold nanoparticles. Although, the high degree of anisotropy causes additional details on the assembly protocols.⁵⁸ One of the popular ways to functionalize the surface of AuNSs is the PEGylation of their surface. This method can stabilize the gold NPs due to the additional stability of polyethylene glycol under physiological conditions and bio-compatibility, both in-vitro and in-vivo.⁸⁴ Together with PEG, dyes, bio polymers, DNA, drugs, and antibiotics are the other desirable molecules for the functionalization of gold NPs.

The surface modification of the AuNPs via self-assembled monolayer (SAM) formation on the gold surface, which is the spontaneous deposition of an organic or biochemical molecule

on the gold surface, affords various applications. The organic molecule is usually an alkanethiol adsorbate that can deposit on the gold surface. The deposition can be done via a ligand exchange process. The SAM can be formed on both curved- and flat surfaces in the ambient conditions without the use of any complicated equipment.⁸⁵ The terminal group of the SAM molecules can bring the desirable modification of NP surfaces for various applications.⁸⁶⁻⁸⁸ Organic thin films on the nanoparticle surfaces are unstable in severe conditions such as heat, UV light or using harsh chemicals. This problem has been addressed in several ways, including using a bidentate thiol to provide better SAM stability on the surface of gold nanoparticles.⁸⁹ Figure 1.7 Shows the AuNPs different shapes, size, surface modification, and surface functionalization.⁹⁰

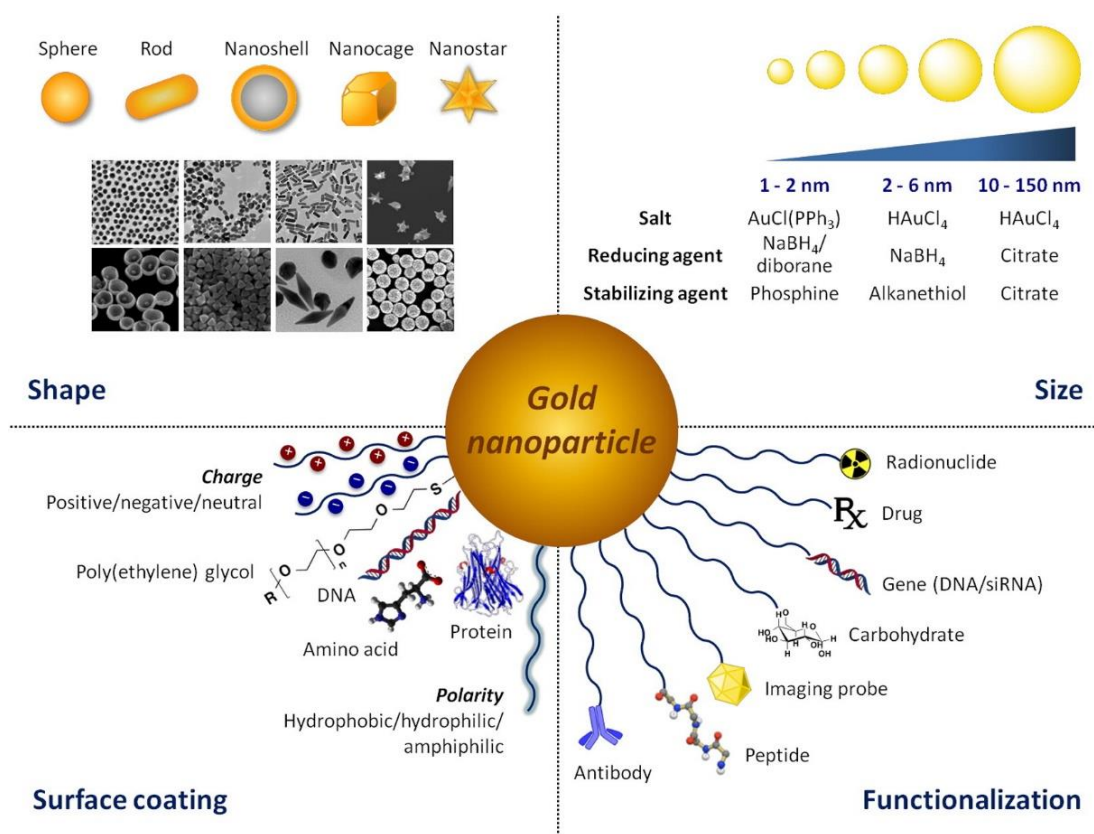


Figure 1.7. AuNP shapes, sizes, surface coating, and functionalization.⁹⁰

1.6 Application of Gold Nanoparticles in LFA

If the visual detection of the signal is desired on the LFA strips, colorful colloidal nanoparticles are used as reporters. The sensitivity of LFA can be improved by the use of gold nanoparticle reporters with different sizes and morphologies that can produce enhanced colorimetric signal intensity.^{32,91,92} Traditional spherical gold-based LFAs possess low sensitivity and higher limits of detection due to lacking sufficient brightness of the nanoparticles.² Plus, using these particles as reporters in LFA brings on “Yes/No” results. The human vision error is likely to happen in visual interpretation of the strips. To address these problems, several ways like applying a reader, silver or gold signal enhancement, dual AuNP-based signal improvement, and enzyme enhancements of the signal from LFA have been reported.³¹

- A reader that can couple with the strips and measure the optical density of the detecting lines, by converting the intensity to optical density (OD) helps to the quantification of the results. Previously it was thought that the measured OD of the test line depends only on analyte concentration. However, the immunoreaction-time and operation temperature are important, too. Later on, it was revealed that obtaining the ratio of OD of TL to OD of CL decreases of all the other parameters' effects but concentration and is a proper way of quantification.^{31,93}
- The signal amplification by modification of AuNPs is another way to offset the low sensitivity of the LFA using traditional AuNPs. For example, replacing pure AuNPs with gold nanocomposites intensifies the effect of dependency on the number of particles. Therefore, using a higher number of nanocomposites lead to darker purple color of TL and CL.⁹⁴ The use of spherical Fe_2O_3 nanoparticles covered by a shell layer of gold decreased the LOD three times in detecting

aflatoxin B₂ in food.⁹⁵ Later, researchers found that the use of other shapes of AuNPs will provide a significant impact on signal enhancement. Silica shelled AuNRs decrease the LOD, hence enhance the sensitivity of LFA toward the detection of proteins.⁹⁶ Multi-branched AuNPs, including AuNSs, have been even more sensitive reporters for their higher optical extinctions.⁹⁷

- The nucleation of gold or silver on the surface of AuNPs by reduction techniques cause the AuNPs to grow in size and that enhances their optical absorbance and improves LFA sensitivity. Using the gold enhancement method increase the signal to background ratio, thus reinforces the sensitivity of LFA by the aggravation of the calorimetric signal.⁹⁸
- The color intensity of the detection lines on LFA depends on the number of particles. Hence, increasing the number of particles used on LFA leads to intense line colors. This is the “dual AuNP-based signal improvement”. Huang *et al.* (2013) showed the improvement of the sensitivity of LFA to four times using this technique.⁹³
- Horseradish peroxidase (HRP), is one of the enzymes usually used in the signal improvement of biological assays and biosensors. The production and concentrated precipitation of an insoluble chromogen, which is the product of an enzymatic reaction, intensifies the color on the detection zones of LFA. HRP-AuNP dual reporters can lower LOD significantly in the detection of a synthetic DNA target.⁹⁹

1.7 Application of Gold Nanostars in LFA

On the contrary to the traditional colloidal gold nanoparticles with the spherical shape, multi-branched anisotropic gold nanoparticles have higher optical brightness. Besides, the stronger binding affinity of the anisotropic AuNPs to the targets due to their huge surface to volume ratio helps their higher capacity for antibody loading.² Among them, the ones with the longer tips boost the detection performance of all the immunochromatographic assays, including LFA, for the profound enhancement of the surface to volume ratio.¹⁰⁰ Thus, using AuNSs reporters is a promising solution for enhancing the sensitivity of LFA toward capturing different biomarkers.

Chapter 2. Gold Nanostars: Sensitive, Highly Capturable, Fast Reporters Improving Visual Limit of Detection of Lateral Flow Assays

2.1 Introduction

Lateral flow assays (LFAs) are point-of-care (POC) diagnostic tests. They fulfill all the ASSURED (Affordable, Sensitive, Specific, User-friendly, Rapid and robust, Equipment-free, and Delivered to the end-users) criteria of World Health Organization (WHO). LFA has been in the center of scientific research due to its commercial and easy usage. LFA has various applications in detection of different specimens, like toxins in agriculture, food, environmental monitoring, safety control, drug industry, medical diagnosis, and animals health.^{1,2} Although LFAs often lack desirable sensitivity or limit of detection (LOD) and give semi-quantitative results, they are still one of the most popular POC diagnosis methods because they are cheaper and more portable than traditional lab assays like enzyme-linked immunosorbent assay (ELISA) and quantitative polymerase chain reaction (q-PCR). This is for their fast, facile, and cost-effective implications, and therefore higher relative potential for wider deployability.^{3,4}

If the visual detection of the signal is desired on the LFA strips, colorful colloidal nanoparticles (NPs) are usually used as reporters for generating the diagnostic signal. Among the NPs, gold nanoparticles with different sizes and morphologies can produce enhanced colorimetric signal intensity to have an improved sensitivity of LFA.^{2, 18, 32, 92} Traditional spherical gold NPs-based LFAs as the reporters possess low sensitivity and higher limit of detection due to lacking sufficient brightness. On the contrary, multi-branched anisotropic shapes of the gold nanoparticles, like gold nanoflowers, gold nano popcorns, or gold nanostars have high optical brightness. Moreover, the anisotropic AuNPs have stronger binding affinity due to their larger

surface to volume ratio that helps higher capacity for antibody loading². Among them, the ones with the longer tips boost the detection performance of all the immunochromatographic assays, including LFA, due to the profound enhancement of the surface to volume ratio compared to the others.¹⁰⁰ Hence, using AuNSs that possess 5-6 long tips for each NP is one promising way for enhancing the sensitivity of LFA toward capturing different biomarkers. Gold nanostars yield such promising results toward detection of different analytes like model protein antigen Procalcitonin which showed to be 10 times more sensitive compared to conventional gold nanospheres.^{92, 101}

In general, the morphology of the particles has always been an effective approach to enhancement of the electromagnetic field, causing localized surface plasmon resonance (LSPR) peak position shifting.⁷⁰ Lin *et al.* (2019) studied the shape influence of different gold nanosystems, including nanostars, nanocubes (NCs), nanorods (NRs), and nanosphere on LFAs for detection of Bisphenol A. They found that nanostar possessed the lowest LOD which was about 80 pg mL⁻¹. They also showed that the LOD of AuNS < spherical AuNPs < AuNR and AuNC.¹⁰² Gold nanostars, in general, exhibit giant electron density localization at their tips, which is proportional to the number of the tips and aspect ratio of the branches. The longer the tips, the more considerable the electron density localization.¹⁰³ These optical properties play an essential role in LFA for the influence on the color they exhibit on the detection zone, and their shaped-depending coupling to the capturing antibodies plotted on the test-line and control-line.¹⁰² This LSPR effect was also used on some paper based surface enhanced Raman spectroscopy (SERS) tests.⁷⁰ SERS is an effective signal amplification method of the weak Raman through charge transfer and electromagnetic mechanism. The LSPR generated on the surface of nanoparticles, especially nanostars with the enhanced electric field on their tips and broad LSPR band, causes the

intense charge transfer from metallic AuNP's to the absorbing species on its surface. This technique can be used in sensing applications.⁷⁰ Therefore, SERS-based immunoassays detect the low-abundance biomarkers, with low concentrations.¹⁰⁴ For example, antibodies and gold particles can be used to quantify proteins in serum with high sensitivity and specificity. The experimental and simulations both showed the SERS enhancement factor follows the order of AuNS > AuNR > Spherical AuNP.¹⁰⁵

In most of the SERS coupled techniques, an expert SERS specialist, as well as a portable SERS reader, is required. SERS has been used to intensify the signal of the detection zone on LFA, too.^{3, 16, 70, 106} The detection of the biomarker is read out by the Raman signal of the reporter molecule. This is why the signal enhancement by the AuNPs, affects the sensitivity of LFA.¹⁰⁷ Although they are one of the most potent techniques when femtograms of the analyte are desired to be detected,²⁸, they hurt the cost-effectiveness and portable application of the LFA strips. Yan *et al.* (2018) used gold nanostars in a SERS improved LFA due to the high SERS sensitivity of the star-shaped gold nanoparticles by the strong electromagnetic field at their tips.²⁰ Xiao *et al.* (2018) converted a turn-off immunochromatographic assay (ICA) strip for Cd²⁺ ion detection based on quantum dots (QDs) to a turn-on mode ICA strip. They used AuNSs taking advantage of their optical properties and the overlapping of the AuNSs spectrum with the QDs fluorescence emission spectrum. This makes the AuNSs able to quench the signal of the QDs, a non-radiative energy transfer from the excited state of QDs to the ground state of AuNSs. Using the AuNSs could lower the LOD to 0.18 ng/mL for cadmium ion detection.¹⁰⁸ In a different study, Kimberly *et al.* (2017) used SERS coded gold nanostars, AuNSs coated with SERS molecules, as the LFA reporters on dipstick strips for a multiplexed strip diagnosing Zika and Dengue, mosquito-borne diseases, with LOD of 0.72 ng/mL and 7.67 ng/mL, respectively. They used 4-(2-hydroxyethyl)-

1-piperazineethanesulfonic acid (HEPES) to synthesize the gold Nanostars.³ Later, they functionalized the same gold nanostars with five different SERS tags on them to quantitatively evaluate the choice of reporters for multiplexed SERS. These SERS tags included 1,2-bis(4-pyridyl)ethylene, 4-mercaptobenzoic acid, 3,5-dichlorobenzenethiol, pentachlorothiophenol, and 5,5'-dithiobis(2-nitrobenzoic acid). These experiments were also done with the dipstick of Raman nanotags, or gold nanostars conjugated to the five reporters and anti-human IgG polyclonal.¹⁰⁹ Comparing different morphology of the gold nanoparticles in SERS signal enhancement, using 4-MBA and BPE (S-Propyl amine-L-cysteine) as their Raman tags on the nanoparticle's surface, they concluded that the sharp-possessing shapes like stars and semi like star particles having boosted electric fields on their tips have higher SERS enhancement factors.¹⁰⁷ In another study, silica-shelled AuNSs with the Raman tags sandwiched in between the silica and gold were used for the development of a SERS based LFA exhibiting superiority compared to its similar calorimetric detection in terms of sensitivity and LOD in a blood plasma-containing sample matrix. The same assays used for neuron-specific enolase (NSE) detection, a traumatic brain injury (TBI) protein biomarker, in diluted blood plasma samples, showed LOD of 0.86 ng/mL.¹⁰⁶ All of these works show highly enhanced sensitivity of LFA. The final goal of the commercialization use of the strips is using robust and user-friendly procedure for the end-users as the home diagnosis test or in general providing simple one-step on-site decision making. Therefore, it is highly desired to provide a technique free of specific help-sheets inside the kits.

Sometimes, an additional step after running the strips, such as gold enlargement or silver enhancement techniques have been applied to enhance the color of the line on the detection zone of the nitrocellulose (NC) membrane like the recent studies by Patferov *et al.* (2018).^{13, 110} In this technique, the performed LFA strips' membrane is immersed in enhancement gold or silver

solution, and is incubated there. The disadvantage of all the mentioned techniques is also the requirement of an additional step in the running of the assays, which makes the procedure more complicated and the LFAs, if becoming commercialized, require to be accompanied with sophisticated directions and methods of use.

In many of the cases of using AuNSs on LFA, one of the problems coming in the design of the gold reporters is the need for the removal of the surfactant used in their synthesis. The elimination of the surfactant is needed for their thiol based self-assembled monolayer (SAM) functionalization. SAM functionalization readies the particles for further conjugation to biomolecules, such as antibodies³² and finally for sensing application.⁷⁰ In most of the cases, the surfactant elimination needs sequential centrifugation and washing steps that can cause irreversible aggregation of gold NPs.^{91, 111} Aggregation causes a change of optical properties of AuNPs. Hence the effective particle size, shape, and dielectric environment will not be the same as the non-aggregated form of the AuNPs.¹¹² This decreases reproducibility of the assays. Furthermore, the aggregation of the particles cause the reporters to have different masses and so particles' rate of flow on LFA that enhances the nonspecific binding on the detection zone. To address this problem, different methods like following a chemically surfactant-free synthesis method³, coating the particles with silica shells³², controllable assembly of the AuNPs¹¹³, or applying either dialysis instead of ultrafast centrifugation techniques¹¹⁴ or size exclusion chromatography¹¹⁵ have been used. In many cases, however, the surfactant-free techniques may not provide the monodisperse nicely shaped particles, and may adversely affect the AuNPs' properties. For gold nanorods (AuNR) which are the ancestors of the anisotropic AuNPs, there have been many papers addressing this issue. Some of these attempts tried to synthesize AuNRs in the presence of the surfactant and do controllable assembly, to have desirable functionalized

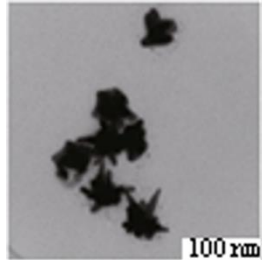
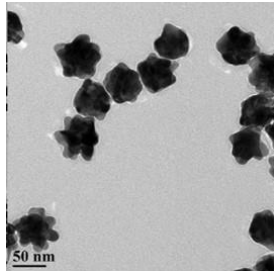
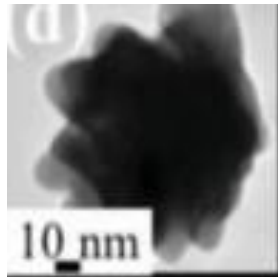
monodispersed particles.^{91, 111, 113} However, for anisotropic AuNPs especially AuNSs, according to our information, nothing other than either taking a surfactant free synthesis⁹² or silica coating after a surfactant-included synthesis have been suggested¹¹⁶ for having the AuNSs ready for bioconjugation and sensing applications.

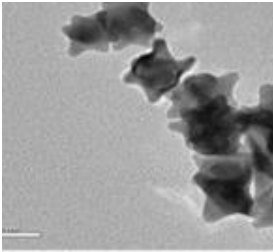
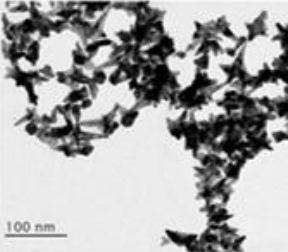
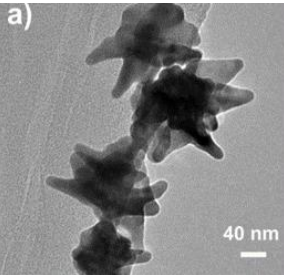
Although the surfactant-free syntheses of AuNSs have been reported,^{117, 118}, they are lacking the advantages of using surfactant-based growth techniques of the gold nanostars. Surfactant provides a longer time for AuNS arm formation and, therefore, produces stable, aggregation-free, and organized spikes, which are required and desirable features to run them in many sensing applications, especially LFA.

To compare the previous studies that used AuNSs as reporters in LFA in a glance, they are summarized in table 2.1. In our study, we reported a simple, unlike SERS or Ag/Au enhancement methods, point of care diagnosis method able to reach low LOD, by using gold nanostars for the detection of hCG. However, our technique solved most of the problem mentioned above by using a modified procedure found in the literature using Triton X-100 as surfactant⁹², which causes the homogeneous production of AuNSs. We also systematically functionalized the AuNSs in the presence of the surfactant using a ligand exchange method with a highly stable organic molecule on the gold nanoparticles' surface¹¹⁵ prohibiting the aggregation of the particles followed by an active bioconjugation of the antibodies using EDC/Sulfo-NHS chemistry. The gold nanostars used in this study decrease the LOD of LFA owing to their capturability and high optical sensitivity due to their LSPR. The EDX-TEM and XPS data provided in this manuscript show the existence of silver mostly on the AuNSs surface since the elemental percentage of silver is higher according to XPS data as a surface technique comparing to TEM-EDX. The silver, mainly on the surface, simplifies visual detection. This result is in accordance with previous studies by Atta *et al.* (2019)

that showed the role of AgNO_3 concentration on these Triton-X-100 stabilized AuNSs characterization data. They concluded that silver deposits mainly on the core and between the bases of neighboring spikes.¹¹⁹ This feature of these AuNSs causes independency on any additional silver enhancement method as a signal amplifying method.

Table 2.1. Summary of AuNS-based LFAs used for sensitivity enhancement

Detection Technique	Target Analyte	LoD (pg/mL)	Ref. Year	Microscopic Image
Silver-enhanced colorimetric detection	Procalcitonin	50	[92] ⁹² 2018	
SERS enhanced using 4-aminothiophenol as Raman reporters	Bisphenol A	73	[70] ⁷⁰ 2013	
Colorimetric –Visual	Bisphenol A	80-530	[102] ¹⁰² 2019	

Competitive assay:				
immunochematographic strip	Cd ²⁺	180	[108] ¹⁰⁸ 2017	
SERS based detection LFA	Zika and Dengue biomarkers	720 and 7620	[3] ³ 2017	
SERS based detection LFA	neuron- specific enolase (NSE)	860	[106] ¹⁰⁶ 2017	

In this study, illustrated in Figure 2.1 the influence of the morphology of the stars on the sensitivity and LOD of the LFA toward human chorionic gonadotropin (hCG) hormone was compared to the commercial 40 nm gold nanospheres, as the typical sensitive reporter.

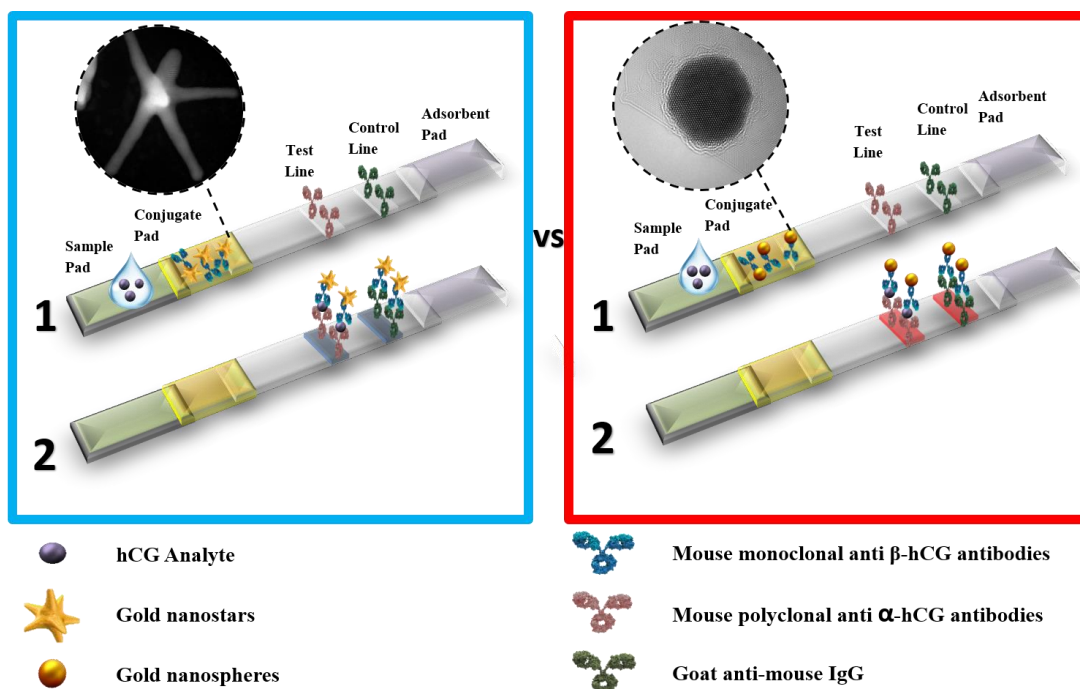


Figure 2.1. Schematic representation of gold nanostars lateral flow assay and gold nanospheres lateral flow assay.

2.2 Materials

Triton X-100, tetrachloroauric acid (HAuCl_4), sodium borohydride (NaBH_4), ascorbic acid (AA), silver nitrate (AgNO_3), 4-mercaptobenzoic acid (4-MBA), 1-Ethyl-3-(3-dimethyl aminopropyl) carbodiimide (EDC), Phosphate-buffered saline (PBS-1X), and N-hydroxysulfosuccinimide (Sulfo-NHS) were purchased from Sigma-Aldrich and used without further purification.

Mouse monoclonal anti- β hCG antibodies (#ABBCG-0402), goat polyclonal anti- α hCG antibodies (#ABACG-0500), and goat polyclonal anti-mouse IgG antibodies (#ABGAM-0500) were purchased from Arista Biologicals (Allentown, PA). Anhydrous ethanol (EtOH) was purchased from Decon Lab, Inc. Deionized water (18 M Ω -cm at 25 °C; Milli-Q *Direct*, Millipore Corporation, Billerica, MA) was used for the preparation of all solutions. All of the glassware used was cleaned in aqua regia solution (3:1 HCl:HNO₃), rinsed with DI water and acetone, and dried in an oven at 90 °C and cooled to room temperature before use. Whatman FF80HP, used as nitrocellulose membrane, and Whatman CF 5, used as adsorbent pad, were both purchased from GE Healthcare. The adhesive card (MIBA-020) used on the LFA strips was purchased from DCN Diagnostics. Colloidal 40 nm gold nanospheres conjugated with β -hCG mAb CGC, clone 2 (#CGBCG-0702) were purchased from Arista Biologicals. Polyethylene glycol (PEG) 20000, potassium carbonate, hydroxylamine, sodium azide (NaN_3), Tween 20, and bovine serum albumin (BSA) were from Sigma-Aldrich, and the Zeba Spin Desalting columns 7K MWCO were from Thermo scientific and used following its accompanying protocol.

2.3 Apparatus and Methods

The images of the obtained AuNSs were created using an LEO-1525 scanning electron microscope (SEM) operating at an accelerating voltage of 15 kV. All SEM samples were deposited on a silicon wafer. For improved resolution, the AuNSs were also evaluated using a high-resolution transmission electron microscope using a Thermo Scientific Themis Z with probe corrector at 300kV. (HRTEM) at an accelerating voltage of 200 kV at different magnification from 100k to 800k. The TEM samples were deposited on 300 mesh carbon-coated copper grids on which the sample was deposited in the aqueous form. All samples were dried overnight, at room temperature, after placing a drop of the diluted sample on 300 mesh holey carbon-coated copper grid.

2.4 Spectroscopic Techniques

UV-Vis spectra were taken on Cary 50 instruments, using quartz cuvettes (1 cm). Energy-dispersive X-ray spectroscopy (EDX) data were collected by an EDX attached to the TEM instrument in order to investigate the local chemical composition of the functionalized AuNSs using Super-X EDS detector on Themis Z HRTEM. X-ray photoelectron spectroscopy (XPS) data were collected using a PHI 5700 XPS equipped with a monochromatic Al K α X-ray source. To prepare all the XPS samples, a highly concentrated aqueous sample of the AuNSs was collected after centrifugation. The concentrated pellet was dropped on a copper-tape-covered slide of silicon wafers, followed by drying overnight in a vacuum desiccator. Prior to the sample preparation, the slides were washed with Milli-Q water and ethanol several times then dried with nitrogen gas. Extinction spectra were obtained using a Cary 50 scan UV-Vis spectrometer.

A Malvern Archimedes Particle Metrology System (MAN0580-03-EN-00) was used for particle mass and size distributions with particles suspended in anhydrous ethanol. The concentration of the colloidal solutions of AuNSs was determined using dilute sample concentrations in deionized water using a NanoSight NS300 (Malvern) with programmable Nanoparticle Tracking Analysis (NTA) software. Nanodrop ND-1000 (Thermo) was used for the optical density (OD) measurements of colloidal solutions and protein concentration measurements. Nuclear magnetic resonance (H-NMR) spectra were collected using JOEL ECX-400 and ECA-500 spectrometers operating at 400 MHz and 500 MHz, respectively. The solvent used was deuterated chloroform (CDCl_3), and the spectra were referenced to δ 7.26. Leelu Reader (Lumos diagnostics) used for the reading of the strips.

2.5 Synthesis of Gold Nanostars

AuNSs were prepared with the seed-mediated growth method as described by Pallavinci *et al.* (2013).¹²⁰

2.5.1 Preparation of Gold Nanoseeds

5 mL of a 0.5 mM HAuCl_4 solution was added to 5 mL of a 100 mM aqueous solution of Triton X-100. 600 μL of a 10 mM NaBH_4 solution was added to form the gold nanoseeds solution, which is stabilized in Triton X-100.

2.5.2 Preparation of Gold Nanostars Growth Solution.

The growth solution was prepared by the addition of 280 μL of a 4 mM AgNO_3 solution and 5 mL of a 1 mM HAuCl_4 solution to 5 mL a 100 mM aqueous solution of Triton X-100. Then,

300 μ L of a 0.08 M ascorbic acid solution was added to the mixture at room temperature. The solution was left under stirring conditions until the solution became colorless.

2.5.3 Preparation of Gold Nanostars

12 μ L of prepared gold nanoseeds solution was added to the as-prepared growth solution. The mixture was mixed at room temperature under stirring conditions until it turned blue. The tips of AuNSs were grown by storing the solution in subdued lighting for 8 h. Incubation time can be varied to obtain different sizes of AuNSs.

2.6 Organic Synthesis of the Linker BMPHA and SAM Functionalization of Gold Nanostar

In order to create a framework on the AuNSs surface suitable for bioconjugation, we functionalized the surface of the AuNSs with a SAM composed of a mixture of two thiol-based adsorbates; a custom-designed bidentate dithiol, 16-(3,5 bis (mercaptomethyl) phenoxy) hexadecanoic acid (BMPHA) and 4-mercaptobenzoic acid (4MBA). BMPHA was reproduced following a slightly modified procedure we previously reported.⁸⁹ The scheme of the synthesis, including modifications, is shown in Figure 2. 2. The H-NMR spectroscopy results of BMPHA (Figure A.1) are reported in Appendix confirm its high purity.

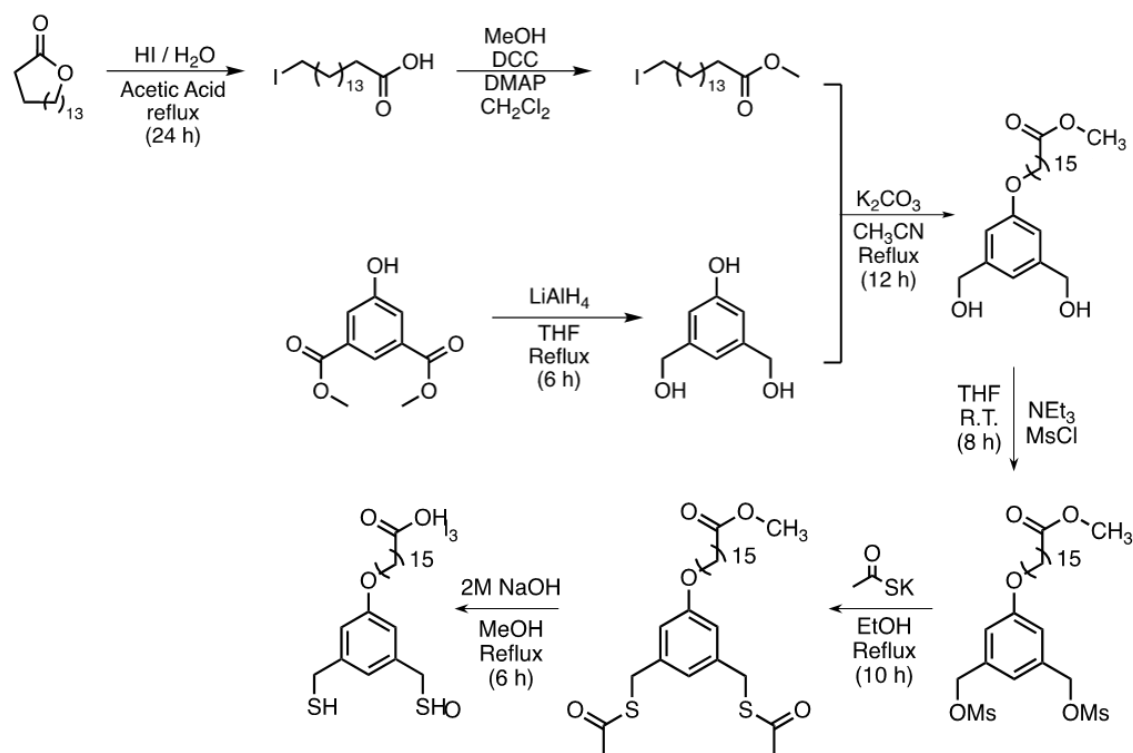


Figure 2.2. The synthesis procedure of BMPHA

2.7 Thiolate- Functionalization of the Gold Nanostars

A self-assembled monolayer (SAM) of BMPHA (16-(3,5bis (mercaptomethyl)phenoxy) hexadecanoic acid) was formed on the surface of the AuNSs by preparing 4.5 ml of a 10 mM ethanolic solution of BMPHA and adding it into the 10 ml of Triton X-100 stabilized gold nanostars. The obtained solution was stirred in the dark overnight. Then 1.4 ml of 18 mM ethanolic solution of 4-mercaptobenzoic acid (4-MBA) was added to fill in the gaps on the surface of the AuNSs. The mixture was left overnight while being stirred. The SAM-coated AuNSs were centrifuged three times to remove the excess BMPHA, 4-MBA, and surfactant. The centrifugation speed plays a significant role since the speeds higher than 3000 g of centrifugation cause irreversible aggregation. Initially, the solution was centrifuged at 2000 g for 15 minutes. The

supernatant was discarded, and a mixture of ethanol and water (1:3, molar ratio) was used to wash the particles. A few drops of 0.1 M NaOH were then added to the colloidal solution of the particles to ensure a negative charge on the SAMs and to avoid particle aggregation. The solution was sonicated for 2 minutes, then centrifuged at 1800 g for 10 minutes. The particles were then redispersed in water. A few drops of NaOH were added again to provide basic pH for the solution. The final centrifugation was done at 1600 g for 7 minutes. The particles were redispersed in 5 mL water and were centrifuged at 2000 g for 5 minutes. The supernatant was removed, and 2.4 ml of 0.02 mM potassium carbonate (pH=9) was added to the pelleted particles, and the solution was sonicated for 30 seconds in the bath sonicator at room temperature. The AuNS particle suspension was stored at refrigerator at 4 °C with $OD_{800} = 3.5$ (optical density at $\lambda=800$ nm) was stable for months until further use without additional purification.

2.8 Bio-Functionalization of Gold Nanostars with Antibodies

The SAM-functionalized AuNSs were bioconjugated with mouse monoclonal anti- β -hCG antibodies using carbodiimide chemistry. 400 μ L of 10 mg/mL ethyl (dimethyl aminopropyl) carbodiimide (EDC) solution and 800 μ L of 10 mg/mL sulfo-NHS solution were added to 2.4 mL of AuNSs ($OD_{800} = 3.5$) to form a final mixture with pH=5, checked by pH paper (This proportions of EDC and NHSS provides this pH). This solution was vortexed and incubated, protected from light, for 30 minutes while rotating at room temperature. The solution was then centrifuged at 2500 g for 5 minutes, and the supernatant was removed. 1 mL of 5 mM potassium phosphate buffer at pH= 7.4, including 0.5% PEG MW 20,000 was added to the pellet. The mixture was vortexed and sonicated for 40 seconds ($OD = 3.5$ in 10mm path length). 48 μ L of 1 μ g/ μ L mouse monoclonal anti- β -hCG antibodies (buffer- exchanged using a Zeba column in 10 mM potassium phosphate pH= 7.4) were added to the sulfo-NHS functionalized AuNSs and vortexed.

The mixture was incubated in an aluminum-wrapped micro-centrifuge tube while rotating in a rotator at room temperature for 1 hour. Then, 20 μL of 50% w/v hydroxylamine was added to the solution to passivate the AuNSs and the mixture was incubated for additional 15 minutes. After incubation, the particles were pelleted by centrifugation at 2500 g for 5 minutes, collected, resuspended at 1 ml of potassium phosphate buffer pH=7.4. The procedure was repeated two more times. The solution was centrifuged at 2500 g for 5 minutes, three times. The potassium phosphate buffer at 5 mM was used for rinsing the particles. After the third time centrifugation, 1 ml of 0.1X PBS pH=8 containing 0.05% sodium azide and 0.5% Tween 20, and 0.5% bovine serum albumin (BSA) was added to the pellet. The mixture was vortexed and sonicated for 40 seconds in a bath sonicator to thoroughly resuspend the particles. The particles were stored at 4 °C until further use.

2.9 Assembling Half Strips (Dipsticks)

The nitrocellulose membrane (length 3.8 cm) adhered to polyvinyl chloride (PVC) backing. CF5 absorbent pad (length 2 cm) was attached with an overlap of 2 mm. The antibodies (goat polyclonal anti- α -hCG and goat polyclonal anti-mouse IgG antibodies for the control line and test line, respectively) were diluted in PBS 1X to a concentration of 1 $\mu\text{g}/\mu\text{L}$. A BioDot XYZ3060 was used to dispense the antibodies (at 1 $\mu\text{g}/\text{cm}$) to form the test and control lines, each with 30 μL (the distance between the two lines was 15 mm; the control line was placed 6mm from the top of the strip). The striped membrane was initially dried at 37 °C for 20 minutes and then further dried at RT in a desiccator overnight. The assembled LFA materials were cut using a ZQ2000 Guillotine Cutter (Diagnostic Tech Co., Shanghai, China) into 3 mm wide LFA strips.

Running the LFA Tests

In this study, hCG was used as a model analyte for the comparative study of LFA with 40 nm gold AuNPs (spheres) and 70 nm gold AuNSs (nanostars).

Human chorionic gonadotropin protein (hCG) was diluted in PBS at 0.010, 0.025, 0.125, 0.250, 0.625, and 6.25 ng/mL. Then, 6 μ L of each sample was added to 18 μ L LFA buffer (PBS 1X containing 1% PEG 3350, 1% BSA, and 0.5 % Tween 20) and 6 μ L (5×10^8 AuNSs particles or 10^9 spherical AuNPs, measured by Nanosight) of anti- β hCG-AuNS conjugates in microcentrifuge tubes. The samples were vortexed and centrifuged for a few seconds. Then the half strips were dipped inside the tubes. The final hCG concentration in the samples were 0, 0.002, 0.005, 0.025, 0.050, 0.125, and 1.25 ng/mL. All samples were analyzed in duplicate. When all of the mixtures has wicked into the nitrocellulose membrane (~7 minutes), the LFA strips were washed twice with 50 μ L of LFA buffer (PBS 1X containing 1% PEG 3350, 1% BSA, and 0.5 % Tween 20).

The brightness of the test and control lines was detected after 10 minutes from the last washing step using the Lumos Leelu LFA reader (red light source, 5.2 ms exposure time for AuNSs, and green light source, 5.2 ms exposure time for AuNPs).

We varied the amount of the antibody used for particle functionalization (12, 24, 36, 48, and 60 μ g 850 μ L of the AuNS at OD=3.5. We observed the trend exhibited by 1 μ L to 7 μ L of the gold nanostar conjugates in 30 μ L total volume of the sample using our LFA buffer (PBS 1X containing 1% PEG 3350, 1% BSA, and 0.5 % Tween 20).

2.10 Characterization of Gold Nanostar Reporters

Gold nanostars, popular for the extraordinary optical properties and providing low limit of detection^{2, 3, 92, 101}, were chosen for LFA sensitivity enhancement studies alongside gold nanospheres, as the typical gold nanoparticle reporters in their optimized size.

We obtained the extinction spectrum, shown in Figure 2.3, to evaluate the optical properties of the AuNSs. The AuNSs show intensive blue color (strong absorption at 500 nm) and exhibit a broad peak at 1100 nm due to the electron oscillation occurring alongside the aligned branches of the neighboring particles and the longitudinal LSPR.¹²¹

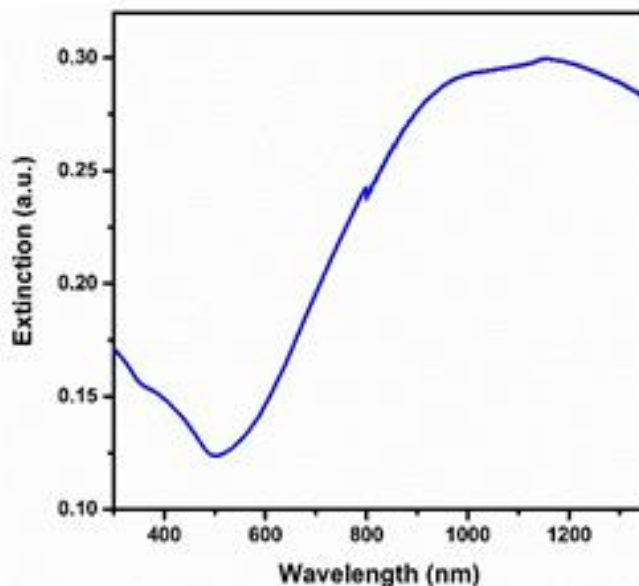


Figure 2.3. Extinction spectra of the synthesized SAM-functionalized AuNSs.

The morphology of the AuNSs was assessed with scanning electron microscopy (SEM), Figure 2.4, and transmission electron microscopy (TEM), Figures 2.5 (a), (c), and (e). According to the SEM and TEM images, the synthesized AuNSs were ~75 nm in diameter (measured from

a tip to the opposite tip), possessing sharp tips. Moreover, these star-shaped particles consist of a spherical core with a diameter of about 20 nm covered by 25-30 nm long tips.

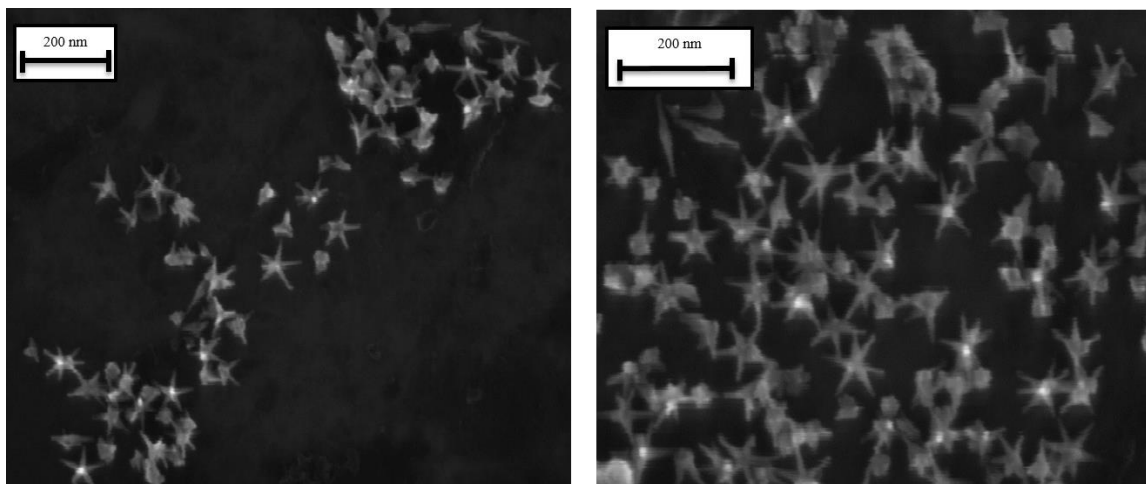


Figure 2.4. SEM images of the AuNSs.

The Nanosight results taken for the gold nanostars confirm their hydrodynamic size distribution. (Figure 2.8.a). The median hydrodynamic diameter of the AuNSs after functionalization with the antibodies is 105 nm. The SEM and TEM results that show the average size of 75 nm for the gold nanostars, themselves. The specific feature of these stars is their more-than-6 sharp branches, which cause their unique absorption peaks due to the different possibilities of the electron oscillation on their surface. Figure 2.5. shows the AuNSs' X-ray diffraction patterns on the right side corresponding to its TEM picture on the left side. (b), (d), and (f) is the diffraction patterns produced by (a), (c), and (e); the AuNS image obtained by TEM. Figure 2.6. shows the high-resolution TEM images of the stars. The rows of the atoms show that the gold atoms form a face-centered cubic (FCC) crystal structure. Figure 2.7. shows (a) TEM image of one arm of AuNSs, (b) the sulfur, and (c) the gold abundance along the drew line perpendicular to it measured by EDX-TEM. As it can be seen through the scanning align the line, the abundance

of Sulfur atoms is highest on the edges and the gold abundance reaches its max in the middle of the tips.

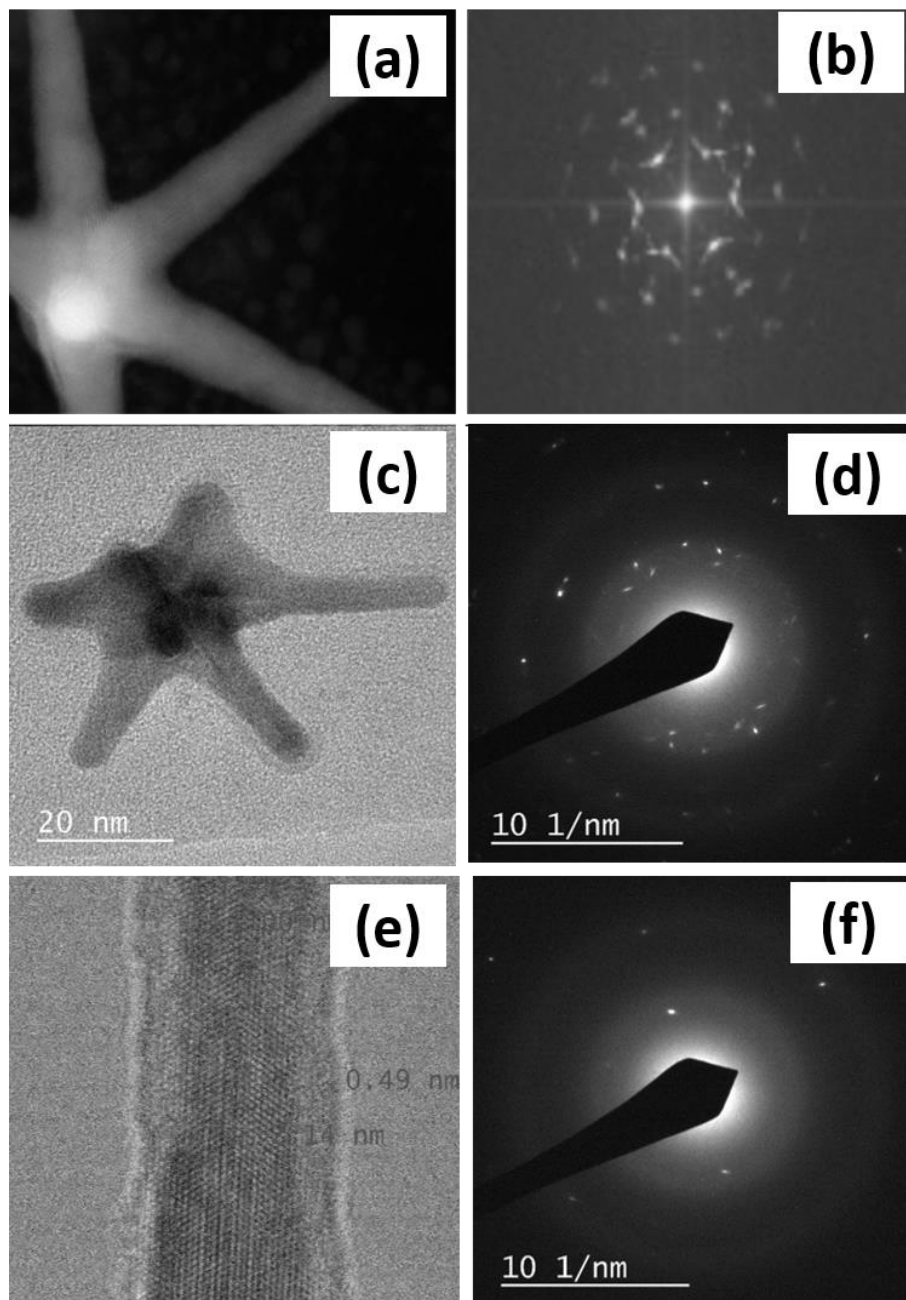


Figure 2. 5. (a), (c), (e) TEM images of the AuNSs and (b), (d), (f) their corresponding X-ray diffraction pattern

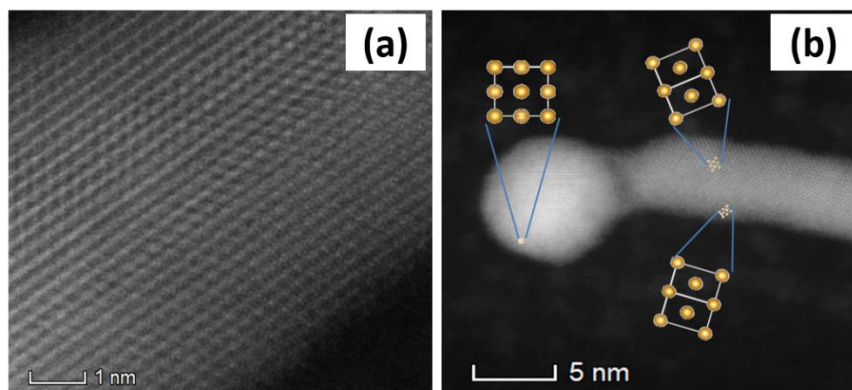


Figure 2.6. (a), (b) TEM images of the AuNSs representing gold face-centered cubic (FCC) structure

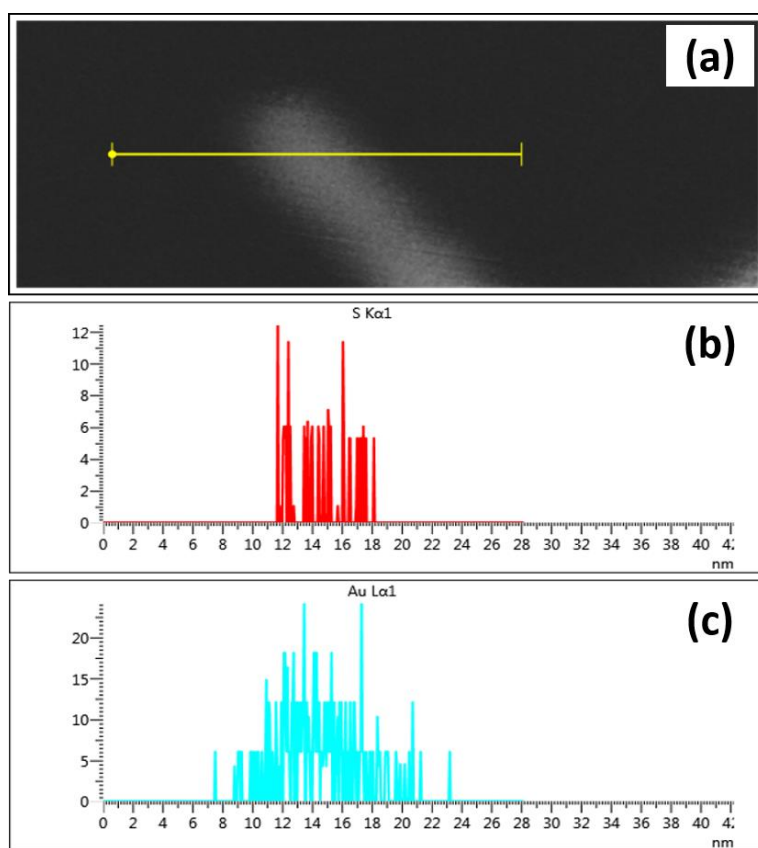


Figure 2.7. (a) TEM image of one arm of AuNSs, (b) the sulfur, and (c) the gold abundance along the drawn line perpendicular to it measured by EDX-TEM.

Nanosight for the antibody conjugated AuNSs figure 2.8 (a), and Archimedes data for BMPHA functionalized AuNSs (figure 2.8 (b)) were obtained to measure the concentration, size, mass, and distribution of the AuNSs. Figure 2.8.b shows the result of Archimedes, which is matched with the expectation for the Gaussian shape of the graph. Though, the mean < 75 nm is due to the assumption of the Archimedes machine, which considers spherical shape for the particles. Therefore reporting the size less than expected.

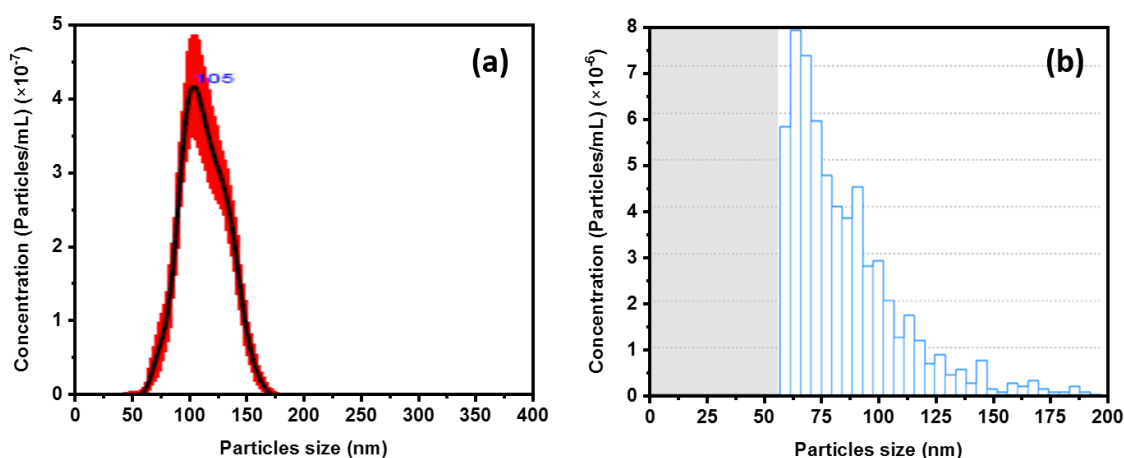


Figure 2.8. Particle size distribution results of the AuNSs measured by (a) Nanosight and (b) Archimedes microchannel resonator; median=62 nm, mean=84 nm, and standard deviation=28 nm. The Nano-chip used in Archimedes could not sense the particles with the size of <50 nm.

The SAM-functionalized AuNSs were analyzed with a Fourier-transform infrared spectrometer (FT-IR) to confirm the presence of the monolayer. As shown in Figure 2.9, the IR spectra of BMPHA exhibit a major peak at 3320 cm^{-1} that corresponds to the O-H stretching of the carboxylic acids. The C=O stretching of the carbonyl group appears at 1697 cm^{-1} , and the C-H stretching of the methylenes of the alkyl chains at 2922 cm^{-1} and 2864 cm^{-1} . For the 4-MBA, the C=O stretching of the carbonyl group appears at a lower wavelength number ($\sim 1667\text{ cm}^{-1}$) compared to BMPHA due to the resonance. To understand how the mixture of the BMPHA and

4-MBA affects the peak shifts, the mixture of BMPHA:4-MBA (1:3 ratio) was also measured with the IR spectroscopy. The result indicates a similar pattern of the peak position of each individual compound from BMPHA and 4-MBA. When compared to the mixture on the gold nanostars, all the peak positions match. This data confirms the presence of the mixture of BMPHA and 4-MBA on the gold nanostars.

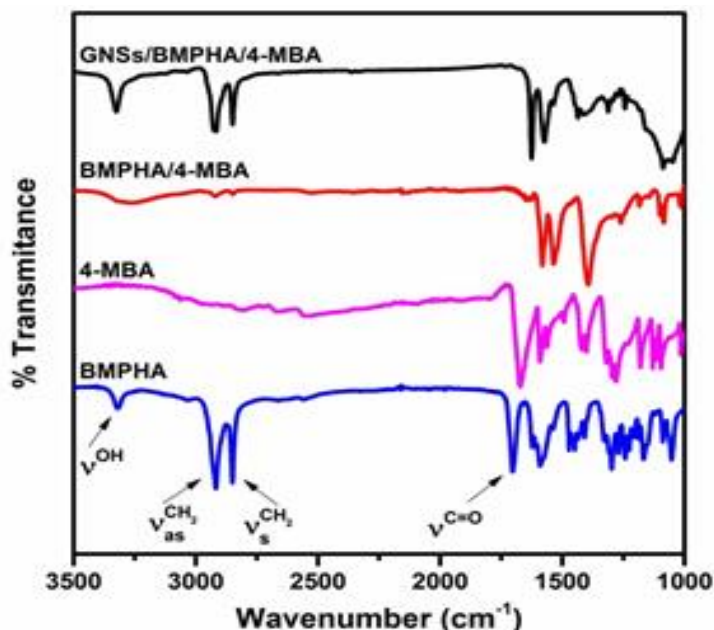


Figure 2.9. FTIR spectra of BMPHA (blue), 4-MBA (purple), the mixture of BMPHA/ 4-MBA (1:3) (red), and the SAM-functionalized AuNSs (black).

Elemental analysis of the SAM-functionalized AuNSs was performed by X-ray photoelectron spectroscopy (XPS). Data obtained by XPS will allow both the assessment of the elemental composition and the identity of the atoms present in the sample. The XPS spectra for the Au (4f, S 2p, C 1s, and Ag 3d regions) are shown in Figure 2.10. The Au 4f spectrum confirms the sample is composed of gold and is used as a reference. Previous studies have established a bound thiolate on gold to produce a doublet in the S 2p region, S 2p_{3/2} and S 2p_{1/2}, with binding energies of 162 and 163.8 eV, respectively, in a 2:1 ratio (S 2p_{3/2}:S 2p_{1/2}).¹⁰¹

For the SAM-functionalized AuNSs, the S 2p region exhibits a broad doublet with a binding energy of ~ 162 eV. However, the $\sim 1:1$ ratio of the peaks indicates a mixture of bound and unbound thiols on the surface. Moreover, the absence of a peak at 169 eV is indicative of a surface free of highly oxidized sulfur species and, therefore, no oxidized sulfur on the surface³⁵. Deconvolution of the S 2p peak revealed $\sim 56\%$ bound thiols. Furthermore, the C 1s region exhibits two peaks, a prominent peak at ~ 285 eV, characteristic of the CH_2 units of the adsorbates, and a small bump at ~ 289 eV, corresponding to the carbonyl carbon. (The deconvolution graph and the summary of its results is shown in Figure 2.11). Ag 3d existence as the element is related to the mechanism of the stars formation that suggests the creation of a silver layer on the surface of the particles.

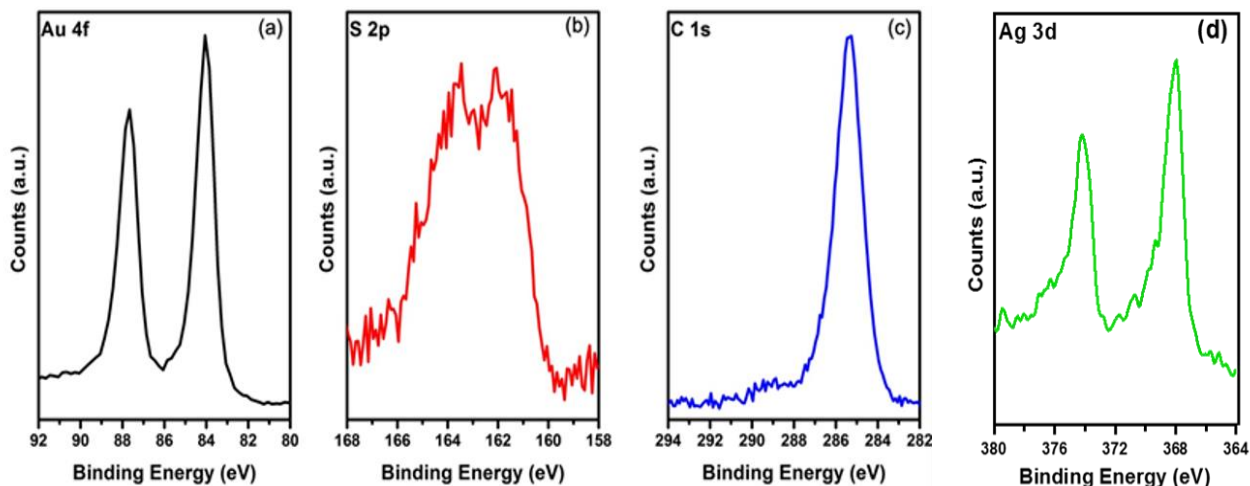


Figure 2.10. XPS spectra of the SAM-functionalized AuNSs in the (a) Au 4f, (b) S 2p, and (c) C 1s, and Ag 3d (d) regions.

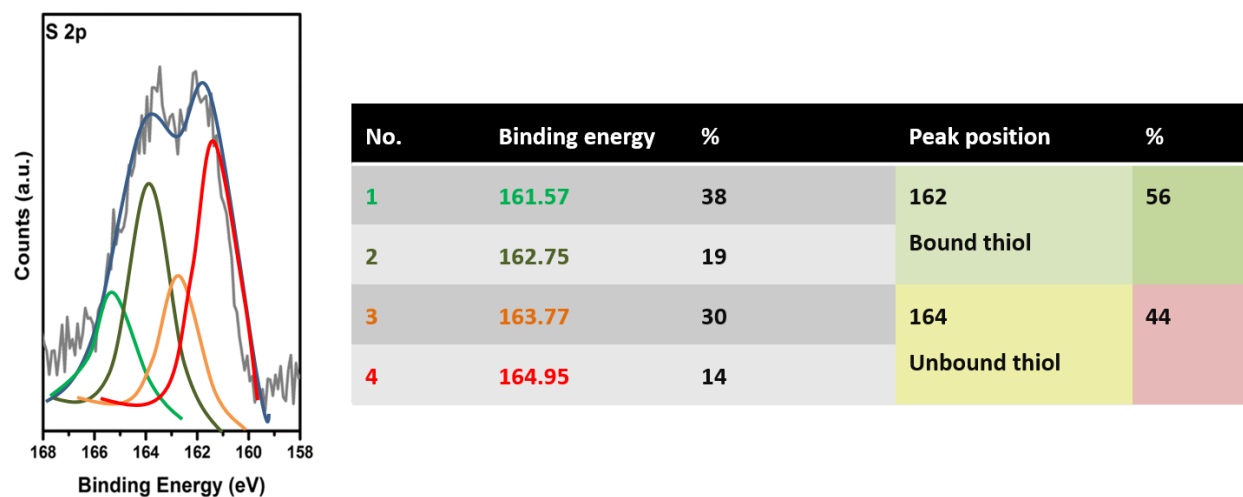


Figure 2.11 Deconvolution of S 2P peak of XPS of the AuNSs and its correlated bound and unbound thiol percentage

The elemental analysis of the SAM-functionalized AuNSs was done by Energy-Dispersive X-ray spectroscopy (EDX) coupled with the TEM. The EDX-TEM data (Figure 2.12) mapping indicates the presence of gold as the main element, and sulfur and silver. The elemental percentage analysis by XPS and EDX confirms the existence of SAM molecules in our samples.

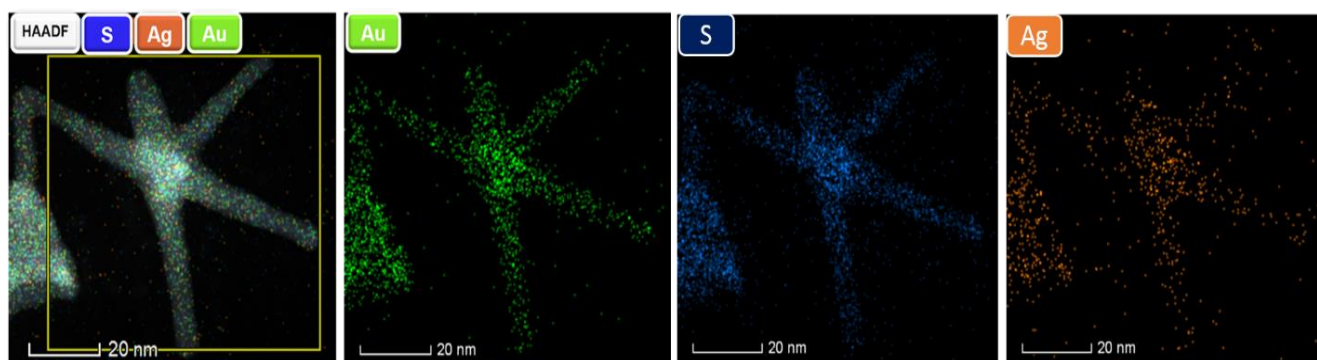


Figure 2.12. EDX-TEM elemental mapping of the BMPHA functionalized stars.

The Ag/ (Ag+Au) ratio, according to EDX obtained as 1:7, however, the XPS data showed this ratio as 7:11. This fact that silver percentage is higher at XPS compared to EDX is because XPS mainly collects the data from the surface of the samples. This shows that the silver atoms are depositing mainly on the surface of the stars. This data is consistent with the previous studies of looking for the role of silver nitrate in the synthesis of these Triton-X-100 stabilized AuNSs¹¹⁹. The full table data of the elemental analysis by EDX and XPS is shown in table 2.2.

Table 2.2. The elemental percentage obtained by EDX and XPS for gold nanostars

Element %	EDX	XPS
Au	65	7
S	4	4
Ag	11	4
C	20	85

2.11 Discussion on Gold Nanostars Formation to Bioconjugation

The AuNSs was synthesized using a seed growth method by applying non-ionic surfactant Triton-X-100 as the shape-directing agent. The preferential adsorption of the surfactant on specific crystalline facets of the gold triggers the anisotropic growth of the particle by changing the growth rates along with different crystallographic directions.^{59, 122, 123} Triton X-100, specifically, stabilizes the [111] facet and encourages the growth of the stars' tips in this direction. Then, a multi-twinned defect causes the anisotropic growth of the tips in three-dimensions.⁶ A schematic representation of particle growth is shown in Figure 2.13. The specific feature of these stars is their more than 6

sharp branches, which cause their unique absorption peaks due to the different possibilities of the electron oscillation on their surface.

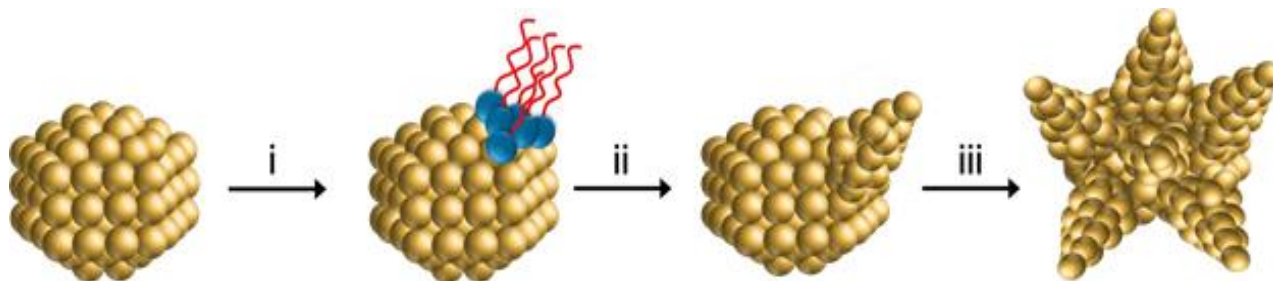


Figure 2.13. Schematic illustration depicting the growth of the AuNSs where: (i) the surfactant stabilizes the [111] facet of the gold particle; (ii) tips grow from the stabilized [111] facet; and finally, (iii) multi-twin defects lead to the formation of the stars

The functionalization of the AuNSs in the presence of Triton X-100 prohibits the aggregation of AuNSs during washing steps. However, the presence of Triton X-100 is not desirable for our application purposes. The choice of Triton X-100 as the synthetic surfactant was made since Triton X-100 is a neutral molecule, and the interaction of it with the surface is weaker compared to other surfactants, especially ionic surfactants. Triton X-100 releases the surface over time once the AuNSs are exposed to the bidentate thiol obtained through a synthetic procedure without the surfactant washing step.

BMPHA was selected for surface functionalization since bidentate thiolate adsorbates are more stable comparing to the monodentate thiolates on the gold surface.⁸⁹ The AuNSs synthesized here were functionalized with dual carboxyl-terminated thiol adsorbates, BMPHA as a long chain, and 4-MBA as a short-chain, being inspired by previous studies for SAM formation on the nanoparticles' surface,¹²⁴ and our optimization experiments. Due to the prevention of any steric hindrance on the complicated surface of the stars, by choosing proper molecules for the surface modification and bioconjugation, aggregation free AuNSs were produced to create a

platform for bioconjugation. The use of the mixture of a stable long-chain bidentate thiol and a short-chain monodentate thiol leads to a better packing density of the SAM on the complicated three-dimensional structure AuNSs. The 4-MBA short-chain possessing the same aromatic ring, fill in the gaps on the surface of the stars. Figure 2.14 illustrates the SAM modification of the as-prepared AuNSs, which is done following a ligand-exchange method.

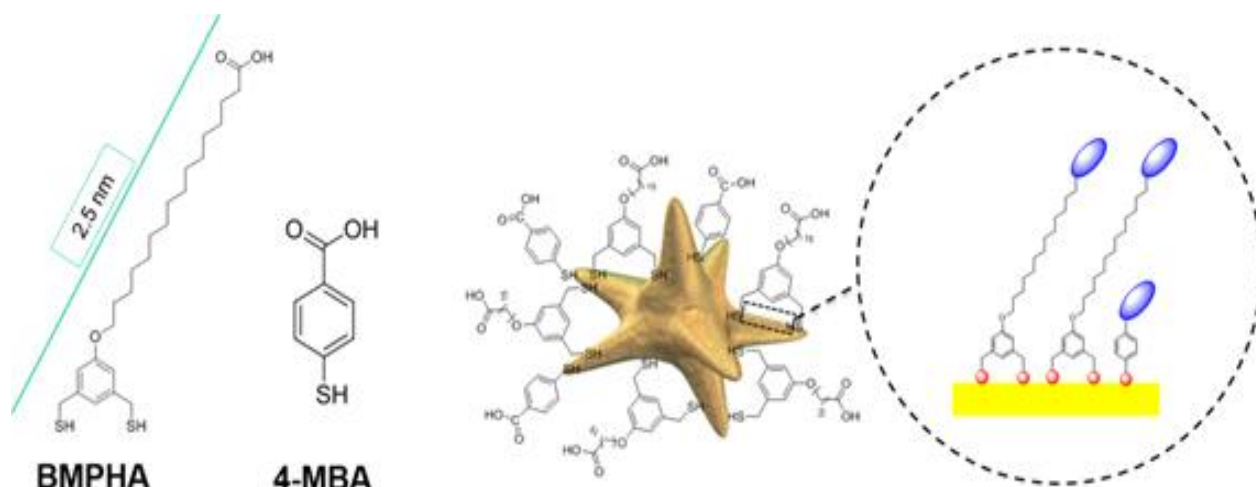


Figure 2.14. SAM Functionalization of the AuNSs

2.12 Gold Nanostars Bioconjugation

For bioconjugation, the EDC-NHSS protocol is used. The EDC reacts with the COOH group to form active ester intermediate that will react with amines to produce an amide product. However, the activated ester intermediate and the EDC itself are readily hydrolyzed by water. Moreover, the reaction of the amine group of proteins with the EDC-carboxyl intermediate is quite slow.¹²⁵ This is why EDC is used along with N-hydroxysulfosuccinimide (NHSS), which possesses hydrophilic reactive groups and couple rapidly with amines on target molecules resulting in a highly stable amide product. Unlike non-sulfonated NHS esters, NHSS is water-soluble,

longer-lived, and does not hydrolyze as fast as NHS in water.¹²⁵ Hydroxylamine was used for quenching instead of bovine serum albumin (BSA) since it is a smaller molecule and does not cause any steric hindrance for the complicated 3D structure of the stars. The complete schematic illustration of the bioconjugation can be found in Figure 2.15.

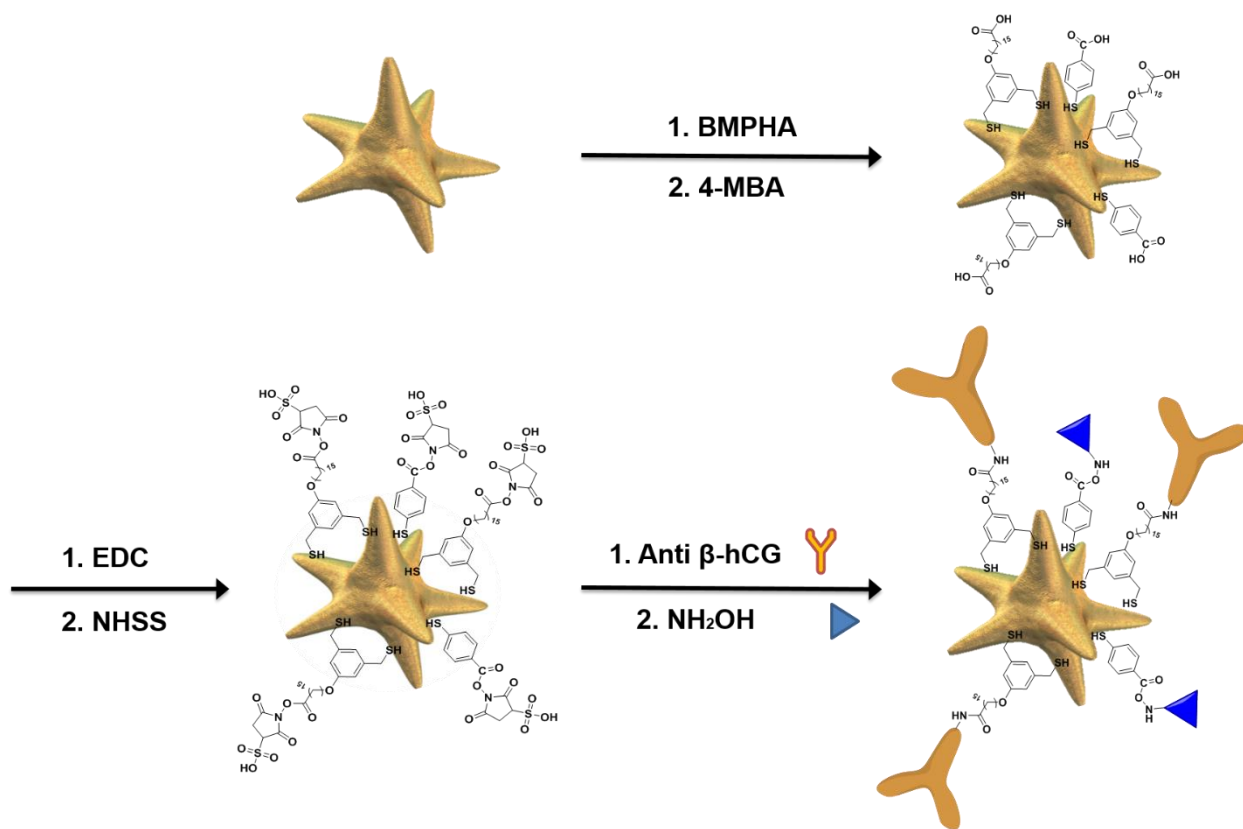


Figure 2.15. Overall steps of bio-functionalization of the AuNSs

The bio-conjugated AuNSs were applied in a lateral flow assay (LFA) biosensor to evaluate the influence of the morphology of the stars on the sensitivity and detection limit of the LFA.

2.13 LFA Data Obtaining

The optimized modes for obtaining data for AuNS- and spherical AuNP- conjugates LFA were obtained, trying every light source (LS) and exposure times in Lumos, analyzing the same strip. (Figures A.2 to A.16) According to the complete set of data, given in the appendix, we determined the optimized mode as the mode which 1) doesn't show too much noise for the TL and CL peaks, and 2) Shows more significant intensities for TL and CL and greater integration of the signal peaks. Therefore, for the AuNSs colloidal, red-blue, red-green, and green-blue will be eliminated for exhibiting too much noise, and lower signal-to-noise ratio. Among the other possible LSs for AuNSs, white LS didn't show a meaningful trend with the enhancement of the exposure time, and signal peak integrations and intensities for it were too low, relative to the others so that we didn't take it as the optimized LS mode. For the rest, including red LS, blue LS, and green LS, the peak area of the TL and CL signals were plotted versus different exposure times for each, given in Figure 2.16. According to the results, the maximum peak area for both TL and CL peaks were observed at red LS at 5.2 ms exposure time. Getting too much noise for spherical AuNPs, when obtaining the data for red-green, red-blue, and green-blue LSs at all exposure times, we concluded that these LSs are not the optimized mode for getting the data. Among the other LSs left, colloidal gold, red, blue, and green, the peak area was plotted versus different exposure times. The green LS showed the maximum signal at 5.2 ms exposure time and was picked as the optimized mode for obtaining all the data related to the spherical AuNPs-based reporters LFA.

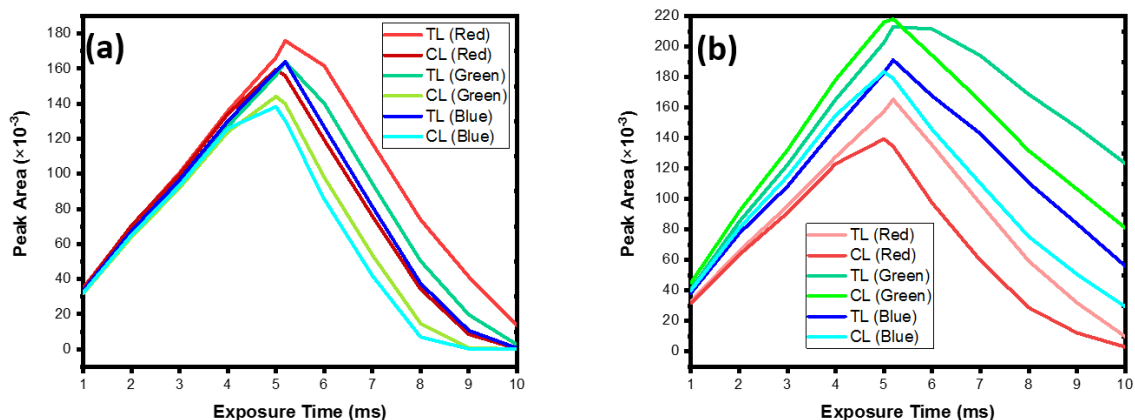


Figure 2.16. Peak area vs exposure time for the data obtained by Lumos using different light sources and exposure times for a) AuNSs and b) spherical AuNPs.

2.14 Amount of Antibodies Used

If the proper amount of antibodies conjugated to the surface of the AuNSs is used, there will be an increasing trend of the peak area of the control lines. After a certain amount of the antibodies conjugated to the AuNSs, the TL related to nonspecific bonding would appear, and false-positive results for negative samples. Therefore, we observe decreasing the peak area of the TL. This trend was observed when 36 μg of the antibody added to 850 μl of the colloidal star samples at OD=3.5. The data is shown in Figure 2.17 for CL.

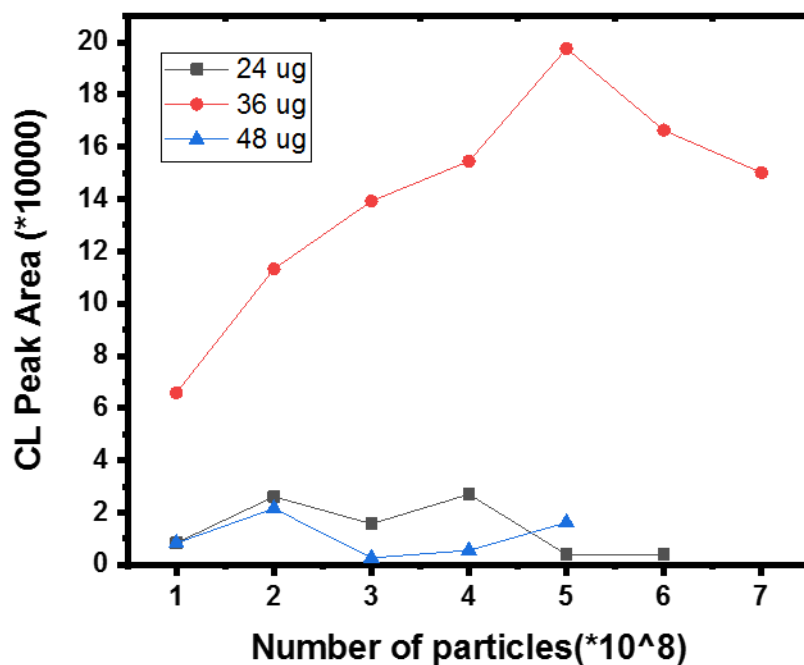


Figure 2.17. Peak area vs. number of the AuNSs for the data obtained by Lumos using different amounts of antibodies for bioconjugation for CL

2.15 Particle Number Optimization

The negative samples were prepared. A variable number of AuNS-conjugates $X=300-800$ million in LFA buffer (PBS 1X containing 1% PEG 3350, 1% BSA, and 0.5 % Tween 20) were prepared.

The highest number of the particles needed for spherical AuNPs and AuNSs needed for having no nonspecific binding, no false positive, and providing maximum brightness, at the same time is optimized. The maximum number of particles that could be used for these experiments were obtained as 5×10^8 particles for stars, 10^9 particles for spheres to only get one visible line for the control line for the negative controls.

2.16 Comparison of LFA Based on Gold Nanospheres and Gold Nanostars

To compare the effect of the star shape on the assay sensitivity, LFA based on the two different shapes of gold nanoparticles was performed. The images of the real strips are found in Figure A.17. The test line and control line's color depends on the reporters used, which are red in the case of spherical AuNPs and dark blue to black in case of using AuNSs as reporters. The XPS and EDX data confirming the silver layer on the surface of these particles, as well as previous studies⁴³ justifies the black color of the AuNS labels on the LFA strips.

All the prepared samples for running in LFA exhibited excellent colloidal stability and homogeneity in terms of composition and size. The ratio of the intensity of the test-line to intensity of the control-line was proportional to hCG concentration. The data obtained from running all of the LFA strips in different hCG concentrations (Figure 2.18.)

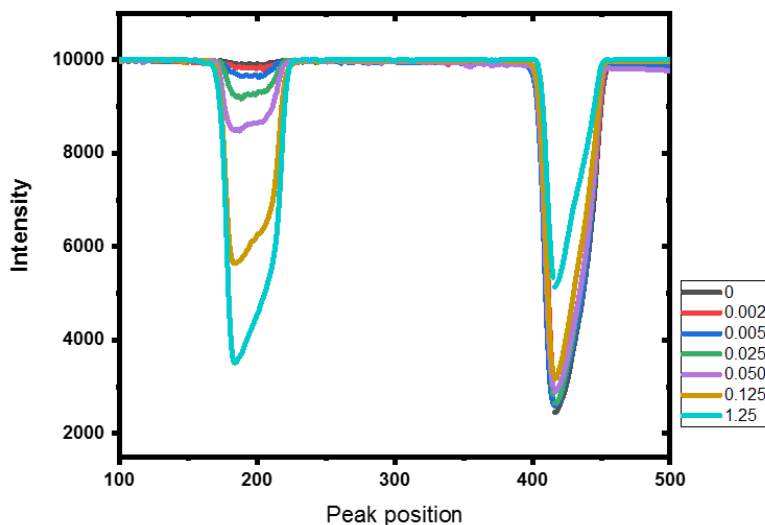


Figure 2.18. The intensity of peaks for TL and CL obtained by Lumos using different concentrations of hCG and AuNS-LFA reporters.

Figure 2.19. TL/CL ratio for different concentrations of hCG using AuNSs and spherical AuNPs. Figure 2. 19 (a) and (b) are the same graphs with varying scales of the y-axis to show the spots of the spheres in low concentrations.

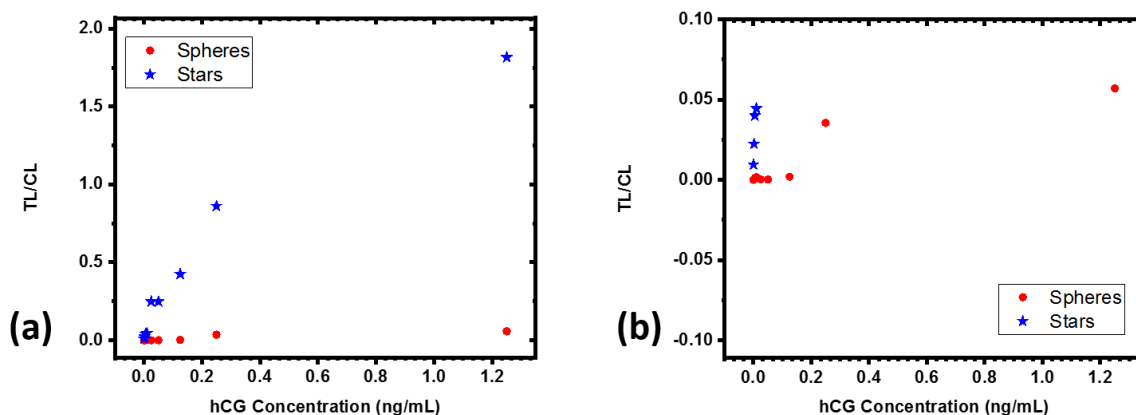


Figure 2.19. TL/CL ratio for different concentrations of hCG using AuNSs and spherical AuNPs with (a) longer y-axis and (b) shorter y-axis

The reporters' size has a profound effect on the sensitivity of the diagnosis assays. The highest detection sensitivity exhibited by of 47 nm to 79 nm gold nanoflowers-based immunographic assays in hCG detection.¹²¹

The 40 nm spherical AuNPs were selected in this work since the increase in the size of AuNPs (up to 40 nm) enhances the sensitivity of LFA. But spherical AuNPs larger than that may reduce the color brightness and nanoparticle stability.^{92, 126}

Spherical AuNPs-based LFA exhibited linearity over the range of with the best limit of detection at 0.1 ng/mL.

AuNSs-based LFAs were the best candidates of the reporters in this study, even capable of detecting 0.002 ng/mL equivalent to 2 pg/ mL of the hCG, which was 50 times better than spherical AuNPs ones in terms of sensitivity. No false-positive results were observed when dealing with negative hCG samples using our proposed protocol based on AuNSs.

Previously, Sebrebrennikova *et al.* (2018) showed the hierarchical use of gold nanoparticles, using different sizes of gold nanospheres, nanopapcorns, and gold nanostars. They mentioned the dependency of the sensitivity of the LFAs to the particle shape more than particle size.⁹² Although, they could not reach detection limit lower than 0.05 ng/mL even using the AuNSs and extra step of silver enhancement method in their approach.

Here in this study, we reported a simple technique using systematically bio-functionalized AuNSs that showed LOD of 0.002 ng/mL. This result is superior to many recent studies for the detection of hCG. The redshift in the LSPR from spherical AuNPs to AuNSs causes them to show the more detectable contrasting color of the test line and control line. This can be due to the fact that the AuNSs used in this work were synthesized using a seed mediated growth technique in the presence of a non-ionic surfactant, Triton X-100. This lead to have long term stabile AuNSs with pointy tips. The SAM functionalization of AuNSs using a stable carboxylic acid-functionalized bidentate thiol like BMPHA, in the presence of the Triton-X-100 causes their thorough functionalization through a ligand exchange process. This is so important since at the same time the aggregation of the nanostars that has been always a big concern is solved and these nanostars are very good candidates for any other applications like drug delivery, photo tumor ablation, given their unique light absorption and scattering spectrum.

The question that might arise here is why these AuNSs can make such a huge difference in results for improving the limit of detection of the LFA, as the POC diagnosis method.

To answer this question, we must see if this is due to the perfect light sensitivity of these particles in response to the detector of the Lumos LFA reader, or if their capturability causes them to show this one-of-a-kind LOD.

Therefore, we did two experiments, accordingly: 1) we compared the light sensitivity of the spherical AuNPs versus AuNSs. A thin layer of nitrocellulose membrane with a width of 2 mm was cut and attached to a rectangular shape 5×20 NC membrane with the same length attached to an adhesive card. Then they were cut using the cutting machine 3 mm wide. Therefore, we could drop the colloidal liquid of each shape of the gold nanoparticles with a controlled dispersing and have a comparison between the integration of the peak produced by the exposure of the strips to Lumos for 5.2 ms exposure time, regardless of any chemical bond between the particles and the nitrocellulose membrane. Then the experiment was done for a different number of the particles, and every plot of the peak area vs. the number of the particles was plotted, Figure 2.20.b. As can be seen, the slope of the graph for nanostars was bigger than nanospheres, indicating the higher light sensitivity of the stars compared to the spheres.

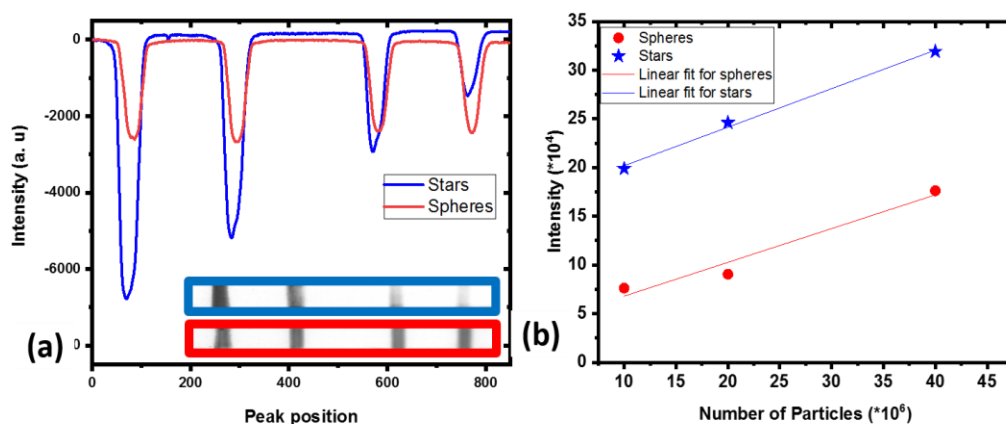


Figure 2.20. (a) Spherical- and star- shaped gold nanoparticles' capturability comparison experiment. (b) Light sensitivity experiment done for gold nanostars (blue), gold nanospheres (red)

We also compared the capturability of spherical AuNPs and AuNSs reporters on LFA. “Capturability” of these particles means how the antibody-functionalized gold nanoparticles are captured by the stationary antibodies on TL and CL. Therefore, four control lines, each with goat anti-mouse antibodies, were plotted on the nitrocellulose membrane attached to an adhesive card with the absorbing pad, each using the concentration of 0.2 mg/mL of the goat anti-mouse. The strips were caught to 4 mm wide strips, and the dipsticks were inserted inside the 30 μ L of the colloidal solution of the spherical AuNPs and AuNSs containing the equal number of particles in the LFA running buffer. Then, they were washed twice, each with 40 μ L of the LFA buffer (PBS 1X containing 1% PEG 3350, 1% BSA, and 0.5 % Tween 20) and the results of the strips were read using the Lumos LFA reader, reported in Figure 2.20.a. As it reveals, the stars were more capturable comparing to spheres by the antibodies on the strips, since the intensity of the control lines on the strips was decreased from the first line to the fourth line for the strips run by the AuNSs. Each experiment was repeated three times.

2.17 Kinetic Analysis of the Gold Nanostar-Lateral Flow Assay

The kinetics of AuNS-LFA was analyzed by using 30 μ L of the sample containing 6.25 ng/mL of hCG in LFA buffer (PBS 1X containing 1% PEG 3350, 1% BSA, and 0.5 % Tween 20) and 5×10^8 particles of spherical AuNPs were poured onto the sample pad. The strips containing the sample pad were put inside the Lumos reader, and the images of the strips were imaged every 10 seconds for 3 minutes. The TL/CL ratio was plotted versus time for each strip. The same experiment was done for the AuNSs. The plot shows that the graph of the star particles using the star-shaped dots in Figure 2.21, is located above spherical AuNPs, proving that the speed of the CL formation for stars is higher than the spheres.

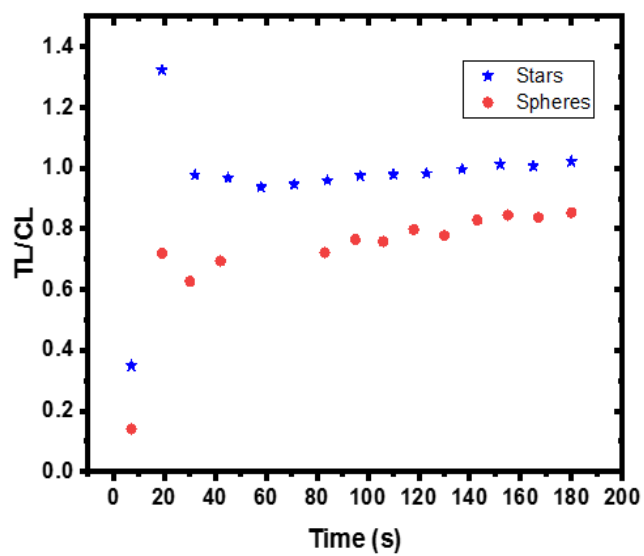


Figure 2.21. Kinetic comparison of nanostars (blue), gold nanospheres (red).

2.18 Conclusion

In this study, AuNS-based LFAs were developed for hCG detection. Gold nanostars (AuNSs) were synthesized in high yield with excellent reproducibility and implemented as novel LFA reporters. The AuNSs exhibit unique optical properties that make them have high visual sensitivity. Analysis by SEM and TEM of the generated nanoparticles confirm that these particles possess a star morphology with ~75 nm in diameter. UV-Visible spectroscopic analysis showed the AuNSs have a wide extinction peak in the NIR region. The synthesized particles were successfully functionalized with the carboxyl-terminated adsorbates, BMPHA and 4-MBA, as confirmed by FT-IR and XPS. The experimental observations besides SEM and TEM images showed no sign of any aggregation.

Furthermore, the SAM-functionalized AuNSs were successfully conjugated with antibody mouse monoclonal anti- β -hCG for suitable use in lateral flow assay (LFA). The influence of the morphology of the stars on the sensitivity and detection limit of the LFA for human chorionic gonadotropin (hCG) hormone was studied. The results were compared to the commercial 40 nm gold nanospheres, as a standard sensitive reporter. These gold nanostars used in this study decrease the limit of detection (LOD) owing to their excellent capturability and high optical sensitivity related to their localized surface Plasmon resonance (LSPR). The preliminary experiments on engineering and evaluation of hCG-targeted reporters of LFA using these colloidal nanostars revealed a limit of detection of 2 pg/mL observable by naked eyes. This LOD is orders of 50 fold magnitude more sensitive than colloidal gold-100 pg/ml, at the same ambient condition, buffer, and strips that work best for the sphere NPs. The existence of silver on the surface of these particles, confirmed by XPS and EDX-TEM data. This surficial silver enhances

the visibility of the line formed on LFA for the formation of a black line as a test line on the strips. That eliminates any additional step using the silver enhancement method for LOD improvement. Therefore, the proposed reporters can be used for the diagnosis of early pregnancy.

2.19 Future Works

The promising result 50 fold improvement of the LFA strips sensitivity using these newly prepared AuNSs shows that it is worth to run these star-shaped reporters with other samples other than hCG. We can also try any other biomarker detection in different samples like urine and human serum, optimizing the conditions using these AuNSs. Also, since this technique does not need any SERS enhancement signal or silver enhancement procedure, it is doable to apply them outside the laboratory. Also, the surfactant included and systematically controlled surface modification method in this work for the gold nanostars solved the problem of the difficulty of having desirable anisotropic shape and aggregation free surface modification simultaneously. This will be an advantage for further sensitive applications like SERS needing these features for the particle. Furthermore, the concentration control of the 4-MBA as a SERS tag molecule on the surface can bring even further promising results in the SERS based LFA even to the femtograms detection. If these stars can replace the commercially used gold nanospheres, they can enhance the sensitivity of the LFA strips and will play a vital role in POC testing, environmental monitoring, or food detection.

Another subject yet to be discovered is the effect of the size of these nanostar particles on the sensitivity improvement of the LFA strips, which can be easily controlled through different time growth of the stars' growth solution.

Bibliography

1. Banerjee, R.; Jaiswal, A., Recent advances in nanoparticle-based lateral flow immunoassay as a point-of-care diagnostic tool for infectious agents and diseases. *Analyst* **2018**, *143* (9), 1970-1996.
2. Zhang, W.; Duan, H.; Chen, R.; Ma, T.; Zeng, L.; Leng, Y.; Xiong, Y., Effect of different-sized gold nanoflowers on the detection performance of immunochromatographic assay for human chorionic gonadotropin detection. *Talanta* **2019**, *194*, 604-610.
3. Sánchez-Purrà, M.; Carré-Camps, M.; de Puig, H.; Bosch, I.; Gehrke, L.; Hamad-Schifferli, K., Surface-enhanced raman spectroscopy-based sandwich immunoassays for multiplexed detection of zika and dengue viral biomarkers. *ACS Infectious Diseases* **2017**, *3* (10), 767-776.
4. Yew, C.-H. T.; Azari, P.; Choi, J. R.; Li, F.; Pingguan-Murphy, B., Electrospin-coating of nitrocellulose membrane enhances sensitivity in nucleic acid-based lateral flow assay. *Analytica Chimica Acta* **2018**, *1009*, 81-88.
5. Koczula, K. M.; Gallotta, A., Lateral flow assays. *Essays in Biochemistry* **2016**, *60* (1), 111-120.
6. Sajid, M.; Kawde, A.-N.; Daud, M., Designs, formats and applications of lateral flow assay: A literature review. *Journal of Saudi Chemical Society* **2015**, *19* (6), 689-705.
7. Bahadır, E. B.; Sezgintürk, M. K., Lateral flow assays: Principles, designs and labels. *TrAC Trends in Analytical Chemistry* **2016**, *82*, 286-306.
8. Tripathi, P.; Upadhyay, N.; Nara, S., Recent advancements in lateral flow immunoassays: A journey for toxin detection in food. *Critical Reviews in Food Science Nutrition* **2018**, *58* (10), 1715-1734.
9. Canfield, R.; O'Connor, J.; Birken, S.; Krichevsky, A.; Wilcox, A., Development of an assay for a biomarker of pregnancy and early fetal loss. *Environmental Health Perspectives* **1987**, *74*, 57-66.
10. Laphorn, A.; Harris, D.; Littlejohn, A.; Lustbader, J.; Canfield, R.; Machin, K.; Morgan, F.; Isaacs, N., Crystal structure of human chorionic gonadotropin. *Nature* **1994**, *369* (6480), 455-461.
11. Esteves, S. C.; Alviggi, C., The role of LH in controlled ovarian stimulation. In *Principles and Practice of Controlled Ovarian Stimulation in ART*, Springer: 2015; pp 171-196.
12. Korevaar, T. I.; Steegers, E. A.; de Rijke, Y. B.; Schalekamp-Timmermans, S.; Visser, W. E.; Hofman, A.; Jaddoe, V. W.; Tiemeier, H.; Visser, T. J.; Medici, M., Reference ranges

and determinants of total hCG levels during pregnancy: the Generation R Study. *European Journal of Epidemiology* **2015**, 30 (9), 1057-1066.

13. Panferov, V. G.; Safenkova, I. V.; Varitsev, Y. A.; Drenova, N. V.; Kornev, K. P.; Zherdev, A. V.; Dzantiev, B. B., Development of the sensitive lateral flow immunoassay with silver enhancement for the detection of *Ralstonia solanacearum* in potato tubers. *Talanta* **2016**, 152, 521-530.

14. Birken, S.; Berger, P.; Bidart, J.-M.; Weber, M.; Bristow, A.; Norman, R.; Sturgeon, C.; Stenman, U.-H., Preparation and characterization of new WHO reference reagents for human chorionic gonadotropin and metabolites. *Clinical Chemistry* **2003**, 49 (1), 144-154.

15. Canfield, R.; Ross, G., A new reference preparation of human chorionic gonadotrophin and its subunits. *Bulletin of the World Health Organization* **1976**, 54 (4), 463.

16. Cheng, X.; Liu, X.; Liu, X.; Guo, Z.; Sun, H.; Zhang, M.; Ji, Z.; Sun, W., Metabolomics of non-muscle invasive bladder cancer: biomarkers for early detection of bladder cancer. *Frontiers in Oncology* **2018**, 8, 494.

17. Kee, J. S.; Lim, S. Y.; Perera, A. P.; Zhang, Y.; Park, M. K., Plasmonic nanohole arrays for monitoring growth of bacteria and antibiotic susceptibility test. *Sensors Actuators B: Chemical* **2013**, 182, 576-583.

18. Mahmoudi, T.; de la Guardia, M.; Shirdel, B.; Mokhtarzadeh, A.; Baradarn, B., Recent advancements in structural improvements of lateral flow assays towards point-of-care testing. *TrAC Trends in Analytical Chemistry* **2019**.

19. Quesada-González, D.; Merkoçi, A., Nanoparticle-based lateral flow biosensors. *Biosensors Bioelectronics* **2015**, 73, 47-63.

20. Yan, L.; Dou, L.; Bu, T.; Huang, Q.; Wang, R.; Yang, Q.; Huang, L.; Wang, J.; Zhang, D., Highly sensitive furazolidone monitoring in milk by a signal amplified lateral flow assay based on magnetite nanoparticles labeled dual-probe. *Food Chemistry* **2018**, 261, 131-138.

21. Paterson, A. S.; Raja, B.; Garvey, G.; Kolhatkar, A.; Hagström, A. E.; Kourentzi, K.; Lee, T. R.; Willson, R. C., Persistent luminescence strontium aluminate nanoparticles as reporters in lateral flow assays. *Analytical Chemistry* **2014**, 86 (19), 9481-9488.

22. Zhang, C.; Zhang, Y.; Wang, S., Development of multianalyte flow-through and lateral-flow assays using gold particles and horseradish peroxidase as tracers for the rapid determination of carbaryl and endosulfan in agricultural products. *Journal of Agricultural Food Chemistry* **2006**, 54 (7), 2502-2507.

23. Yang, W.; Li, X.-b.; Liu, G.-w.; Zhang, B.-b.; Zhang, Y.; Kong, T.; Tang, J.-j.; Li, D.-n.; Wang, Z., A colloidal gold probe-based silver enhancement immunochromatographic assay for the rapid detection of abrin-a. *Biosensors Bioelectronics* **2011**, 26 (8), 3710-3713.

24. Mahler, B.; Spinicelli, P.; Buil, S.; Quelin, X.; Hermier, J.-P.; Dubertret, B., Towards non-blinking colloidal quantum dots. *Nature Materials* **2008**, 7 (8), 659-664.
25. Danthanarayana, A. N.; Finley, E.; Vu, B.; Kourentzi, K.; Willson, R. C.; Brgoch, J., A multicolor multiplex lateral flow assay for high-sensitivity analyte detection using persistent luminescent nanophosphors. *Analytical Methods* **2020**.
26. Paterson, A. S.; Raja, B.; Mandadi, V.; Townsend, B.; Lee, M.; Buell, A.; Vu, B.; Brgoch, J.; Willson, R. C., A low-cost smartphone-based platform for highly sensitive point-of-care testing with persistent luminescent phosphors. *Lab on a Chip* **2017**, 17 (6), 1051-1059.
27. Goux, H. J.; Raja, B.; Kourentzi, K.; Trabuco, J. R.; Vu, B. V.; Paterson, A. S.; Kirkpatrick, A.; Townsend, B.; Lee, M.; Truong, V. T. T., Evaluation of a nanophosphor lateral-flow assay for self-testing for herpes simplex virus type 2 seropositivity. *PloS one* **2019**, 14 (12).
28. Li, X.; Yang, T.; Song, Y.; Zhu, J.; Wang, D.; Li, W., Surface-enhanced Raman spectroscopy (SERS)-based immunochromatographic assay (ICA) for the simultaneous detection of two pyrethroid pesticides. *Sensors Actuators B: Chemical* **2019**, 283, 230-238.
29. Lin, L.-K.; Stanciu, L. A., Bisphenol A detection using gold nanostars in a SERS improved lateral flow immunochromatographic assay. *Sensors Actuators B: Chemical* **2018**, 276, 222-229.
30. Gumustas, A.; Caglayan, M. G.; Eryilmaz, M.; Suludere, Z.; Soykut, E. A.; Uslu, B.; Boyaci, I. H.; Tamer, U., Paper based lateral flow immunoassay for the enumeration of *Escherichia coli* in urine. *Analytical methods* **2018**, 10 (10), 1213-1218.
31. Huang, X.; Aguilar, Z. P.; Xu, H.; Lai, W.; Xiong, Y., Membrane-based lateral flow immunochromatographic strip with nanoparticles as reporters for detection: a review. *Biosensors Bioelectronics* **2016**, 75, 166-180.
32. Elahi, N.; Kamali, M.; Baghersad, M. H., Recent biomedical applications of gold nanoparticles: A review. *Talanta* **2018**, 184, 537-556.
33. Liz-Marzán, L. M.; Murphy, C. J.; Wang, J., Nanoplasmonics. *Chemical Society Reviews* **2014**, 43 (11), 3820-3822.
34. Bohren, C. F.; Huffman, D. R., *Absorption and scattering of light by small particles*. John Wiley & Sons: 2008.
35. Kreibig, U.; Vollmer, M., *Optical properties of metal clusters*. Springer Science & Business Media: 2013; Vol. 25.
36. Mejía-Salazar, J.; Oliveira Jr, O., Plasmonic biosensing: focus review. *Chemical Reviews* **2018**, 118 (20), 10617-10625.
37. Naik, G. V.; Shalae, V. M.; Boltasseva, A., Alternative Plasmonic Materials: Beyond Gold and Silver. **2013**, 25 (24), 3264-3294.

38. García de Abajo, F. J.; Howie, A., Relativistic Electron Energy Loss and Electron-Induced Photon Emission in Inhomogeneous Dielectrics. *Physical Review Letters* **1998**, *80* (23), 5180-5183.
39. Link, S.; El-Sayed, M. A., Size and Temperature Dependence of the Plasmon Absorption of Colloidal Gold Nanoparticles. *The Journal of Physical Chemistry B* **1999**, *103* (21), 4212-4217.
40. Xing, S.; Tan, L. H.; Yang, M.; Pan, M.; Lv, Y.; Tang, Q.; Yang, Y.; Chen, H., Highly controlled core/shell structures: tunable conductive polymer shells on gold nanoparticles and nanochains. *Journal of Materials Chemistry* **2009**, *19* (20), 3286-3291.
41. Lee, K.-S.; El-Sayed, M. A., Gold and Silver Nanoparticles in Sensing and Imaging: Sensitivity of Plasmon Response to Size, Shape, and Metal Composition. *The Journal of Physical Chemistry B* **2006**, *110* (39), 19220-19225.
42. Dykman, L.; Khlebtsov, N., Gold nanoparticles in chemo-, immuno-, and combined therapy: review. *Biomedical Optics Express* **2019**, *10* (7), 3152-3182.
43. Park, H.; Lim, D.-J.; Vines, J. B.; Yoon, J.-H.; Ryu, N.-E., Gold nanoparticles for photothermal cancer therapy. *Frontiers in Chemistry* **2019**, *7*, 167.
44. Langer, R., Biomaterials in Drug Delivery and Tissue Engineering: One Laboratory's Experience. *Accounts of Chemical Research* **2000**, *33* (2), 94-101.
45. Ghosh, S. K.; Pal, T., Interparticle Coupling Effect on the Surface Plasmon Resonance of Gold Nanoparticles: From Theory to Applications. *Chemical Reviews* **2007**, *107* (11), 4797-4862.
46. Qian, X.; Peng, X.-H.; Ansari, D. O.; Yin-Goen, Q.; Chen, G. Z.; Shin, D. M.; Yang, L.; Young, A. N.; Wang, M. D.; Nie, S., In vivo tumor targeting and spectroscopic detection with surface-enhanced Raman nanoparticle tags. *Nature Biotechnology* **2008**, *26* (1), 83-90.
47. Sajjadi, A. Y.; Suratkar, A.; Mitra, K.; Grace, M. S., Short-Pulse Laser-Based System for Detection of Tumors: Administration of Gold Nanoparticles Enhances Contrast. *Journal of Nanotechnology in Engineering and Medicine* **2012**, *3* (2).
48. Niidome, T.; Yamagata, M.; Okamoto, Y.; Akiyama, Y.; Takahashi, H.; Kawano, T.; Katayama, Y.; Niidome, Y., PEG-modified gold nanorods with a stealth character for in vivo applications. *Journal of Controlled Release* **2006**, *114* (3), 343-347.
49. Giljohann, D. A.; Seferos, D. S.; Prigodich, A. E.; Patel, P. C.; Mirkin, C. A., Gene Regulation with Polyvalent siRNA–Nanoparticle Conjugates. *Journal of the American Chemical Society* **2009**, *131* (6), 2072-2073.
50. McMahon, S. J.; Hyland, W. B.; Muir, M. F.; Coulter, J. A.; Jain, S.; Butterworth, K. T.; Schettino, G.; Dickson, G. R.; Hounsell, A. R.; O'Sullivan, J. M.; Prise, K. M.; Hirst, D. G.; Currell, F. J., Biological consequences of nanoscale energy deposition near irradiated heavy atom nanoparticles. *Scientific Reports* **2011**, *1* (1), 18.

51. Li, Y.; Schluesener, H. J.; Xu, S., Gold nanoparticle-based biosensors. *Gold Bulletin* **2010**, *43* (1), 29-41.
52. Priyadarshini, E.; Pradhan, N., Gold nanoparticles as efficient sensors in colorimetric detection of toxic metal ions: a review. *Sensors Actuators B: Chemical* **2017**, *238*, 888-902.
53. Zhang, Z.; Chen, Z.; Wang, S.; Qu, C.; Chen, L., On-Site Visual Detection of Hydrogen Sulfide in Air Based on Enhancing the Stability of Gold Nanoparticles. *ACS Applied Materials & Interfaces* **2014**, *6* (9), 6300-6307.
54. Lohse, S. E.; Murphy, C. J., The quest for shape control: a history of gold nanorod synthesis. *Chemistry of Materials* **2013**, *25* (8), 1250-1261.
55. Thiele, M.; Soh, J. Z. E.; Knauer, A.; Malsch, D.; Stranik, O.; Mueller, R.; Csaki, A.; Henkel, T.; Koehler, J. M.; Fritzsche, W., Gold nanocubes—Direct comparison of synthesis approaches reveals the need for a microfluidic synthesis setup for a high reproducibility. *Chemical Engineering Journal* **2016**, *288*, 432-440.
56. Requejo, K. I.; Liopo, A. V.; Zubarev, E. R., High yield synthesis and surface chemistry exchange of small gold hexagonal nanoprisms. *Chemical Communications* **2019**, *55* (76), 11422-11425.
57. Patel, A. S.; Juneja, S.; Kanaujia, P. K.; Maurya, V.; Prakash, G. V.; Chakraborti, A.; Bhattacharya, J., Gold nanoflowers as efficient hosts for SERS based sensing and bio-imaging. *Nano-Structures Nano-Objects* **2018**, *16*, 329-336.
58. Chirico, G.; Borzenkov, M.; Pallavicini, P., *Gold nanostars: synthesis, properties and biomedical application*. Springer: 2015.
59. Sau, T. K.; Murphy, C. J., Room temperature, high-yield synthesis of multiple shapes of gold nanoparticles in aqueous solution. *Journal of the American Chemical Society* **2004**, *126* (28), 8648-8649.
60. Ahmadi, T. S.; Wang, Z. L.; Green, T. C.; Henglein, A.; El-Sayed, M. A., Shape-controlled synthesis of colloidal platinum nanoparticles. *Science* **1996**, *272* (5270), 1924-1925.
61. Li, M.; Schnablegger, H.; Mann, S., Coupled synthesis and self-assembly of nanoparticles to give structures with controlled organization. *Nature* **1999**, *402* (6760), 393-395.
62. Jin, R.; Cao, Y. C.; Hao, E.; Métraux, G. S.; Schatz, G. C.; Mirkin, C. A., Controlling anisotropic nanoparticle growth through plasmon excitation. *Nature* **2003**, *425* (6957), 487-490.
63. Sun, Y.; Gates, B.; Mayers, B.; Xia, Y., Crystalline silver nanowires by soft solution processing. *Nano letters* **2002**, *2* (2), 165-168.
64. Yacamán, M. J.; Ascencio, J.; Liu, H.; Gardea-Torresdey, J., Structure shape and stability of nanometric sized particles. *Journal of Vacuum Science Technology B: Microelectronics Nanometer Structures Processing, Measurement, Phenomena* **2001**, *19* (4), 1091-1103.

65. Yang, C. Y.; Heinemann, K.; Yacaman, M.; Poppa, H., A structural analysis of small vapor-deposited “multiply twinned” gold particles. *Thin Solid Films* **1979**, 58 (1), 163-168.
66. Renou, A.; Gillet, M., Growth of Au, Pt and Pd particles in a flowing argon system: observations of decahedral and icosahedral structures. *Surface Science* **1981**, 106 (1-3), 27-34.
67. Huang, X.; El-Sayed, M. A., Gold nanoparticles: Optical properties and implementations in cancer diagnosis and photothermal therapy. *Journal of Advanced Research* **2010**, 1 (1), 13-28.
68. Sosa, I. O.; Noguez, C.; Barrera, R. G., Optical Properties of Metal Nanoparticles with Arbitrary Shapes. *The Journal of Physical Chemistry B* **2003**, 107 (26), 6269-6275.
69. Barbosa, S.; Agrawal, A.; Rodríguez-Lorenzo, L.; Pastoriza-Santos, I.; Alvarez-Puebla, R. A.; Kornowski, A.; Weller, H.; Liz-Marzán, L. M., Tuning Size and Sensing Properties in Colloidal Gold Nanostars. *Langmuir* **2010**, 26 (18), 14943-14950.
70. Mehn, D.; Morasso, C.; Vanna, R.; Bedoni, M.; Prosperi, D.; Gramatica, F., Immobilised gold nanostars in a paper-based test system for surface-enhanced Raman spectroscopy. *Vibrational Spectroscopy* **2013**, 68, 45-50.
71. Mallick, K.; Wang, Z.; Pal, T., Seed-mediated successive growth of gold particles accomplished by UV irradiation: a photochemical approach for size-controlled synthesis. *Journal of Photochemistry Photobiology A: Chemistry* **2001**, 140 (1), 75-80.
72. Sau, T. K.; Rogach, A. L.; Döblinger, M.; Feldmann, J., One-step high-yield aqueous synthesis of size-tunable multipiked gold nanoparticles. *Small* **2011**, 7 (15), 2188-2194.
73. Guerrero-Martínez, A.; Barbosa, S.; Pastoriza-Santos, I.; Liz-Marzán, L. M., Nanostars shine bright for you: colloidal synthesis, properties and applications of branched metallic nanoparticles. *Current Opinion in Colloid Interface Science* **2011**, 16 (2), 118-127.
74. Xia, Y.; Xiong, Y.; Lim, B.; Skrabalak, S. E., Shape-controlled synthesis of metal nanocrystals: simple chemistry meets complex physics? *Angewandte Chemie International Edition* **2009**, 48 (1), 60-103.
75. Chirumamilla, M.; Gopalakrishnan, A.; Toma, A.; Zaccaria, R. P.; Krahne, R., Plasmon resonance tuning in metal nanostars for surface enhanced Raman scattering. *Nanotechnology* **2014**, 25 (23), 235303.
76. Chirumamilla, M.; Toma, A.; Gopalakrishnan, A.; Das, G.; Zaccaria, R. P.; Krahne, R.; Rondanina, E.; Leoncini, M.; Liberale, C.; De Angelis, F., 3D nanostar dimers with a sub-10-nm gap for single-/few-molecule surface-enhanced Raman scattering. *Advanced Materials* **2014**, 26 (15), 2353-2358.
77. Murphy, C. J.; Sau, T. K.; Gole, A. M.; Orendorff, C. J.; Gao, J.; Gou, L.; Hunyadi, S. E.; Li, T., Anisotropic metal nanoparticles: synthesis, assembly, and optical applications. ACS Publications: 2005.

78. Nikoobakht, B.; El-Sayed, M. A., Preparation and growth mechanism of gold nanorods (NRs) using seed-mediated growth method. *Chemistry of Materials* **2003**, *15* (10), 1957-1962.
79. Chen, S.; Wang, Z. L.; Ballato, J.; Foulger, S. H.; Carroll, D. L., Monopod, bipod, tripod, and tetrapod gold nanocrystals. *Journal of the American Chemical Society* **2003**, *125* (52), 16186-16187.
80. Mousavi, S. M.; Zarei, M.; Hashemi, S. A.; Ramakrishna, S.; Chiang, W.-H.; Lai, C. W.; Gholami, A., Gold nanostars-diagnosis, bioimaging and biomedical applications. *Drug Metabolism Reviews* **2020**, 1-20.
81. Tian, F.; Conde, J.; Bao, C.; Chen, Y.; Curtin, J.; Cui, D., Gold nanostars for efficient in vitro and in vivo real-time SERS detection and drug delivery via plasmonic-tunable Raman/FTIR imaging. *Biomaterials* **2016**, *106*, 87-97.
82. Yuan, H.; Khoury, C. G.; Wilson, C. M.; Grant, G. A.; Bennett, A. J.; Vo-Dinh, T., In vivo particle tracking and photothermal ablation using plasmon-resonant gold nanostars. *Nanomedicine: Nanotechnology, Biology, Medicine* **2012**, *8* (8), 1355-1363.
83. Tiwari, P. M.; Vig, K.; Dennis, V. A.; Singh, S. R., Functionalized gold nanoparticles and their biomedical applications. *Nanomaterials* **2011**, *1* (1), 31-63.
84. Sanna, V.; Pala, N.; Sechi, M., Targeted therapy using nanotechnology: focus on cancer. *International Journal of Nanomedicine* **2014**, *9*, 467.
85. Love, J. C.; Estroff, L. A.; Kriebel, J. K.; Nuzzo, R. G.; Whitesides, G. M., Self-assembled monolayers of thiolates on metals as a form of nanotechnology. *Chemical Reviews* **2005**, *105* (4), 1103-1170.
86. Bensebaa, F.; Ellis, T.; Badia, A.; Lennox, R., Probing the different phases of self-assembled monolayers on metal surfaces: Temperature dependence of the C–H stretching modes. *Journal of Vacuum Science Technology A: Vacuum, Surfaces, and Films* **1995**, *13* (3), 1331-1336.
87. Tam-Chang, S.-W.; Biebuyck, H. A.; Whitesides, G. M.; Jeon, N.; Nuzzo, R. G., Self-assembled monolayers on gold generated from alkanethiols with the structure RNHCOCH₂SH. *Langmuir* **1995**, *11* (11), 4371-4382.
88. Zamborini, F. P.; Crooks, R. M., In-situ electrochemical scanning tunneling microscopy (ECSTM) study of cyanide-induced corrosion of naked and hexadecyl mercaptan-passivated Au (111). *Langmuir* **1997**, *13* (2), 122-126.
89. Lee, H. J.; Jamison, A. C.; Yuan, Y.; Li, C.-H.; Rittikulsittichai, S.; Rusakova, I.; Lee, T. R., Robust carboxylic acid-terminated organic thin films and nanoparticle protectants generated from bidentate alkanethiols. *Langmuir* **2013**, *29* (33), 10432-10439.

90. Her, S.; Jaffray, D. A.; Allen, C., Gold nanoparticles for applications in cancer radiotherapy: Mechanisms and recent advancements. *Advanced Drug Delivery Reviews* **2017**, *109*, 84-101.
91. Thierry, B.; Ng, J.; Krieg, T.; Griesser, H. J., A robust procedure for the functionalization of gold nanorods and noble metal nanoparticles. *Chemical Communications* **2009**, (13), 1724-1726.
92. Serebrennikova, K.; Samsonova, J.; Osipov, A., Hierarchical nanogold labels to improve the sensitivity of lateral flow immunoassay. *Nano-micro Letters* **2018**, *10* (2), 24.
93. Huang, X.; Aguilar, Z. P.; Li, H.; Lai, W.; Wei, H.; Xu, H.; Xiong, Y., Fluorescent Ru (phen) 32+-doped silica nanoparticles-based ICTS sensor for quantitative detection of enrofloxacin residues in chicken meat. *Analytical Chemistry* **2013**, *85* (10), 5120-5128.
94. Omidfar, K.; Khorsand, F.; Azizi, M. D., New analytical applications of gold nanoparticles as label in antibody based sensors. *Biosensors Bioelectronics* **2013**, *43*, 336-347.
95. Tang, D.; Saucedo, J.; Lin, Z.; Ott, S.; Basova, E.; Goryacheva, I.; Biselli, S.; Lin, J.; Niessner, R.; Knopp, D., Magnetic nanogold microspheres-based lateral-flow immunodipstick for rapid detection of aflatoxin B2 in food. *Biosensors Bioelectronics* **2009**, *25* (2), 514-518.
96. Xu, H.; Chen, J.; Birrenkott, J.; Zhao, J. X.; Takalkar, S.; Baryeh, K.; Liu, G., Gold-nanoparticle-decorated silica nanorods for sensitive visual detection of proteins. *Analytical Chemistry* **2014**, *86* (15), 7351-7359.
97. Ji, Y.; Ren, M.; Li, Y.; Huang, Z.; Shu, M.; Yang, H.; Xiong, Y.; Xu, Y., Detection of aflatoxin B1 with immunochromatographic test strips: enhanced signal sensitivity using gold nanoflowers. *Talanta* **2015**, *142*, 206-212.
98. Rohrman, B. A.; Leautaud, V.; Molyneux, E.; Richards-Kortum, R. R., A lateral flow assay for quantitative detection of amplified HIV-1 RNA. *PLoS One* **2012**, *7* (9).
99. He, Y.; Zhang, S.; Zhang, X.; Baloda, M.; Gurung, A. S.; Xu, H.; Zhang, X.; Liu, G., Ultrasensitive nucleic acid biosensor based on enzyme-gold nanoparticle dual label and lateral flow strip biosensor. *Biosensors Bioelectronics* **2011**, *26* (5), 2018-2024.
100. Yang, Y.; Ozsoz, M.; Liu, G., Gold nanocage-based lateral flow immunoassay for immunoglobulin G. *Microchimica Acta* **2017**, *184* (7), 2023-2029.
101. Truong, P. L.; Kim, B. W.; Sim, S. J., Rational aspect ratio and suitable antibody coverage of gold nanorod for ultra-sensitive detection of a cancer biomarker. *Lab on a Chip* **2012**, *12* (6), 1102-1109.
102. Lin, L. K.; Huang, P. Y.; Dutta, S.; Rochet, J. C.; Stanciu, L. A., Tuning a Bisphenol A Lateral Flow Assay Using Multiple Gold Nanosystems. *Particle Particle Systems Characterization* **2019**, *36* (7), 1900133.

103. Zhu, J.; Liu, M.-J.; Li, J.-J.; Zhao, J.-W., Synthesis of gold nanostars with fractal structure: application in surface-enhanced Raman scattering. *The European Physical Journal B* **2017**, 90 (11), 216.
104. Joseph, M. M.; Narayanan, N.; Nair, J. B.; Karunakaran, V.; Ramya, A. N.; Sujai, P. T.; Saranya, G.; Arya, J. S.; Vijayan, V. M.; Maiti, K. K., Exploring the margins of SERS in practical domain: An emerging diagnostic modality for modern biomedical applications. *Biomaterials* **2018**, 181, 140-181.
105. Li, M.; Cushing, S. K.; Zhang, J.; Lankford, J.; Aguilar, Z. P.; Ma, D.; Wu, N., Shape-dependent surface-enhanced Raman scattering in gold-Raman-probe-silica sandwiched nanoparticles for biocompatible applications. *Nanotechnology* **2012**, 23 (11), 115501.
106. Gao, X.; Zheng, P.; Kasani, S.; Wu, S.; Yang, F.; Lewis, S.; Nayeem, S.; Engler-Chiurazzi, E. B.; Wigginton, J. G.; Simpkins, J. W., based surface-enhanced Raman scattering lateral flow strip for detection of neuron-specific enolase in blood plasma. *Analytical Chemistry* **2017**, 89 (18), 10104-10110.
107. Sánchez-Purrà, M.; Roig-Solvas, B.; Versiani, A.; Rodriguez-Quijada, C.; de Puig, H.; Bosch, I.; Gehrke, L.; Hamad-Schifferli, K., Design of SERS nanotags for multiplexed lateral flow immunoassays. *Molecular Systems Design Engineering* **2017**, 2 (4), 401-409.
108. Xiao, M.; Fu, Q.; Shen, H.; Chen, Y.; Xiao, W.; Yan, D.; Tang, X.; Zhong, Z.; Tang, Y., A turn-on competitive immunochromatographic strips integrated with quantum dots and gold nano-stars for cadmium ion detection. *Talanta* **2018**, 178, 644-649.
109. Sánchez-Purrà, M.; Roig-Solvas, B.; Rodriguez-Quijada, C.; Leonardo, B. M.; Hamad-Schifferli, K., Reporter Selection for Nanotags in Multiplexed Surface Enhanced Raman Spectroscopy Assays. *ACS omega* **2018**, 3 (9), 10733-10742.
110. Panferov, V. G.; Safenkova, I. V.; Zherdev, A. V.; Dzantiev, B. B., Post-assay growth of gold nanoparticles as a tool for highly sensitive lateral flow immunoassay. Application to the detection of potato virus X. *Microchimica Acta* **2018**, 185 (11), 506.
111. Vigderman, L.; Khanal, B. P.; Zubarev, E. R., Functional gold nanorods: synthesis, self-assembly, and sensing applications. *Advanced Materials* **2012**, 24 (36), 4811-4841.
112. Ghosh, S. K.; Pal, T., Interparticle coupling effect on the surface plasmon resonance of gold nanoparticles: from theory to applications. *Chemical Reviews* **2007**, 107 (11), 4797-4862.
113. Zhu, Y.; Kuang, H.; Xu, L.; Ma, W.; Peng, C.; Hua, Y.; Wang, L.; Xu, C., Gold nanorod assembly based approach to toxin detection by SERS. *Journal of Materials Chemistry* **2012**, 22 (6), 2387-2391.

114. Tao, Y.; Yang, J.; Chen, L.; Huang, Y.; Qiu, B.; Guo, L.; Lin, Z., Dialysis assisted ligand exchange on gold nanorods: Amplification of the performance of a lateral flow immunoassay for E. coli O157: H7. *Microchimica Acta* **2018**, *185* (7), 350.
115. Bogliotti, N.; Oberleitner, B.; Di-Cicco, A.; Schmidt, F.; Florent, J.-C.; Semetey, V., Optimizing the formation of biocompatible gold nanorods for cancer research: functionalization, stabilization and purification. *Journal of Colloid Interface Science* **2011**, *357* (1), 75-81.
116. Lu, X.; Guo, Q.; Zhou, W.; Li, X.; Chen, J.; Zhou, X.; Sun, N.; Fang, Z., Improved performance of lateral flow immunoassays for alpha-fetoprotein and vanillin by using silica shell-stabilized gold nanoparticles. *Microchimica Acta* **2019**, *186* (1), 2.
117. Yuan, H.; Khoury, C. G.; Hwang, H.; Wilson, C. M.; Grant, G. A.; Vo-Dinh, T., Gold nanostars: surfactant-free synthesis, 3D modelling, and two-photon photoluminescence imaging. *Nanotechnology* **2012**, *23* (7), 075102.
118. Xu, Q.; Guo, X.; Xu, L.; Ying, Y.; Wu, Y.; Wen, Y.; Yang, H., Template-free synthesis of SERS-active gold nanopopcorn for rapid detection of chlorpyrifos residues. *Sensors Actuators B: Chemical* **2017**, *241*, 1008-1013.
119. Atta, S.; Beetz, M.; Fabris, L., Understanding the role of AgNO₃ concentration and seed morphology in the achievement of tunable shape control in gold nanostars. *Nanoscale* **2019**, *11* (6), 2946-2958.
120. Pallavicini, P.; Donà, A.; Casu, A.; Chirico, G.; Collini, M.; Dacarro, G.; Falqui, A.; Milanese, C.; Sironi, L.; Taglietti, A., Triton X-100 for three-plasmon gold nanostars with two photothermally active NIR (near IR) and SWIR (short-wavelength IR) channels. *Chemical Communications* **2013**, *49* (56), 6265-6267.
121. Pesavento, M.; Cennamo, N.; Donà, A.; Pallavicini, P.; D'Agostino, G.; Zeni, L., A new approach for selective optical fiber sensors based on localized surface plasmon resonance of gold nanostars in molecularly imprinted polymer. *Recent Advances In Biomedical Chemical Engineering Materials Science* **2014**, 71.
122. Nehl, C. L.; Liao, H.; Hafner, J. H., Optical properties of star-shaped gold nanoparticles. *Nano letters* **2006**, *6* (4), 683-688.
123. Wu, H.-L.; Chen, C.-H.; Huang, M. H., Seed-mediated synthesis of branched gold nanocrystals derived from the side growth of pentagonal bipyramids and the formation of gold nanostars. *Chemistry of Materials* **2009**, *21* (1), 110-114.
124. Jehn, C.; Küstner, B.; Adam, P.; Marx, A.; Ströbel, P.; Schmuck, C.; Schlücker, S., Water soluble SERS labels comprising a SAM with dual spacers for controlled bioconjugation. *Physical Chemistry Chemical Physics* **2009**, *11* (34), 7499-7504.
125. Hermanson, G. T., *Bioconjugate techniques*. Academic press: 2013.

126. Safenkova, I.; Zherdev, A.; Dzantiev, B., Factors influencing the detection limit of the lateral-flow sandwich immunoassay: a case study with potato virus X. *Analytical Bioanalytical Chemistry* **2012**, *403* (6), 1595-1605.

Appendix

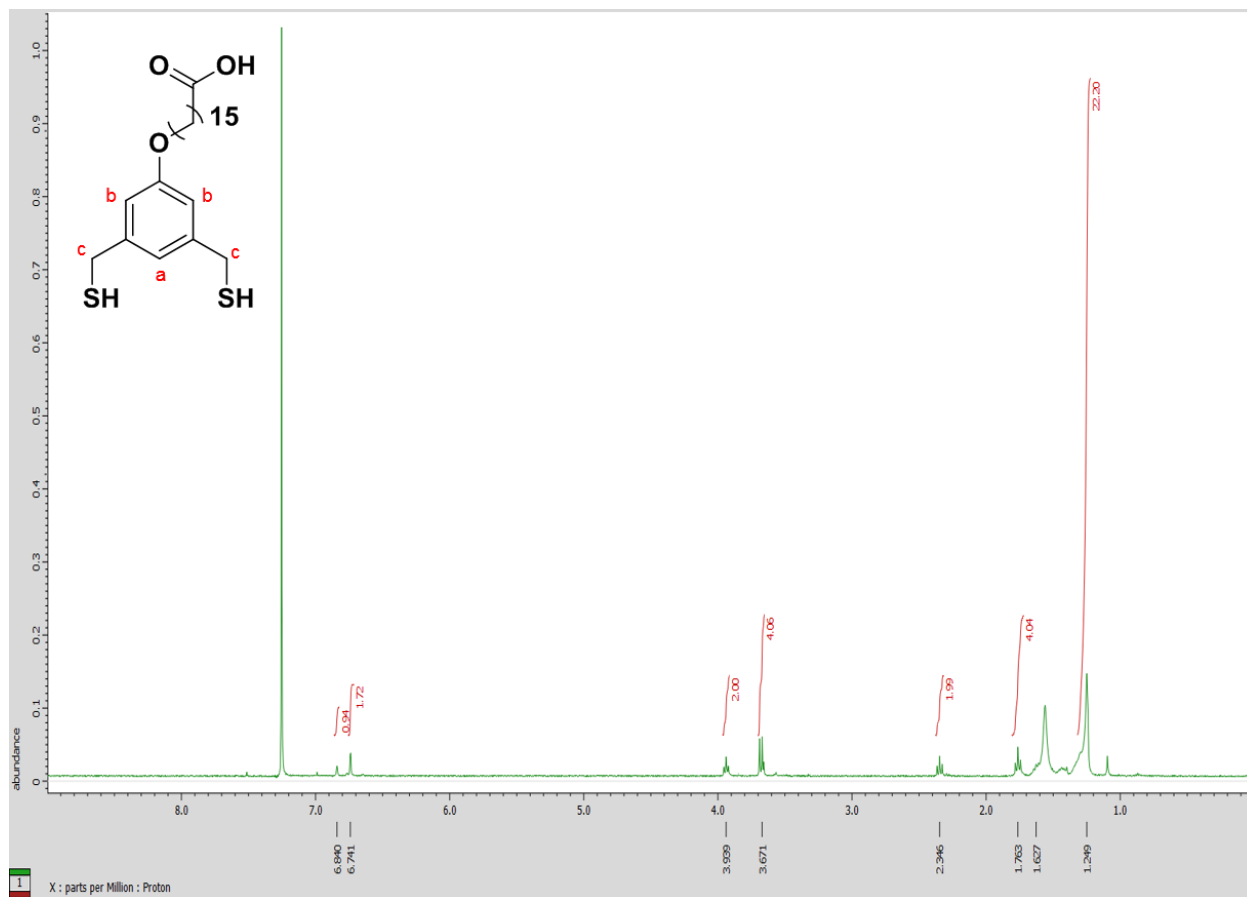


Figure A.1. ^1H NMR of the 16-(3,5 bis (mercaptomethyl) phenoxy) hexadecanoic acid (BMPHA)

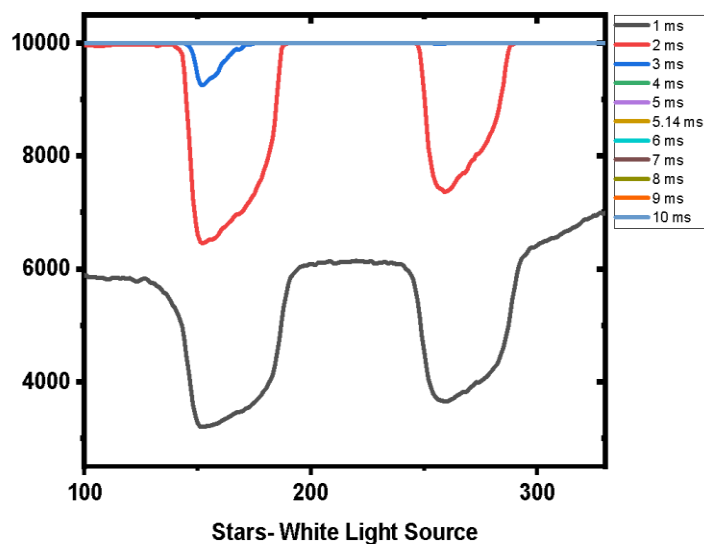


Figure A.2. The intensity of CL and TL vs. detection lines positions on LFA using AuNSs reporters with the white LS of Lumos trying different exposure times, from 1 msec. to 10 msec.

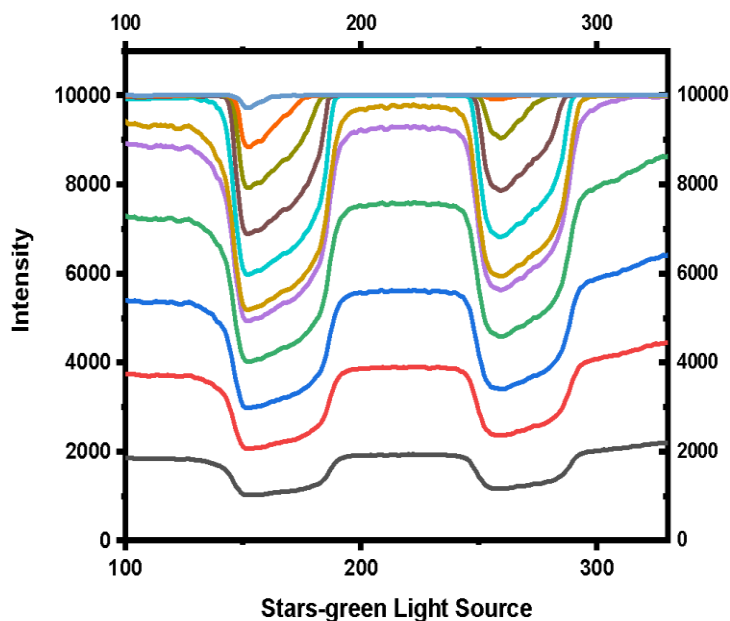


Figure A.3. The intensity of CL and TL vs. detection lines positions on LFA using AuNSs reporters with the green LS of Lumos trying different exposure times, from 1 msec. to 10 msec.

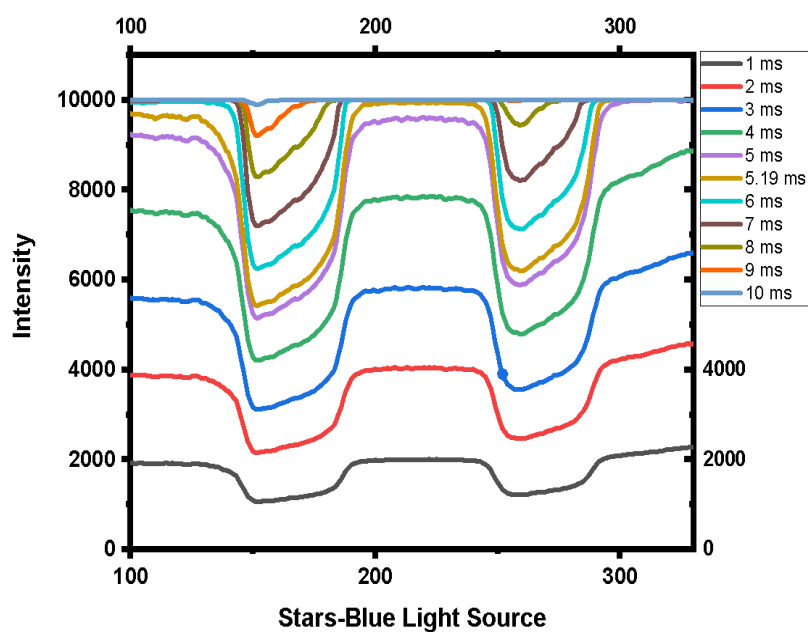


Figure A.4. The intensity of CL and TL vs. detection lines positions on LFA using AuNSs reporters with the blue LS of Lumos trying different exposure times, from 1 msec. to 10 msec.

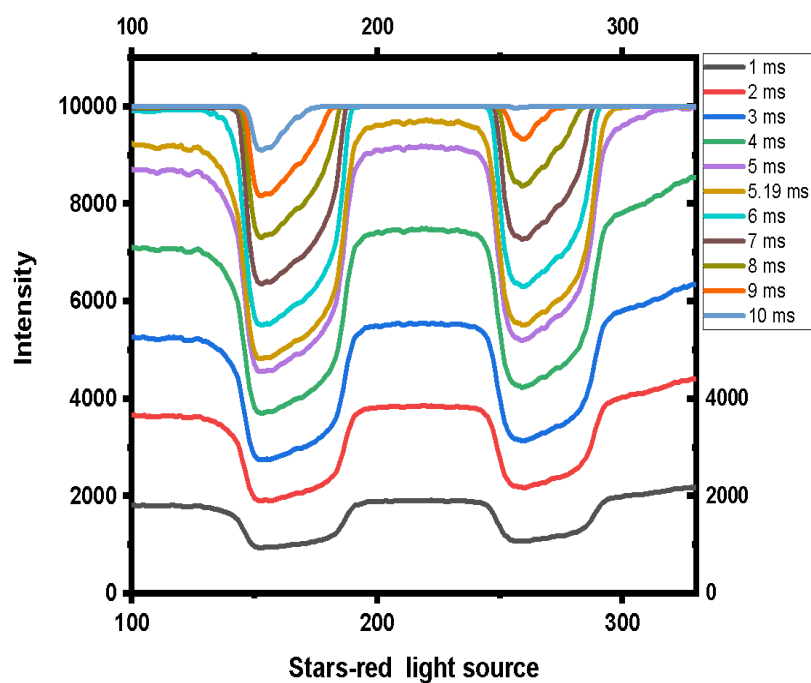


Figure A.5. The intensity of CL and TL vs. detection lines positions on LFA using AuNSs reporters with the red LS of Lumos trying different exposure times, from 1 msec. to 10 msec.

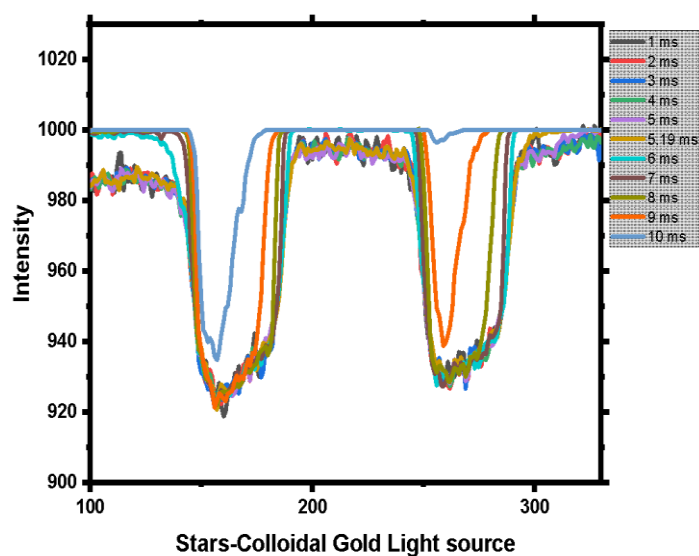


Figure A.6. The intensity of CL and TL vs. detection lines positions on LFA using AuNSs reporters with the “colloidal old” LS of Lumos trying different exposure times, from 1 msec. to 10 msec.

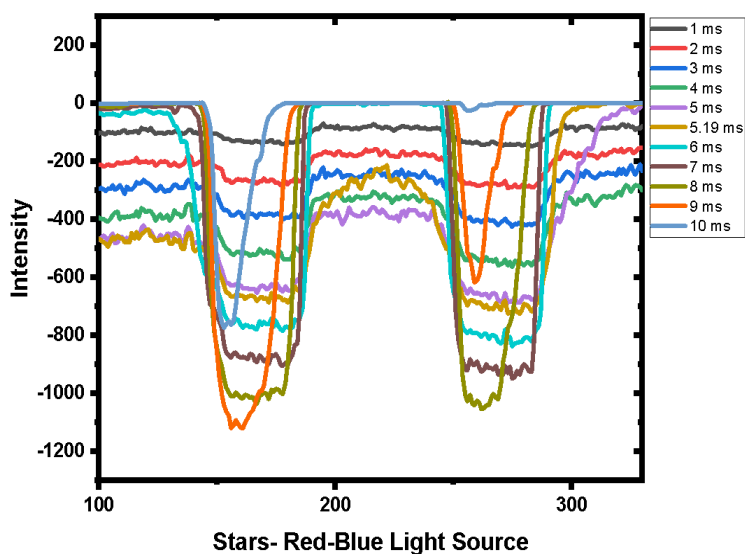


Figure A.7. The intensity of CL and TL vs. detection lines positions on LFA using AuNSs reporters with the red-blue LS of Lumos trying different exposure times, from 1 msec. to 10 msec.

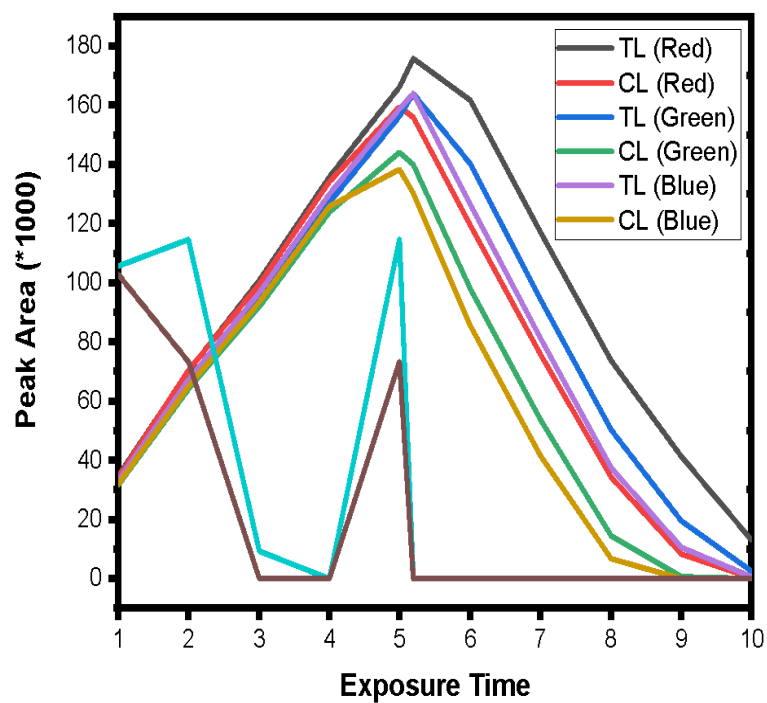


Figure A.8. AuNSs peak area of TL and CL vs. different exposure times using the various light sources of Lumos reader.

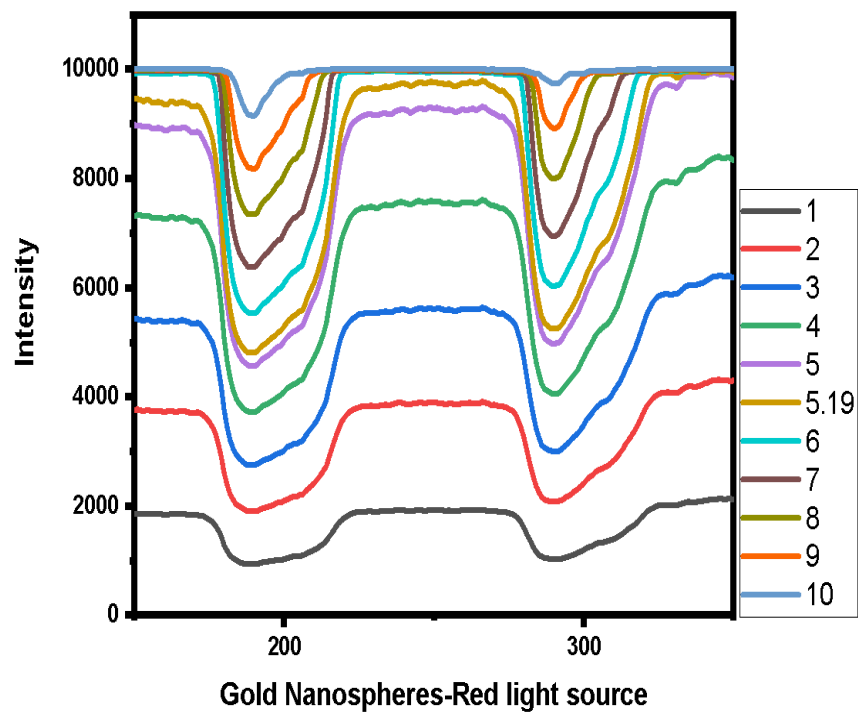


Figure A.9. The intensity of CL and TL vs. detection lines positions on LFA using spherical AuNPs reporters with the red LS of Lumos trying different exposure times, from 1 msec. to 10 msec.

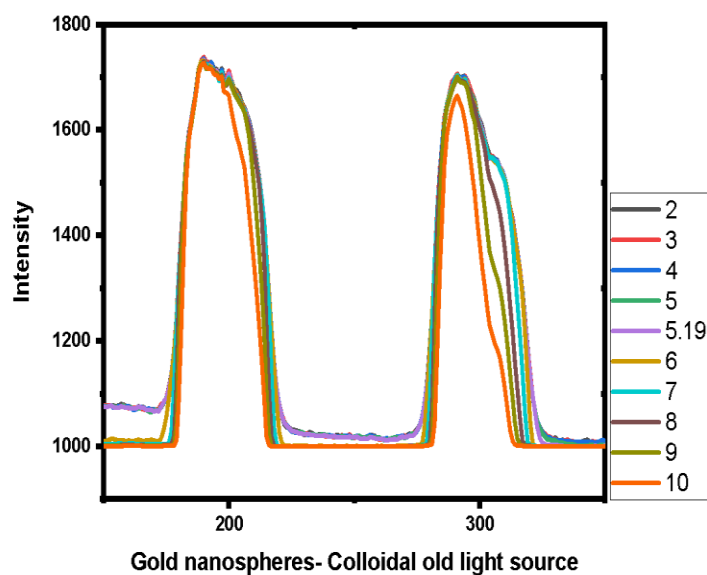


Figure A.10. The intensity of CL and TL vs. detection lines positions on LFA using spherical AuNPs reporters with the “colloidal gold” LS of Lumos trying different exposure times, from 1msec. to10 msec.

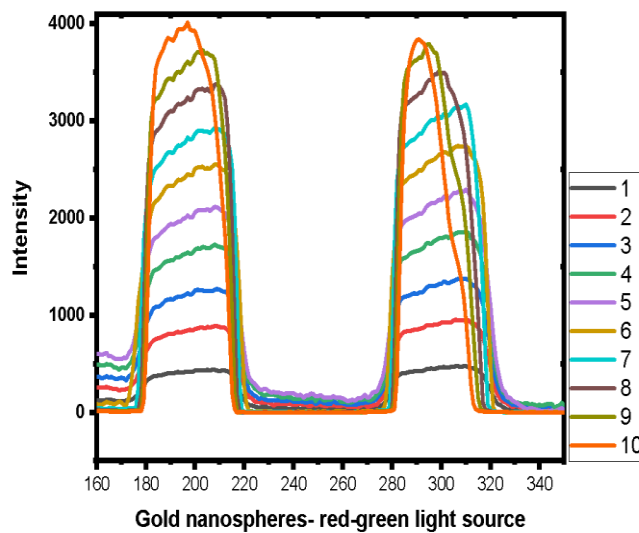


Figure A.11. The intensity of CL and TL vs. detection lines positions on LFA using spherical AuNPs reporters with the red-green LS of Lumos trying different exposure times, from 1 msec. to 10 msec.

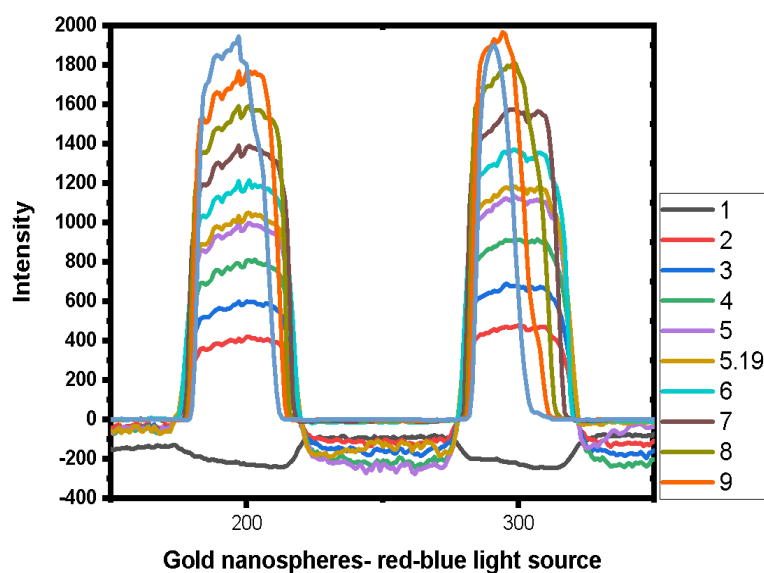


Figure A.12. The intensity of CL and TL vs. detection lines positions on LFA using spherical AuNPs reporters with the red-blue LS of Lumos trying different exposure times, from 1 msec. to 10 msec.

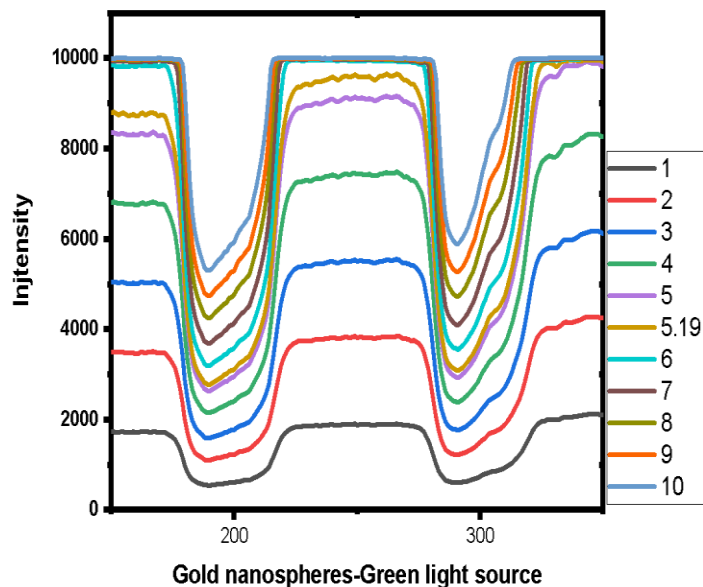


Figure A.13. The intensity of CL and TL vs. detection lines positions on LFA using spherical AuNPs reporters with the green LS of Lumos trying different exposure times, from 1 msec. to 10 msec.

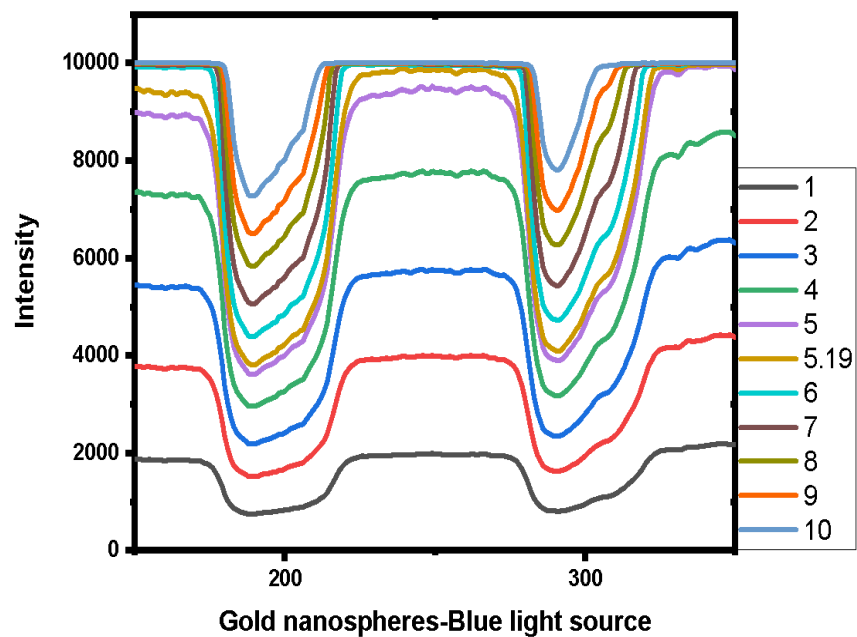


Figure A.14. The intensity of CL and TL vs. detection lines positions on LFA using spherical AuNPs reporters with the blue LS of Lumos trying different exposure times, from 1 msec. to 10 msec.

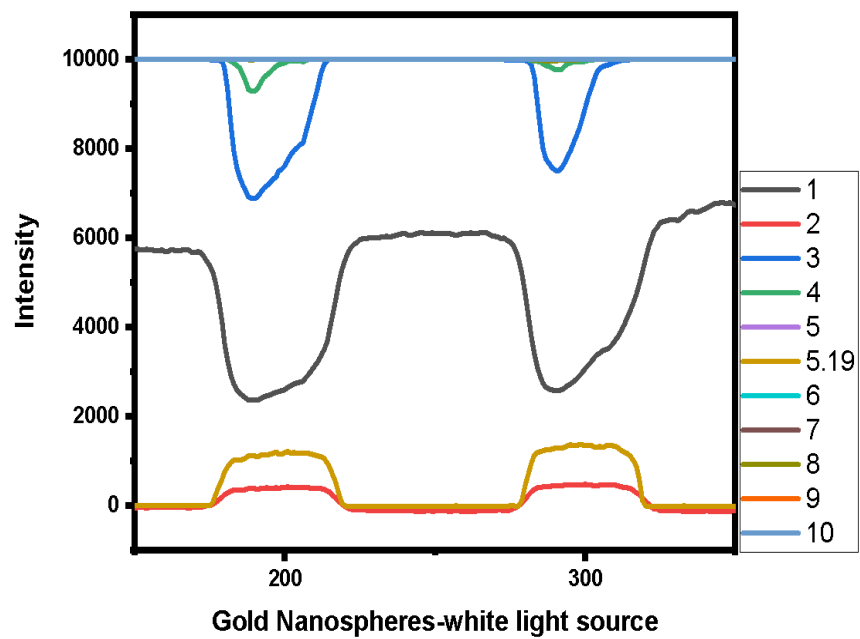


Figure A.15. The intensity of CL and TL vs. detection lines positions on LFA using spherical AuNPs reporters with the white LS of Lumos trying different exposure times, from 1 msec. to 10 msec.

s

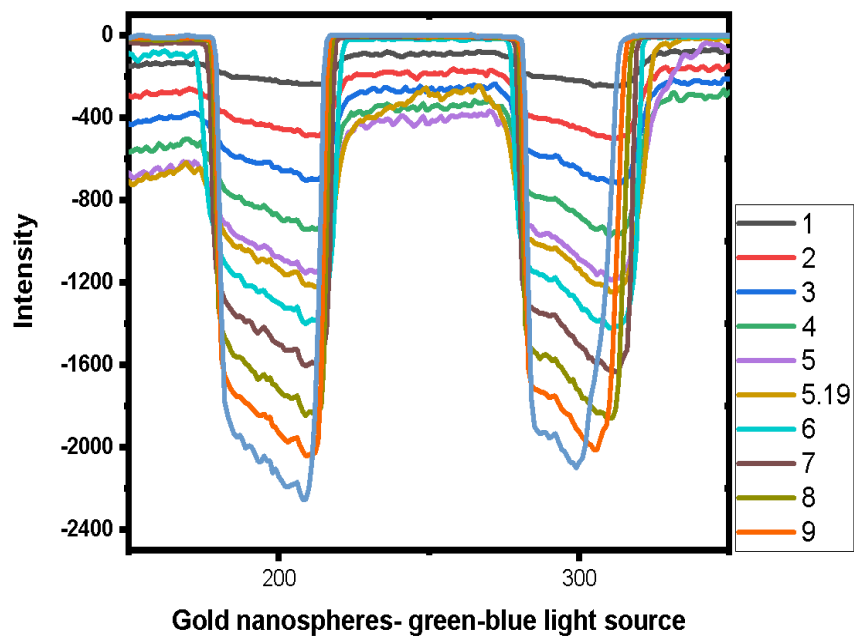


Figure A.16. The intensity of CL and TL vs. detection lines positions on LFA using spherical AuNPs reporters with the green-blue LS of Lumos trying different exposure times, from 1 msec. to 10 msec.

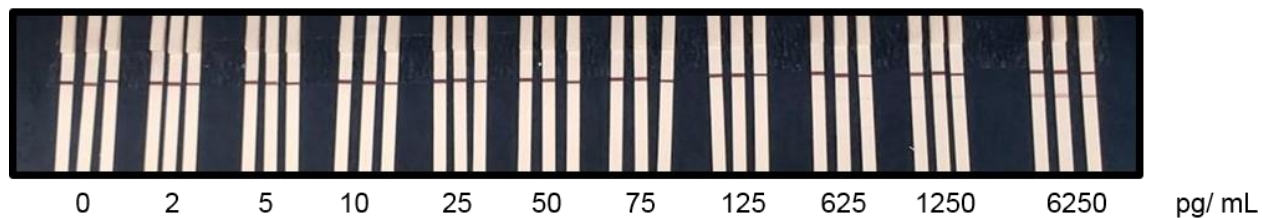
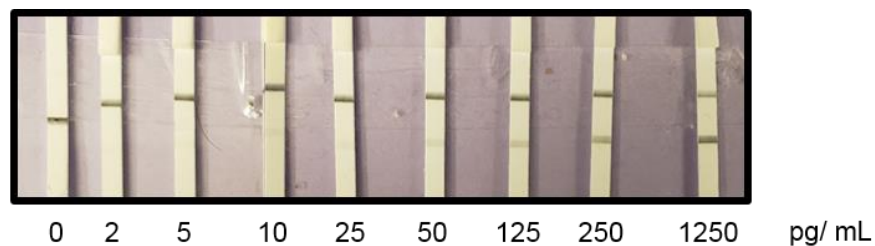


Figure A.17. LFA results using gold nanostars with different concentrations of hCG (on top) and spherical gold nanoparticles in different concentrations of hCG (on bottom)

Table A.1. Frequently used abbreviation table

LFA	lateral flow assay	MBA	Mercapto Benzoic Acid
POC	point of care	EDC	1-Ethyl-3-(3-dimethylaminopropyl)carbodiimide
AuNS	gold Nanostar	NHSS	N-hydroxysulfosuccinimide (Sulfo-NHS)
LOD	limit of detection	SEM	Scanning electron microscopy
hCG	human chorionic gonadotropin	TEM	transmission electron microscopy
LSPR	localized surface Plasmon resonance	EDX	Energy dispersive X-ray spectroscopy
AuNC	gold nanocube	XPS	X-ray photoelectron spectroscopy
Au	gold nano	OD	Optical density
AuNP	gold nanoparticle	NMR	Nuclear magnetic resonance
NC	Nitrocellulose	BMPHA	16- (3,5bis(mercaptomethyl)phenoxy)hexadecanoic acid
TL	test line	MQW	milli-Q water
CL	control line	BSA	Bovine serum albumin
PBS	phosphate-buffered saline	PVC	Polyvinyl Chloride
SAM	self-assembled monolayer	FTIR	Fourier transform infrared
AuNR	gold nanorods	SERS	surface-enhanced Raman spectroscopy